Review

Smart Ligands for Efficient 3d-, 4d- and 5d-Metal Single-Molecule Magnets and Single-Ion Magnets [†]

Panagiota S. Perlepe [1] [ID]**, Diamantoula Maniaki** [1]**, Evangelos Pilichos** [1]**, Eugenia Katsoulakou** [1,]***and Spyros P. Perlepes** [1,2,]*

[1] Department of Chemistry, University of Patras, 265 04 Patras, Greece; pennyperlepes@gmail.com (P.S.P.); dia.maniaki@gmail.com (D.M.); pilvag@gmail.com (E.P.)
[2] Institute of Chemical Engineering Sciences, Foundation for Research and Technology-Hellas (FORTH/ICE-HT), Platani, P.O.Box 1414, 265 04 Patras, Greece
* Correspondence: eugeniachem@gmail.com (E.K.); perlepes@patreas.upatras.gr (S.P.P.); Tel.: +30-2610-996019 (E.K.); +30-2610-996730 (S.P.P.)
[†] This work is devoted to Research Director Vassilis Psycharis on the occasion of his 60th birthday. Dr. Psycharis is an excellent structural scientist, a fantastic collaborator and a precious friend.

check for updates

Abstract: There has been a renaissance in the interdisciplinary field of Molecular Magnetism since ~2000, due to the discovery of the impressive properties and potential applications of d- and f-metal Single-Molecule Magnets (SMMs) and Single-Ion Magnets (SIMs) or Monometallic Single-Molecule Magnets. One of the consequences of this discovery has been an explosive growth in synthetic molecular inorganic and organometallic chemistry. In SMM and SIM chemistry, inorganic and organic ligands play a decisive role, sometimes equally important to that of the magnetic metal ion(s). In SMM chemistry, bridging ligands that propagate strong ferromagnetic exchange interactions between the metal ions resulting in large spin ground states, well isolated from excited states, are preferable; however, antiferromagnetic coupling can also lead to SMM behavior. In SIM chemistry, ligands that create a strong axial crystal field are highly desirable for metal ions with oblate electron density, e.g., Tb^{III} and Dy^{III}, whereas equatorial crystal fields lead to SMM behavior in complexes based on metal ions with prolate electron density, e.g., Er^{III}. In this review, we have attempted to highlight the use of few, efficient ligands in the chemistry of transition-metal SMMs and SIMs, through selected examples. The content of the review is purely chemical and it is assumed that the reader has a good knowledge of synthetic, structural and physical inorganic chemistry, as well as of the properties of SIMs and SMMs and the techniques of their study. The ligands that will be discussed are the azide ion, the cyanido group, the tris(trimethylsilyl)methanide, the cyclopentanienido group, soft (based on the Hard-Soft Acid-Base model) ligands, metallacrowns combined with click chemistry, deprotonated aliphatic diols, and the family of 2-pyridyl ketoximes, including some of its elaborate derivatives. The rationale behind the selection of the ligands will be emphasized.

Keywords: ligands; molecular magnetism; single-ion magnets (SIMs) or monometallic single-molecule magnets; single-molecule magnets (SMMs); synthetic strategies; 3d-, 4d- and 5d-metal complexes as SIMs and SMMs

1. The History of Molecular Magnetism in Brief—The Era of Single-Molecule Magnets (SMMs) and Single-Ion Magnets (SIMs)

Molecular magnetism [1] is currently a "hot" interdisciplinary research field which started almost 35 years ago. It was a rather natural extension of the field of Magnetochemistry which was developed in the 1955–1985 period. In the latter field, inorganic chemists were using experimental values of magnetic moment and their variation with temperature to draw chemical and structural conclusions for molecular complexes. Well known examples [2,3] were: (i) The distinction between several stereochemistries (tetrahedral, square planar, octahedral) in complexes of some 3d-metal ions, e.g., Ni(II) and Co(II); (ii) the recognition of high-spin and low-spin configurations in octahedral complexes of $3d^4$–$3d^7$ metal ions; and (iii) the elegant determination of the singlet-triplet gap in copper(II) acetate hydrate by Bleaney and Bowers, before the X-ray solution of its dinuclear $[Cu_2(O_2CMe)_4(H_2O)_2]$ structure.

Before proceeding to a brief history of molecular magnetism, we can mention two advantages that molecular systems offer over conventional atom- or ion-based magnetic materials [4]: (a) The structures that can be formed are more complicated and more diverse that the structural types we normally meet in conventional inorganic materials. Molecular crystals can provide scientists with ensembles of identical structures and iso-orientated magnetic objects which permit the in-depth study of their physical behavior. Such molecular materials offer model systems to test existing theories on many-body problems and discover, e.g., new quantum, behavior; and (b) Molecular systems are ideal for incorporation of other useful functionalities, e.g., optical properties, conductivity, etc. This may be a synergistic property not coupled with magnetism, or it may be a coupling of different physical properties, e.g., light-induced magnetic ordering in spin-crossover (SCO) Prussian blue phases. This type of materials may find novel, highly specific applications.

In the field of molecular magnetism, chemists, chemical engineers, physicists and material scientists, both experimentalists and theoreticians, closely collaborate trying to design, synthesize, fully characterize and model the magnetic properties of molecule-based materials. In the initial period of its development, the focus of research was on simple model systems (homo- and heterometallic dinuclear complexes and coordination clusters); the goal was to test theories in solids about exchange interactions and electron delocalization at the molecular scale [5]. The field later expanded towards the study of 1D systems [1,6,7], e.g., homometallic chains, heterometallic chains and homometallic chains in which the metal centers are bridged by an organic radical. In the late 1980s and during the 1990s, chemists prepared a great variety of 3D complexes exhibiting spontaneous magnetization below a critical temperature (T_c) [8–10]. The Miller and Epstein groups broke the critical temperature barrier record ($T_c > 350$ K) with the ferrimagnet $\{[V^{III}(TCNE)_2] \cdot x CH_2Cl_2\}_n$ [11], where $TCNE^-$ is the radical anion of tetracyanoethylene, while other groups came close by using Prussian blue derivatives [9,10].

Simultaneously with the above developments, the molecular magnetism community paid more attention on octahedral $3d^4$–$3d^7$ systems (mainly on $3d^6$ iron(II) complexes) with a SCO behavior [12,13]. This phenomenon, discovered by Cambi in 1931, continues to attract the intense interest of scientists even after 90 years [14,15]. The goals are to construct systems which undergo spin transition near 300 K and to study the possibility of tuning this molecular bistability through application of external stimuli (temperature, pressure, light). The SCO phenomenon has already led to applications, e.g., sensors [16], actuators [17] and thermal displays [18].

Thus, the initial growth of molecular magnetism was mainly based on the deep understanding of the factors that could be used to design and synthesize novel crystalline molecule-based materials exhibiting useful magnetic properties, e.g., ferromagnetism and ferrimagnetism, similar to those observed in inorganic atom-/ion-based materials. More importantly, those molecular materials had special features such as low density, insulating nature and optical transparency; these distinctive physical properties provide

material scientists with a number of fabrication advantages, as the materials are most often prepared using solution methods.

After the period of initial growth of molecular magnetism, its community turned the attention to three large classes of molecular compounds. The first class comprises the Single-Molecule Magnets (SMMs) and the Single-Ion Magnets (SIMs), the second the Single-Chain Magnets (SCMs) and the third involves the multifunctional molecular magnetic materials [19,20]. The focus of this review is on transition-metal SMMs and SIMs.

In the presence of axial magnetic anisotropy (D), the M_S levels of a transition-metal complex with total spin S will split under zero magnetic field according to the Hamiltonian $\hat{H} = D\hat{S}_z^2$. If the value of D is negative, the two $\pm M_S$ levels of maximal projection along the z axis form a bistable ground state because they are degenerate. If we reverse the magnetic moment by converting $-M_S$ to $+M_S$, this requires traversal of a spin-inversion barrier. This barrier is $U = S^2|D|$ for integer S or $U = (S^2 - 1/4)|D|$ for non-integer S, and the system passes through the $M_S = 0$ or the $M_S = 1/2$ levels, respectively, at the height of the energy barrier. The existence of such a barrier can lead to the slow relaxation of the magnetic moment at very low temperatures upon removal of the external dc field [21,22]. The presence of this barrier is often proven by the appearance of magnetic hysteresis of molecular origin as first observed for the iconic $[Mn_{12}O_{12}(O_2CMe)_{16}(H_2O)_4]$ (**1**, Figure 1) SMM [21–23]. Clusters containing polynuclear molecules that exhibit such behavior have been named Single-Molecule Magnets. The magnetic behavior of each of these clusters can be described as a giant anisotropic spin as a result of the exchange coupling between the spins of neighboring metal ions. Because of the magnetic bistability, these polynuclear molecules were proposed for use in magnetic memory devices since they can remain magnetized in one of the two spin states, thus giving rise to a "bit" of memory. The aim during the first decade of SMM research (1993–2003) was to prepare SMMs with memory effects at higher temperatures [19]. Although synthetic inorganic chemists made many efforts to achieve this goal, the progress was little and the energy barriers that stabilize the magnetic bits against thermal fluctuations remained small. Another tremendously important consequence of the discovery of SMMs was the observation of quantum effects in mesoscopic magnets. At that time, physicists were looking for small magnetic particles, all identical to each other, to investigate if quantum effects could be observed in ensembles of such identical particles; however, the preparation of these collections proved difficult. Chemists solved the problem using a molecular approach to prepare identical cluster molecules in crystalline SMMs. A few years after the characterization of **1**, scientists revealed that its crystals exhibit quantum tunneling of magnetization (QTM) [24,25]; this phenomenon is considered one of the milestones in the study of spin during the 20th century [19]. Synthetic efforts were followed by advanced theoretical studies, and the latter provided strong evidence that the magnitude of D decreases as S increases; this implied that the construction of efficient SMMs with a large U cannot be achieved by only maximizing S and that control of D is equally important [21,22].

In the last 15 years or so, another exciting subclass of SMMs was discovered, the so-called Single-Ion Magnets (SIMs). These represent the smallest molecular nanomagnets we can imagine [21,26–34]. In the literature, SIMs are often referred to as mononuclear SMMs. However, neither SIMs nor mononuclear SMMs are perfect descriptors [26]. Monometallic SMMs is probably better, but herein we have chosen to use the SIM acronym rather, e.g., MSMM, which is probably more awkward. SIMs are mononuclear complexes containing a single magnetic d- or f-metal ion. The motivation behind the SIM research evolution was the belief of scientists that incorporating many paramagnetic centers into a cluster molecule may be a disadvantage in terms of generating complexes with large cluster anisotropies (D or better $D_{cluster}$). Many metal ions can, in principle, lead to a large S, but as the nuclearity of the molecule increases it is becoming very difficult (practically impossible) to control the mutual alignment of the anisotropy axes of the individual metal ions; this gives small $D_{cluster}$ values [27]. These considerations, combined with the observation of slow magnetization relaxation in complexes $(Bu^n_4N)[Ln(pc)_2]$ (**2**), where Ln = Tb, Dy and

pc = the dianion of phthalocyanine [35], by Ishikawa and co-workers, turned the attention of researchers to single-ion systems [19,21]. If we compare 4f-(Ln) and d-metal ions for use in SIMs, the former appear better because they possess: (i) larger magnetic moments, (ii) higher spin-orbit coupling constants, and (iii) weak coupling of the f orbitals to the ligand field which cannot quench first-orbital contributions to the magnetic moment. As a consequence, magnetic hysteresis has been observed at temperatures as high as 80 K for mononuclear organometallic Dy(III) complexes [36]. However, d-metal ion SIMs are important and cannot be considered simply as academic research curiosities. As scientists understand deeper the physics of d single ions in a ligand field, they can begin to design strategies to couple the anisotropy of individual transition metal ions together in order to create cluster SMMs in a rational way; such clusters could be ideal molecular analogues for magnetic nanoparticles. Additionally, the utilization of well-studied and understood SIM building blocks in the modular synthesis of 1D SCMs with high spin and uniaxial anisotropies (a concept which is active in the 4f-metal chemistry), and Metal–Organic Frameworks (MOFs) with SIM units as nodes (e.g., for the design of porous magnetic materials) is a currently "hot" research area, see information provided in reference [27].
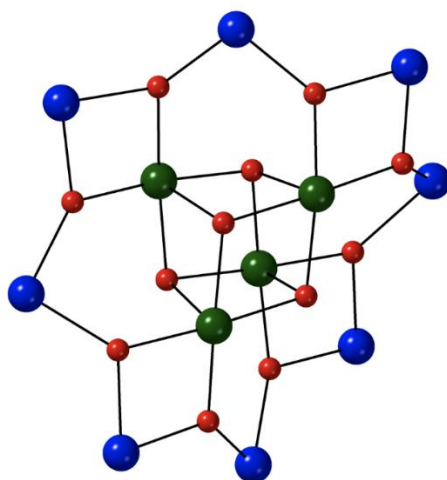

Figure 1. The $\{Mn^{III}_8Mn^{IV}_4(\mu_3\text{-}O)_{12}\}^{16+}$ core of the archetype Single-Molecule Magnet (SMM) **1**. The Mn^{III} centers are shown with blue color, the Mn^{IV} centers with green color and the oxido ions are shown with red color. The four central Mn^{IV} atoms are weakly ferromagnetically coupled, and the remaining $Mn^{III}\cdots Mn^{IV}$ and $Mn^{III}\cdots Mn^{III}$ exchange interactions are all antiferromagnetic, with the former much stronger than the latter. As a result, the stronger $Mn^{III}\cdots Mn^{IV}$ interactions overcome the weaker $Mn^{III}\cdots Mn^{III}$ ones within each triangular $Mn^{III}_2Mn^{IV}$ subunit of the core, aligning the spins of the outer Mn^{III} atoms all parallel, and thus antiparallel to the central Mn^{IV} atoms; this gives an $S = 16 - 6 = 10$ ground state.

Despite high energy barriers for magnetization reversal, often SMMs and SIMs suffer from fast relaxation processes, not just via QTM, but also via interactions between the spin states and lattice phonons [27,30]. The complex behavior of relaxation dynamics is a specialized topic beyond the scope of this review. However, it is helpful to consider the SMM and SIM systems as being composed of two parts, the spin part and the lattice part. The interaction between lattice vibrations (phonons) and spin provide the system with additional relaxation processes, which "shortcut" the desired thermal pathway. The spin-lattice relaxation mechanisms are of three types (direct, Orbach and Raman processes). Since the tunneling pathways are very sensitive to changes of molecular symmetry, synthetic chemists try to control the molecular symmetry of SMMs/SIMs through careful design of the ligands used. Additional tools for minimizing QTM through the ground state are magnetic dilution and utilization of a Kramers metal ion; for the latter, breaking of the M_S degeneracy and therefore QTM is formally forbidden in strictly zero

magnetic field. However, the fast quantum tunneling offers an advantage because these molecules are candidates to realize quantum bits (qubits), the basic units of quantum computers [37].

A second class of molecular compounds which has captured the intense interest of the molecular magnetism community consists of slow-relaxing 1D magnets, or SCMs [20,21,38,39]. These consist of chains, isolated from each other, presenting a slow relaxation of the magnetization; they cannot present a long-range magnetic order. However, they exhibit a short-range order caused by the occurrence of domains where N spins are oriented in the same direction, interrupted by a reversed spin or by chain defects. A finite magnetization can thus be frozen in the absence of an applied magnetic field at low temperatures. Like in SMMs, the system should have an Ising-type magnetic anisotropy, i.e., the spins must preferentially orient in one direction. The main concept of dynamics is the probability of a spin to flip within the chain, taking into account only the nearest neighbors' interactions, with an Hamiltonian of the type $\hat{H} = -J\Sigma_{i=1,N-1}\hat{S}_i\hat{S}_{i+1}$. The prototype compound is the 1D complex $\{[Co^{II}(hfac)_2(NITPhOMe)]\}_n$ (**3**) [40], where hfac is the hexafluoroacetylacetonato(−1) ligand and NITPhOMe is the neutral nitronyl nitroxide, bridging radical 4'-methoxyphenyl-4,4,5,5-tetramethylimidazoline-1-oxyl-3-oxide. The Ising nature of the chain has been attributed to the presence of Co(II) as this center yields significant anisotropic effects when it is 6-coordinate.

The third class of molecular compounds, of great interest to scientists, consists of multifunctional materials whose study is beyond molecular magnetism. These molecular materials combine two, technologically interesting, electronic properties, e.g., ferromagnetism and superconductivity, or SMM properties and photoluminescence; such properties are very difficult to be included in purely inorganic solids. Examples of crystalline, multifunctional molecular materials include porous magnets [41], chiral magnets [42,43], conducting magnets [44] and luminescent SMMs [45,46], among others.

In the last few years, the interdisciplinary field of molecular magnetism is rapidly shifting to magnetic molecules and materials in physics- and nanotechnology-related fields [19], such as molecular spintronics, quantum technologies, 2D materials and MOFs [37,47–51]. For example, in the field of quantum technologies, the achievements in the design of molecular spin qubits with long quantum coherence times and in the implementation of quantum operations give hopes for the use of molecular spin qubits in quantum computation.

Closing this introductory section, we would like to emphasize some advantages of the use of nd metal ions (compared to nf ones) in the SMM/SIM research. The magnetic anisotropy of a transition metal center can be more rationally tuned by chemical design. For a given d^n configuration, both the sign and the magnitude of *D* are controlled, mainly by the geometry of the coordination sphere of the nd metal ion, and thus they can be tuned more easily than for a nf metal ion by the chemist. Very large |*D*| values are found for complexes with low coordination numbers, which are more accessible for the nd metal ions (at least with $n = 3$) than for the nf metal centers. Such chemical control on the magnetic anisotropy of monometallic SMMs can help scientists to develop more efficient polynuclear molecular magnetic species.

2. Ligands in SMM and SIM Chemistry

Alfred Stock, a pioneer in borane and silane chemistry, was the first scientist to introduce the term "ligand" in the second decade of the 20th century; the word has its roots in the Latin language where "ligare" means "to bind" [52]. The term came into use among English-speaking inorganic chemists after the 2nd world war, mainly through the wide popularity of the PhD Thesis of Jannik Bjerrum [52]. The proper utilization of known ligands and the design of new ones is behind many spectacular developments in coordination and metallosupramolecular chemistry [53]. Theoretical concepts related to ligands are the chelate effect, the macrocycle effect, the cryptate effect, the isoelectronic and isolobal relationships, the conformation of chelating rings and the reactivity of coordinated ligands [54].

In SMM and SIM chemistry, the ligands play a crucial role [55,56], sometimes equally important to that of the magnetic metal ions. An impressive example comes from the 4f-metal SIM chemistry. By combining two different organometallic ligands of sufficient bulk (but not too bulky to avoid close approach of the ligands), the groups of Tong, Mansikkamäki and Layfield synthesized the mononuclear complex $[(Cp^{iPr5})Dy^{III}(Cp^*)][B(C_6F_5)_4]$ (**4**), Equations (1) and (2), Figure 2; Cp^{iPr5} is the penta-iso-propylcyclopentadienyl(−1) ligand and Cp^* is the pentamethylcyclopentadienyl(−1) ligand. This design of ligand framework allowed the two key structural parameters—that is, the Dy–Cp$_{cent}$ distances (cent refers to the centroids of the cyclopentadienyl ligands) and the Cp–Dy–Cp bend angle-to be short and wide, respectively, thus achieving an axial crystal field of sufficient strength to give a SIM that shows magnetic hysteresis above 77 K [36]; this is the first step for the development of nanomagnet devices that function at relatively practical temperatures.
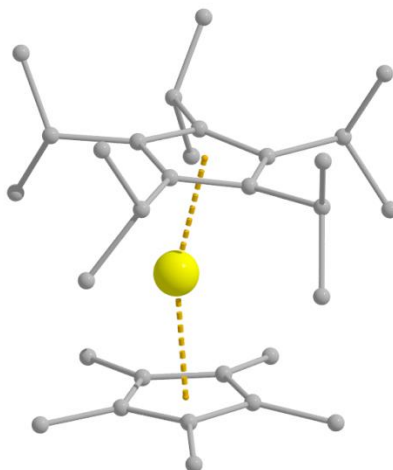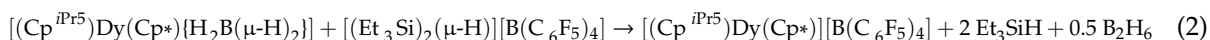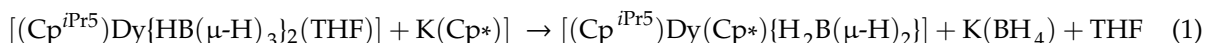
$$[(Cp^{iPr5})Dy\{HB(\mu\text{-}H)_3\}_2(THF)] + K(Cp^*)] \rightarrow [(Cp^{iPr5})Dy(Cp^*)\{H_2B(\mu\text{-}H)_2\}] + K(BH_4) + THF \quad (1)$$

$$[(Cp^{iPr5})Dy(Cp^*)\{H_2B(\mu\text{-}H)_2\}] + [(Et_3Si)_2(\mu\text{-}H)][B(C_6F_5)_4] \rightarrow [(Cp^{iPr5})Dy(Cp^*)][B(C_6F_5)_4] + 2\,Et_3SiH + 0.5\,B_2H_6 \quad (2)$$

Figure 2. The molecular structure of the cation $[(Cp^{iPr5})Dy^{III}(Cp^*)]^+$ that is present in the Single-Ion Magnets (SIM) **4**, which holds the world record for the magnetic blocking temperature (T_B = 80 K); one description of this parameter refers to the maximum temperature at which it is possible to observe hysteresis in the field dependence of the magnetization, subject to the field sweep rate. The Dy^{III} center is shown in yellow color. Modified from reference [36].

3. Scope and Organization of this Review

As briefly mentioned in Section 1, in the last 25 years there has been a renaissance in the field of molecular magnetism. The main reason for this was the discovery of the exciting properties and the efforts for improvement of SMMs and SIMs. One of the consequences of these discoveries was an explosive growth of synthetic molecular inorganic and organometallic chemistry. Many groups around the world have been working on the synthesis of SMMs and SIMs with higher effective energy barriers for magnetization reversal (U_{eff}) and T_B values, with the Holy Grail in this area being their technological applications. Novel structural types of metal complexes and new, smart synthetic methods have been reported to realize this general goal. *Inorganic and organic ligands are central "players" in this game.* Concerning transition-metal ion polynuclear SMMs, the ligands are of various types. The inorganic ligands are mainly the hydroxido, oxido, azido, dicyanamido, cyanato, cyanido and halogenido groups.

Simple carboxylato, azolato, deprotonated diol and triol, and thiolato organic ligands are frequently used, but the most employed ones are polydentate ligands involving a combination of functional groups, e.g., alkoxido, phenoxido, carboxylato, oximato, etc. Concerning transition-metal ion monometallic SMMs (SIMs), the ligands should be terminal and the most popular ones are simple heterocycles, phosphines and thioureas, thiolates, phenolates, bis(trimethylsilyl)amide, 2,9-dialkylcarboxylate-1,10-phenantrholines, 6,6′-dialkylcarboxylate-2,2′-bipyridines, chelating Schiff bases and various organometallic-type ligands, including tris(trimethylsilyl)methanide. We should mention here that the U_{eff} term is used to indicate thermally induced reversal of the magnetization, the rate of which is dependent on the energy barrier in which the system must surmount to reverse the spin [30]. Due to tunneling effects, U_{eff} is always lower than U defined in Section 1.

The general aim of this review is to highlight the use of few (we emphasize the word "few") inorganic and organic ligands in the chemistry of 3d-, 4d-, and 5d-metal SMMs and SIMs, through selected examples. According to the authors' opinion (a subjective opinion!), these ligands have contributed much into the development of the transition-metal SMM/SIM area, but simultaneously they are promising and have the potential for exciting achievements in the future. Ligands that have been used in f-metal-containing (both homometallic and heterometallic) SMM and SIM chemistry will not be described.

The review's content is shaped by a few specific features. First, it is important to specify *what this review is not*. It is *not* a comprehensive review on the chemistry of transition-metal SMMs and SIMs; there are excellent reviews and books covering this wide topic [21–23,26,27,29,57–60]. We never considered the idea of being exhaustive; each of the sections could have been on its own a subject of another review. It is *not* a survey of recent interesting results; such results can be found in the current literature. Thus, we apologize to the outstanding researchers whose excellent work will not be cited.

Second, the content of the review is chemical and we assume that the readers have a good knowledge of synthetic, structural and physical coordination and organometallic chemistry, as well as of the properties of SMMs/SIMs and the techniques of their study. Structural and magnetic information will be confined to the absolute minimum. To avoid long synthetic discussions, balanced chemical equations (written using molecular and not-ionic formulae) will be used. This, of course, implies that only one reaction occurs in solution (which is certainly not the case, at least in SMM chemistry that involves polynuclear species); however, we do believe that writing chemical equations offers a great help to the reader to understand the processes, better than presenting a long text. We shall try to explain the synthetic philosophy behind the reactions with emphasis on the choice of ligands and metal ion sources. Many of the references for the general information are reviews and book chapters.

Third, the method that will be used to describe the coordination of ligands to transition-metal ions is mainly the "Harris Notation"; occasionally, and in simple cases, the traditional η/μ rotation will be also used. The "Harris Notation" [61] is an already widely accepted method for the description of the ligands' binding to metal ions. It is written in the form $X.Y_1Y_2Y_3 \ldots Y_i$, where X is the total number of metal ions bound by the whole ligand, and each Y value refers to the number of metal centers attached to the different donor atoms. The order of Y atoms follows the Cahn–Ingold–Prelog priority rules; hence, for most of the ligands reported in this review, O comes before N. For clarity, the coordination modes of the ligands in most examples of this work will be presented schematically.

A fourth, more personal point, is that this review is a distillation from life-long experience of our group as a synthetic one, preparing molecules and molecular assemblies specially designed to exhibit given physical properties. Few of the ligands that will be discussed reflect our poor knowledge of and minor contributions into the area of the chemistry of SMMs and SIMs with 3d- and 4f-metal ions. Thus, few examples (but not the majority of them) will be work from our group.

Fifth, it is important to realize that the discipline of designing appropriate ligands for efficient transition-metal SMMs and SIMs has reached such a state of maturity that the present attempt cannot give

(we are afraid) innovative ideas, but it will be a trip to the great achievements of selected (and not all) groups in the area.

As far as we are aware, this is the first attempt to highlight in a review the great influence of ligands on SMM and SIM properties. The topic has been partly covered in many of the books [21,22], chapters in books [55] and reviews [23,26,27,57–60] available dealing with the chemistry, physics, properties and potential applications of molecular nanomagnets.

4. The Azide Ion: An Evergreen "Tree" in the Chemistry of Transition-Metal SMMs

The azide ion (N_3^-) is the conjugate base of hydrazoic acid. Aqueous solutions of HN_3 were first prepared by T. Curties in 1890, Equation (3). Such solutions are weakly acidic (pK_a = 4.75).

$$N_2H_5^+ + HNO_2 \rightarrow HN_3 + H^+ + 2\,H_2O \tag{3}$$
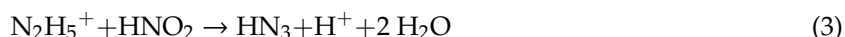
The azido ligand is very popular in transition-metal chemistry and especially for the synthesis of coordination clusters and coordination polymers [62–64]. In Coordination Chemistry, it is found either as a terminal ligand (η^1) or as a bridging one. The to-date crystallographically established coordination modes of the bridging azido ligand are illustrated in Figure 3.
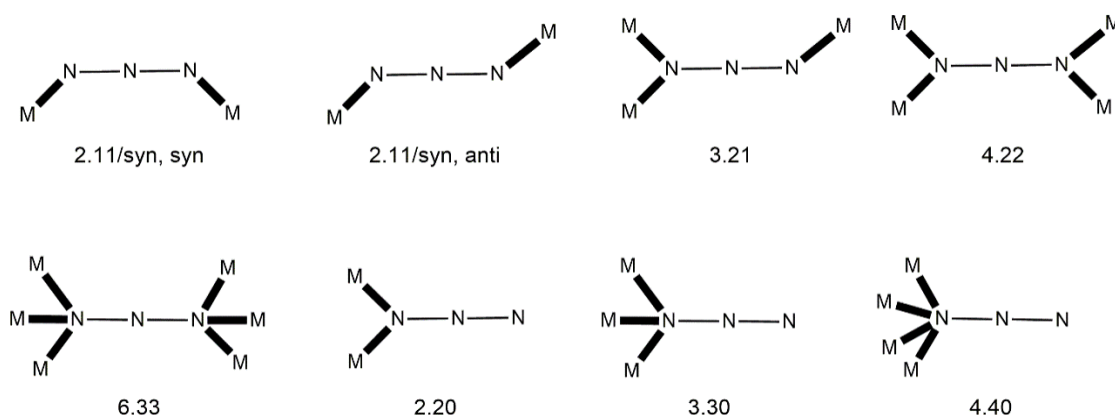

Figure 3. The to-date crystallographically established bridging coordination modes of the azido ligand and the Harris notation [61] that describes these modes. Coordination bonds are drawn with bold lines.
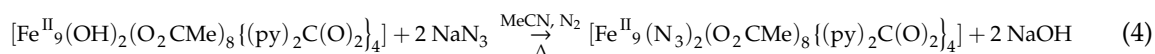
The bridging azido ligand has been one of the most investigated ligands in Magnetochemistry and Molecular Magnetism [63]. The variety of its bridging modes and its ability to propagate exchange interactions has led to compounds with several kinds of magnetic behaviors, such as antiferromagnetism, ferrimagnetism, ferromagnetism, canted weak ferromagnetism, spin-flop, and SMM and SCM properties [63]. End-to-end (EE) azido groups generally propagate antiferromagnetic interactions between paramagnetic metal ions, whereas end-on (EO) N_3^- ions are generally ferromagnetic couplers; exceptions of this general rules are known [63]. In addition to the coordination mode, other structural and electronic parameters (bridging and dihedral angles, bond lengths, orthogonality of magnetic orbitals, spin polarization, delocalization of unpaired electrons, et al.) play an important role in determining the sign and strength of the magnetic coupling. The ability of N_3^- to promote ferromagnetic exchange interaction has been utilized in the SMM chemistry of 3d-metal ions [62–64].

We should mention here that an excellent experimental and theoretical study by Sarkar, Neese, Meyer and coworkers [65] has opened the doors for the use of the terminal azido group in 3d-metal SIM chemistry. Contrary to previous suggestions, it was shown that the N_3^- ligand behaves as a strong σ

and π donor. Magnetostructural correlations have revealed a remarkable increase in the negative D value with shortening of the axial $Co^{II}-N_{azido}$ bond lengths, i.e., with increasing Lewis basicity.

Returning to SMM chemistry, our group, in collaboration with the group of Escuer at Barcelona, have developed a general synthetic strategy for the remarkable increase of the ground-state spin in coordination clusters, which often "switches on" SMM behavior [66–69]. The strategy is based on the substitution of bridging hydroxido or alkoxido groups, which most often propagate antiferromagnetic exchange interactions, in pre-formed coordination clusters by EO azido groups which propagate ferromagnetic interactions. The core changes, but the nuclearity does not. The incoming azido groups (always EO) introduce ferromagnetic components in the superexchange scheme of the molecule and, as a consequence, the ground-state spin increases significantly, sometimes inducing SMM behavior.

The reaction between the pre-formed cluster $[Fe^{II}_9(OH)_2(O_2CMe)_8\{(py)_2C(O)_2\}_4]$ (**5**) and a slight excess of NaN_3 in refluxing MeCN under N_2 gives the corresponding azido cluster $[Fe^{II}_9(N_3)_2(O_2CMe)_8\{(py)_2C(O)_2\}_4]$ (**6**) in ~40% yield, Equation (4); $(py)_2C(O)_2^{2-}$ is the dianion of the *gem*-diol form of di-2-pyridyl ketone, $(py)_2CO$ [68,69]. The reactant and the product have similar molecular structures, the only difference being the presence of two 4.40 azido groups in the latter instead of two 4.4 hydroxido groups in the former. The nine Fe^{II} atoms in **6** adopt the topology of two square pyramids sharing a common apex. Bridging within each square base is achieved through four syn, syn 2.11 $MeCO_2^-$ ligands, four alkoxido oxygen atoms from the four 5.3311 $(py)_2C(O)_2^{2-}$ ligands (**A** in Figure 4) and one extremely rare 4.40 azido group (Figure 3). Each alkoxido oxygen is μ_3 bridging connecting two metal centers from a square base to the central Fe^{II} atom; the latter is thus 8-coordinate. The core is $\{Fe^{II}_9(4.40\text{-}N_3)_2(\mu_3\text{-}OR)_8\}^{8+}$, Figure 5. The two square bases have a slightly staggered conformation which results in a square antiprismatic coordination geometry about the central Fe^{II} atom, the chromophore being $\{Fe^{II}O_8\}$. Dc magnetic susceptibility studies in the 2–300 K temperature range indicate that the substitution of the 4.4 OH^-s in **5** by the 4.40 N_3^-s in **6** induces ferromagnetic coupling in the latter; its ground spin state is not well isolated from low-lying excited states and it cannot be accurately determined. Compound **6** is EPR silent at the X-band frequency at 4.2 K, but it is an SMM with a U_{eff} value of 29(1) cm^{-1}. The slow magnetic relaxation is also evident using zero-field ^{57}Fe Mössbauer spectroscopy.

$$[Fe^{II}_9(OH)_2(O_2CMe)_8\{(py)_2C(O)_2\}_4] + 2\,NaN_3 \xrightarrow[\Delta]{MeCN,\,N_2} [Fe^{II}_9(N_3)_2(O_2CMe)_8\{(py)_2C(O)_2\}_4] + 2\,NaOH \qquad (4)$$

Almost all the azido-bridged transition-metal clusters and SMMs contain chelating or bridging organic ligands. The presence of bridging organic ligands is usually a disadvantage because it introduces antiferromagnetic components in the superexchange scheme, thus decreasing the effect of the ferromagnetic EO azido groups. The group of Stamatatos have recently developed [70–72] a novel strategy for the synthesis of 3d-metal, EO azido-bridged coordination clusters with high-spin S values and SMM properties by avoiding the presence of any organic chelating/bridging ligand. The azido groups in the cores of the clusters are exclusively EO, which ensures the presence of ferromagnetic exchange interactions between the metal spin carriers and therefore the attainment of the maximum S value. In the presence of magnetic anisotropy, induced by the choice of the appropriate metal ion, some of the clusters also exhibit remarkable SMM properties. The peripheral ligation around the metallic core is completed by terminal, volatile MeCN ligands, whose solvation/de-solvation effects sometimes lead to interesting magnetic phenomena. The key reagent for this chemistry is Me_3SiN_3. This has some remarkable differences compared to its all-inorganic analogue, which is almost 100% used in metal–azide chemistry. Firstly, Me_3SiN_3 is more soluble in organic solvents than NaN_3, and this allows reactions to be performed in a variety of such solvents. Secondly, Me_3SiN_3 can abstract OH^- ions from the reaction media and thus bridging hydroxide ligands are not incorporated in the products; this allows the dominance of the N_3^- ions in solution which can act as ligands without competition from the OH^- species. And third, Me_3Si^+ cannot coordinate and Na^+ ions are not

incorporated in the clusters, which is often the case when NaN_3 is used as the azide source. Representative examples of this strategy are briefly mentioned below.
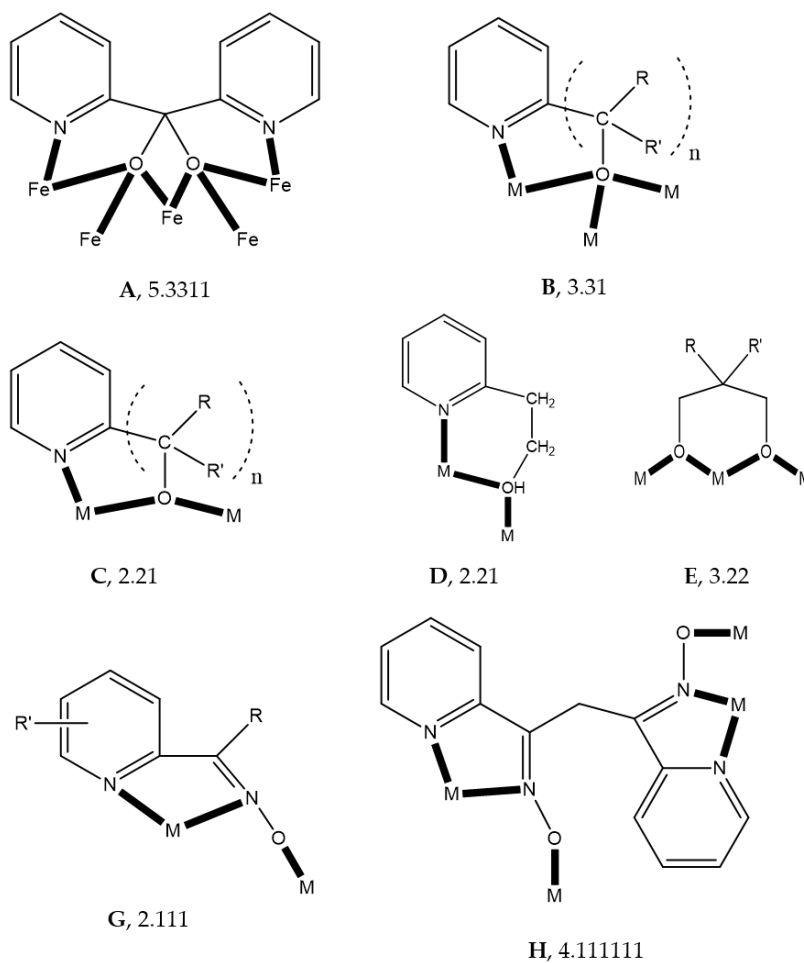

A, 5.3311

B, 3.31

C, 2.21

D, 2.21

E, 3.22

G, 2.111

H, 4.111111

Figure 4. The coordination modes of some of the ligands discussed in the text and the Harris notation that describes these modes. M = metal ion (this is specified in the cited examples); n = 1, 2.
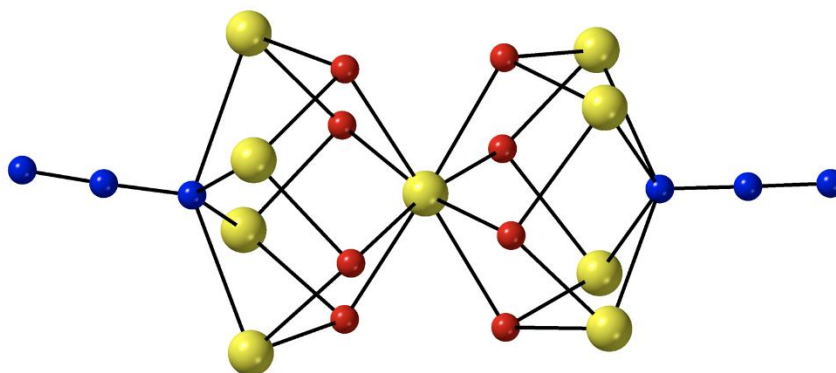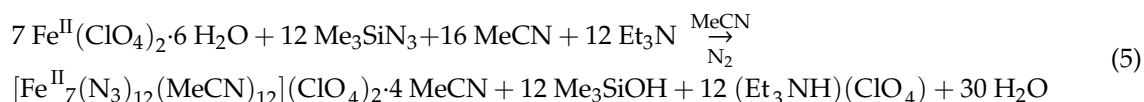

Figure 5. The $\{Fe^{II}{}_9(4.40\text{-}N_3)_2(\mu_3\text{-}OR)_8\}^{8+}$ core of cluster **6**. The Fe^{II} centers are shown in dark yellow, the nitrogen atoms in blue and the oxygen atoms are shown in red. Modified from reference [69].

The 1:1:4 reaction between $Fe^{II}(ClO_4)_2 \cdot 6H_2O$, Et_3N and Me_3SiN_3 in MeCN under N_2 gives a dark red solution from which orange crystals of $[Fe^{II}_7(N_3)_{12}(MeCN)_{12}](ClO_4)_2 \cdot 4MeCN$ (**7·4MeCN**) can be isolated in a ~55% yield, Equation (5). The crystals were treated in two ways for magnetic and spectroscopic studies [70,71]. A portion of the crystalline material was immediately transferred and sealed in an NMR tube representing the structurally characterized sample. The other portion was collected by filtration and dried under N_2 for 3 h; its analytical data corresponded to the formula $\{Fe^{II}_7(N_3)_{12}(MeCN)_2(ClO_4)_2\}$ (**7a**). The IR spectra of **7·4MeCN** and **7a** indicate the presence of the EO azido group, with the band due to the $\nu_{as}(N_3)$ mode appearing at ~2100 cm^{-1}. The almost complete de-solvation of **7·4MeCN** to give **7a** is evidenced by the nearly complete disappearance of the IR bands due to the $\nu(C\equiv N)$ mode of the MeCN molecules from the spectrum of the latter (at 2310 and 2279 cm^{-1} in the spectrum of the former).

$$7\, Fe^{II}(ClO_4)_2 \cdot 6\, H_2O + 12\, Me_3SiN_3 + 16\, MeCN + 12\, Et_3N \xrightarrow[N_2]{MeCN}$$
$$[Fe^{II}_7(N_3)_{12}(MeCN)_{12}](ClO_4)_2 \cdot 4\, MeCN + 12\, Me_3SiOH + 12\, (Et_3NH)(ClO_4) + 30\, H_2O \tag{5}$$

The heptanuclear cation that is present in the crystal structure of **7·4MeCN** (Figure 6) contains a nearly ideal planar hexagon of metal ions centered on the seventh, central Fe^{II} atom [71]. The central Fe^{II} atom is a crystallographic inversion center; the $\{Fe^{II}_7\}$ disk-like cation possesses virtual S_6 symmetry. The seven octahedral Fe^{II} atoms are held together through six 2.20 and six 3.30 EO azido groups. The six 3.30 azides connect the outer $\{Fe^{II}_6\}$ hexagon with the central metal ion, while the six 2.20 azides bridge exclusively the outer Fe^{II} centers. Peripheral ligation is completed by twelve MeCN molecules, two on each of the outer metal ions. The $\{Fe^{II}_7(3.30\text{-}N_3)_6(2.20\text{-}N_3)_6\}^{2+}$ core can also be described as consisting of six $\{Fe^{II}_3(N_3)_4\}$ defective cubane units, each double face-sharing; a vertex of each cubane unit is shared with the common vertex of the six cubanes which is the central Fe^{II} atom. The metal–nitrogen bond lengths are indicative of high-spin $(t_{2g})^4(e_g)^2$ Fe^{II} atoms with N-ligation. The intramolecular $Fe^{II} \cdots Fe^{II}$ distances are ~3.35 Å, while the Fe^{II}–N–Fe^{II} angles span the range 95.5–105°. The intermolecular $Fe^{II} \cdots Fe^{II}$ distances are large (>8 Å) due to the packing of the heptanuclear cations and to the presence of the coordinated MeCN molecules.

Both the as-synthesized (**7·4MeCN**) and dried (**7a**) forms of the complex were magnetically studied [70,71]. Dc magnetic susceptibility studies reveal the maximum possible ground-state spin ($S = 14$). Both forms are SMMs; however, their ac magnetic dynamics are different, revealing a "Janus"-faced SMM behavior for the pristine and dried samples which have been attributed to solvation/de-solvation effects from the coordinated solvent molecules. Sample **7a** exhibits two individual relaxation processes, which are both thermally assisted; the 2.7–5.0 K process is characterized by a U_{eff} value of 30.5(1) cm^{-1}, and the 1.8–2.6 K process by a U_{eff} value of 15.3(2) cm^{-1}. Data are shown in Figure 7. In contrast, the as-synthesized (pristine) sample **7·4MeCN** exhibits only one relaxation process below ~3 K with a U_{eff} value of 10.0(2) cm^{-1}. The different number of relaxation processes and the different values of effective energy barriers for magnetization reversal can be rationalized in terms of the differences in intermolecular, i.e., intercationic, interactions and the different molecular anisotropies arising from different crystal fields around the peripheral Fe^{II} atoms [71].

Complexes $[Co_7(N_3)_{12}(MeCN)_{12}](ClO_4)_2$ (**8**) and $[Ni_7(N_3)_{12}(MeCN)_{12}](ClO_4)_2$ (**9**) were prepared by a reaction similar to that used for **7·4MeCN**, simply replacing the metal perchlorate starting material [72]. The crystal structures of **8** and **9** (these complexes are isomorphous) do not contain solvent molecules in the lattice. The clusters have a similar molecular structure to its $\{Fe^{II}_7\}$ analogue. The crystals of **8** and **9** are stable at room temperature and no degradation is observed after 24 h exposure to the normal laboratory atmosphere; the static and dynamic properties of their wet- and "dried"-forms are identical for each complex. As expected, both clusters are strongly ferromagnetically coupled. The Ni(II) cluster ($S = 7$) has a negligible magnetoanisotropy and, consequently, it does not exhibit out-of-phase ac magnetic

susceptibility signals, i.e., it is not a SMM, in either the absence or the presence of an external dc field. The Co(II) cluster exhibits SMM properties under the application of a weak external dc field of 0.1 T with a U_{eff} value of 19.6(1) cm^{-1} [72]. The application of weak dc fields during the dynamic susceptibility studies helps to suppress QTM, which is otherwise strong for systems in low-symmetry crystal environments. This experimental practice is very helpful in elucidating the mechanisms operating in magnetization relaxation processes. However, the researchers should be cautious when interpreting ac susceptibility results in the presence of external dc fields; an excellent description of such a cautionary note is provided in reference [27].
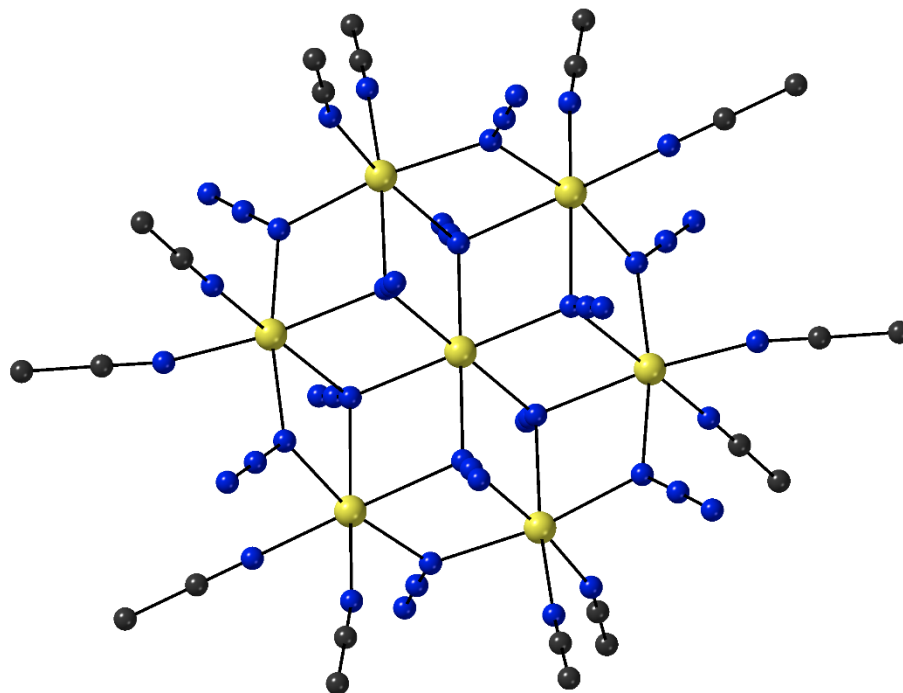

Figure 6. The molecular structure of the heptanuclear cation of cluster **7·4MeCN**. The Fe$^{\text{II}}$ centers are shown with dark yellow color, the nitrogen atoms with blue color and the carbon atoms with black color. Modified from reference [31].

The great utility of the above mentioned synthetic approach, which can potentially stimulate the research in transition-metal azido chemistry to meet new directions, is demonstrated by the 2-nm-sized spherical cluster $[\text{Mn}_{29}\text{O}_{24}(\text{N}_3)_{10}(\text{dma})_{28}]$ (**10**) [73], where dma is the 3,3-dimethylacrylate(−1) ligand. The cluster contains a $\{\text{Mn}^{\text{II}}\text{Mn}^{\text{III}}_{28}(4.4\text{-O})_8(3.3\text{-O})_{16}(4.40\text{-N}_3)_2(2.20\text{-N}_3)_8\}^{28+}$ core, and has an $S = 9/2$ ground state. Despite the appreciable number of EO azido groups, the complex is not an SMM due to the simultaneous presence of bridging oxido and carboxylato groups, which promote antiferromagnetic exchange interactions and "force" the Mn–N$_{\text{azido}}$–Mn angles to be rather large (average 111.4°) presaging antiferromagnetic interactions between the respective azido-bridged metal ions.
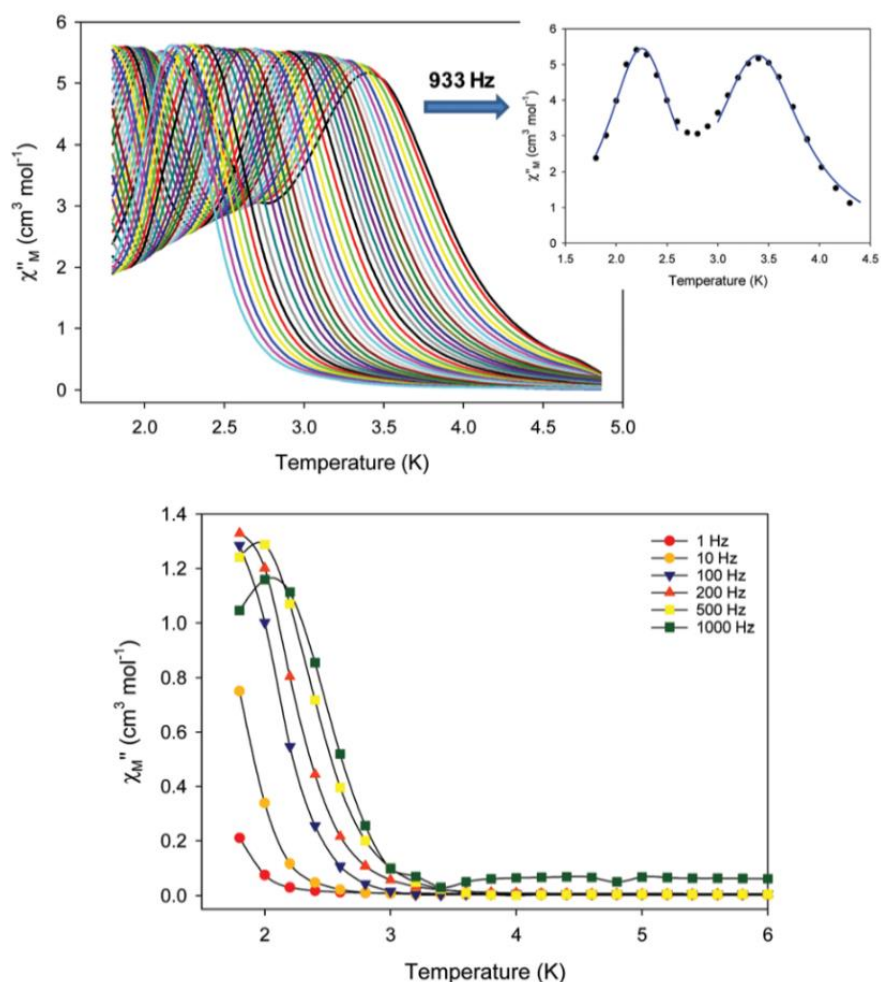
Figure 7. (Top) Out-of-phase (χ''_M) ac molar magnetic susceptibility signals for **7a**. The inset shows the χ''_M vs. *T* plot at the representative ac frequency of 933 Hz revealing the two separation relaxation processes in two different *T* regions for the sample; the solid blue lines are the fits of the data. (Bottom) Frequency dependent χ''_M signals of **7**·4MeCN. Reproduced from reference [70] with permission from the Royal Society of Chemistry.

5. Cyanido-Directed Assembly of Transition-Metal SMMs

Many transition-metal SMMs contain hydroxido (OH^-), alkoxido-type (RO^-) or oxido (O^{2-}) bridging groups. The problem is that the oxygen atom can bridge two or more (up to six with the O^{2-} ligand) metal centers, with a wide variety of M–O–M angles. Since the pairwise magnetic exchange interactions (which should be ferromagnetic and strong for an efficient SMM) are very sensitive to the bridging angles (and more generally to local geometry), chemists cannot often predict the magnetic properties of a complex structure. As a consequence, the search for new metal–hydroxido/alkoxido/oxido SMMs remains a rather serendipitous effort. The "good news" is that there is an alternative small-sized inorganic bridging ligand which might overcome the aforementioned difficulty. This is the cyanide (CN^-) group. Given that Prussian Blue, $Fe^{III}_4[Fe^{II}(CN)_6]_3 \cdot xH_2O$ ($x = 14$–16), the first coordination complex and the first molecule-based magnetic solid was discovered in 1704 by the painter Diesbach in Berlin, it is amazing that after more than 300 years the CN^- ion is in the forefront of coordination chemistry and

molecular magnetism [74]. Perhaps, Andreas Ludi, who called Prussian Blue "An Inorganic Evergreen" in an article written in 1981, was more visionary when he gave this nickname [75].

The preference of CN^- for binding just two metal sites, one at each end, leading to a linear bridging arrangement is well established in inorganic chemistry. Thus, solution assembly reactions can be designed with the expectation that the product will possess linear M–CN–M′ groups, thus providing synthetic chemists with a degree of synthetic and structural control [58]. In addition, because of the linear bridging arrangement, there is a satisfactory level of predictability in the expected nature of the magnetic exchange coupling between octahedral M and M′ spin carriers. Unpaired spin density from orthogonal metal-based orbitals (t_{2g} + e_g) will leak over into orthogonal CN^--based orbitals, leading to ferromagnetic exchange via Hund's rule. On the contrary, the unpaired spin density from metal-based orbitals of compatible symmetry (t_{2g} + t_{2g} or e_g + e_g) will leak over into the same cyanide-based orbitals, leading to antiferromagnetic exchange via Pauli exclusion principle. The antiferromagnetic exchange interactions are generally stronger and tend to dominate the superexchange in a competitive coupling scheme. Such predictions are useful in the design of cyanido-bridged clusters with high values of the ground-state spin [21,55,58].
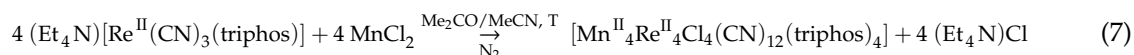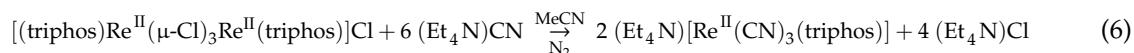
Metal–cyanido chemistry can rather easily lead to molecules with high-spin ground states [21,58]. The difficult problem is to introduce axial magnetic anisotropy in these systems, i.e., negative *D*. The incorporation of metal centers that have a large single-ion anisotropy is a good first step in obtaining large *D* values in a cluster. The anisotropy of an individual metal ion is determined by the coupling between its spin angular momentum and its orbital angular momentum. Thus, metal ions with orbitally degenerate ground states are expected to have a large zero-field splitting and would be appropriate for incorporation in SMMs. This is, for example, the case in **1** (Figure 1) where the outer Mn^{III} atoms, with a $t_{2g}^3 e_g^1$ configuration contribute much to the anisotropy barrier. Thus, there are two approaches for instilling magnetic anisotropy in metal–cyanido clusters. The first one is to utilize metal ions already known to give hydroxido-, alkoxido- and/or oxido-bridged 3d-metal SMMs, e.g., V^{III}, high-spin Mn^{III}, high-spin Co^{II}, etc. Such high-spin configurations are obtained easily with O-based donors; however, low-spin configurations often occur in metal–cyanido clusters and certain of these (with orbital degeneracy) may be particularly effective. The second approach is to utilize 4d- and 5d-metal ions. Because of the relativistic nature of the spin-orbit coupling phenomenon (which is a source of magnetic anisotropy), this will generally result in significant increase of single-ion anisotropy for heavier transition-metal ions. For example, replacement the Cr^{III} atoms in known cyanide clusters with Mo^{III} atoms can lead to clusters with enhanced magnetic anisotropy while preserving the ground-state spin [58]. Of particular importance in this context is that theory has predicted that single-ion anisotropy originating from spin-orbit coupling will give SMMs with higher T_B values [76].

Based on the facts mentioned above, the main method for synthesizing cyanido-based homo- and, especially, heterometallic transition-metal SMMs is a building-block approach, often called modular process or "complexes as ligands and complexes as metal ions" strategy. A typical cluster preparation involves two building units. One bears one or more coordination sites occupied by labile (loosely coordinated) solvent molecules (the "metal ion") and the other is a complex that possesses one or more terminal cyanido ligands (the "metalloligand") [21,55,58,77–85]. In solution, the nucleophilic "free" nitrogen atoms of the terminal cyanido ligands displace the labile solvent molecules, leading to dinuclear or polynuclear assemblies. An important synthetic parameter is the nature and denticity of the capping (chelating) ligands for either of the two building units (precursors); these characteristics often control the nuclearity of the product. The "metal ion" in this building-block approach can also be a simple metal "salt" without a capping ligand and/or labile solvent molecules. In addition to this structural control, there are available qualitative rules for predicting the nature and the strength of the magnetic exchange interaction between the cyanido-bridged metal spin carriers established via detailed studies on hundreds of Prussian

Blue analogues [15,21,58,86]. This fruitful combination of structural and magnetic predictability has led to the rational design, synthesis and study of many cyanido-bridged SMMs.

A significant advantage of transition metal–cyanido cluster chemistry is that once a stable new structural motif is identified, the researcher can be confident that she/he can replace some metal ions with certain other metal ions in the structure [58].

After this, rather long, introduction we proceed with few representative examples. The metalloligand $(Et_4N)[Re^{II}(CN)_3(triphos)]$, where triphos is the bulky tridentate phosphine 1,1,1-tris(diphenylphosphinomethyl)ethane (Figure 8a), was prepared by Dunbar's group. Direct reaction of $[(triphos)Re^{II}(\mu-Cl)_3Re^{II}(triphos)]Cl$ with 6 equivs of $(Et_4N)CN$ in MeCN leads to homolytic scission of the $\{Re^{II}\equiv Re^{II}\}^{4+}$ unit to give the bright yellow precursor metalloligand, Equation (6), in ~35% yield [87]. The coordination geometry of Re^{II} in the mononuclear anion is *fac* pseudo-octahedral; three coordination sites are occupied by the C-bonded cyanido ligands, while the other three sites are filled by the P atoms of the tridentate chelating triphos ligand. Mononuclear 17-electron complexes of Re(II) are attractive in molecular magnetism due to strong spin-orbit coupling effects ($\lambda = 2000–3000$ cm^{-1}) arising from the low-spin 5d^5 configuration. The 1:1 reaction between $(Et_4N)[Re^{II}(CN)_3(triphos)]$ and anhydrous $MnCl_2$ in Me_2CO/MeCN under reflux gives the orange-red cluster $[Mn^{II}_4Re^{II}_4Cl_4(CN)_{12}(triphos)_4]$ (**11**), Equation (7). The octanuclear molecule has an approximate cubic topology (Figure 8b) [78,79] with alternating octahedral Re^{II} and tetrahedral Mn^{II} concerns. The edges of the cube are spanned by the 12 bridging cyanido groups (Re^{II}–CN–Mn^{II}) that link the metal ions. The coordination geometry around the Re^{II} atoms is similar to that of the mononuclear starting metalloligand, i.e., distorted octahedral with the triphos ligand behaving as a facially capping, tridentate chelating ligand with the carbon end of the three cyanido ligands completing the coordination sphere. The Mn^{II} centers adopt a distorted tetrahedral geometry, the donor atoms for each metal ion being three coordinated nitrogen atoms from bridging cyanido groups and a fourth terminal chlorido ligand extending out of the cube. It is obvious that the steric bulk of the triphos ligands enforces the distorted tetrahedral coordination environments at each of the 3d-metal sites. The structurally similar cubic complexes $[Mn^{II}_4Re^{II}_4I_4(CN)_{12}(triphos)_4]$ (**12a**) and $[M^{II}_4Re^{II}_4Cl_4(CN)_{12}(triphos)_4]$ (M = Fe, **12b**; M = Co, **12c**; M = Ni, **12d**; M = Zn, **12e**) have also been prepared through analogous reactions [79]. Variable-temperature dc magnetic susceptibility data for **11** indicate antiferromagnetic coupling between the "*S* = 1/2" Re^{II} and *S* = 5/2 Mn^{II} atoms. The complex is a weak SMM with a U_{eff} value of ~9 cm^{-1}. Micro-SQUID temperature-dependent scans reveal hysteretic behavior for the cluster. The data also show a prominent step at zero field, resulting from fast QTM. The step becomes temperature-independent below 0.2 K but remains sweep rate-dependent, suggesting a ground-state resonant tunneling process at $H = 0$ [79].

$$[(triphos)Re^{II}(\mu-Cl)_3Re^{II}(triphos)]Cl + 6\,(Et_4N)CN \xrightarrow[N_2]{MeCN} 2\,(Et_4N)[Re^{II}(CN)_3(triphos)] + 4\,(Et_4N)Cl \qquad (6)$$

$$4\,(Et_4N)[Re^{II}(CN)_3(triphos)] + 4\,MnCl_2 \xrightarrow[N_2]{Me_2CO/MeCN,\,T} [Mn^{II}_4Re^{II}_4Cl_4(CN)_{12}(triphos)_4] + 4\,(Et_4N)Cl \qquad (7)$$

Staying at Re, an interesting metalloligand is $[Re^{IV}(CN)_7]^{3-}$, which was prepared by Long's group through a simple ligand metathesis reaction [88], Equation (8). This anion has a low-spin 5d^3 pentagonal bipyramidal geometry. The complex has a strong magnetic anisotropy which can be attributed to a combination of its large spin-orbit coupling associated with the heavy rhenium ion and the unquenched orbital angular momentum of its $^2E_1'$ electronic ground state. Thus, the incorporation of $[Re^{IV}(CN)_7]^{3-}$ into a high-spin coordination cluster would "transfer" magnetic anisotropy to the product, possibly leading to slow magnetic relaxation. Complex $[Mn^{II}(PY5Me_2)(MeCN)](PF_6)_2$ is an ideal "metal ion" for a building-block reaction for three reasons: (i) The Mn^{II} ion has 5 unpaired electrons; (ii) the six-coordinate cation possesses a labile MeCN molecule; and (iii) the potentially pentadentate

chelating ligand 2,6-bis(1,1-bis(2-pyridyl)ethyl)pyridine ligand (PY5Me$_2$, Figure 9a) is an efficient capping moiety which can ensure the formation of star-like clusters that are magnetically isolated. Reaction of $(Bu^n_4N)_3[Re^{IV}(CN)_7]$ with 4 equivs of $[Mn^{II}(PY5Me_2)(MeCN)](PF_6)_2$ in MeCN at −40 °C produces a blue solution from which the blue, temperature-sensitive cluster $[Mn^{II}_4Re^{IV}(CN)_7(PY5Me_2)_4](PF_6)_5$ (**13**) is isolated in a good yield, Equation (9). If the same reaction is performed at room temperature, an immediate color change from blue to green and then to yellow is observed affording complex $[Mn^{II}_4Re^{III}(CN)_7(PY5Me_2)_4](PF_6)_4$ (**13a**); this complex is formed via a spontaneous reduction of Re^{IV} ($S = 1/2$) to Re^{III} ($S = 0$) within the cluster [80].

$$(Bu^n_4N)_2[Re^{IV}Cl_6] + 7\ (Bu^n_4N)CN\ \xrightarrow[\text{3 days, N}_2]{\text{DMF, 85 °C}}\ (Bu^n_4N)_3[Re^{IV}(CN)_7] + 6\ (Bu^n_4N)Cl \tag{8}$$

$$(Bu^n_4N)_3[Re^{IV}(CN)_7] + 4\ [Mn^{II}(PY5Me_2)(MeCN)](PF_6)_2\ \xrightarrow[\text{N}_2]{\text{MeCN, −40 °C}}$$
$$[Mn^{II}_4Re^{IV}(CN)_7((PY5Me_2)_4](PF_6)_5 + 3\ (Bu^n_4N)(PF_6) + 4\ MeCN \tag{9}$$
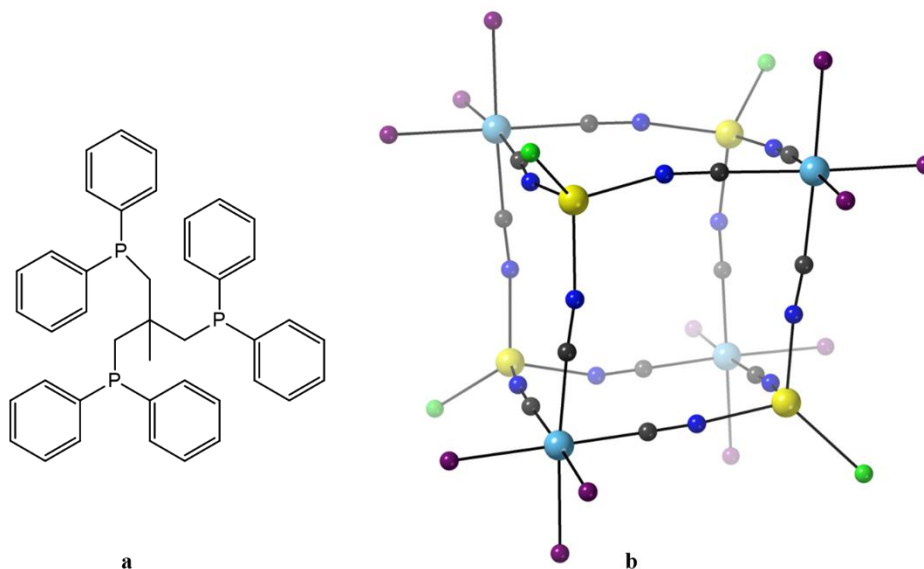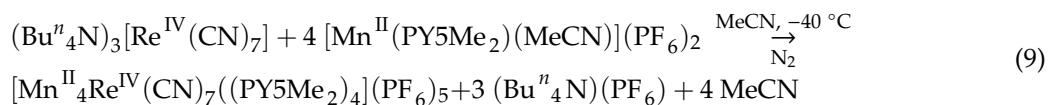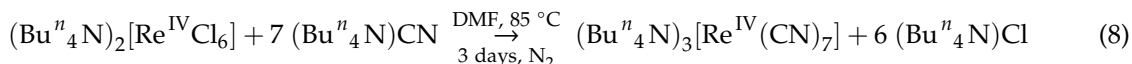

Figure 8. (**a**) The structural formula of triphos. (**b**) An aspect of the molecular structure of the cubic cluster **11**; only the P atoms of the tridentate chelating phosphine triphos have been drawn. The Re^{II}, Mn^{II}, Cl$^-$, N, C and P atoms/ions are shown with turquoise, yellow, green, blue, gray and mauve colors, respectively. Modified from reference [78].

X-ray analysis on single crystals of **13** reveals the presence of a four-point star-like topology for the cation of the complex, as shown in Figure 9. The $[Re^{IV}(CN)_7]^{3-}$ unit is at the center of the star and is bridged through cyanido groups to four $\{Mn^{II}(PY5Me_2)\}^{2+}$ pendant units; three cyanido ligands remain terminal at the central Re^{IV} atom. The coordination polyhedron of the 5d-metal ion is close to that of an ideal pentagonal bipyramid, with an essential liner axial C_{ax}–Re^{IV}–C_{ax} angle of 179.9°. The arrangement of the four 3d-metal ions can be described as a square, with two of the Mn^{II} atoms binding axial cyanido groups of Re^{IV} and the other two binding non-neighboring equatorial cyanido groups of Re^{IV}. The magnetic exchange interactions between the central Re^{IV} atom ($S = 1/2$) and the surrounding Mn^{II} centers ($S = 5/2$ each) are ferromagnetic, resulting in a high-spin ground state (most probably 21/2). The high-spin ground state of the cluster, combined with the negative D value of −0.44 cm^{-1} gives SMM properties in **13** with an effective

relaxation barrier of U_{eff} = 33 cm^{-1} [80]. Analogous reaction schemes lead to structurally similar clusters [M$^{II}_4$Re^{IV}(CN)$_7$(PY5Me$_2$)$_4$](PF$_6$)$_5$ (M = Ni, **13b**; M = Cu, **13c**), which are also SMMs with U_{eff} values of ~17 and ~8 cm^{-1}, respectively [81]; the D values are −0.93 cm^{-1} (**13b**) and −1.33 cm^{-1} (**13c**), the corresponding S values being 9/2 and 5/2.
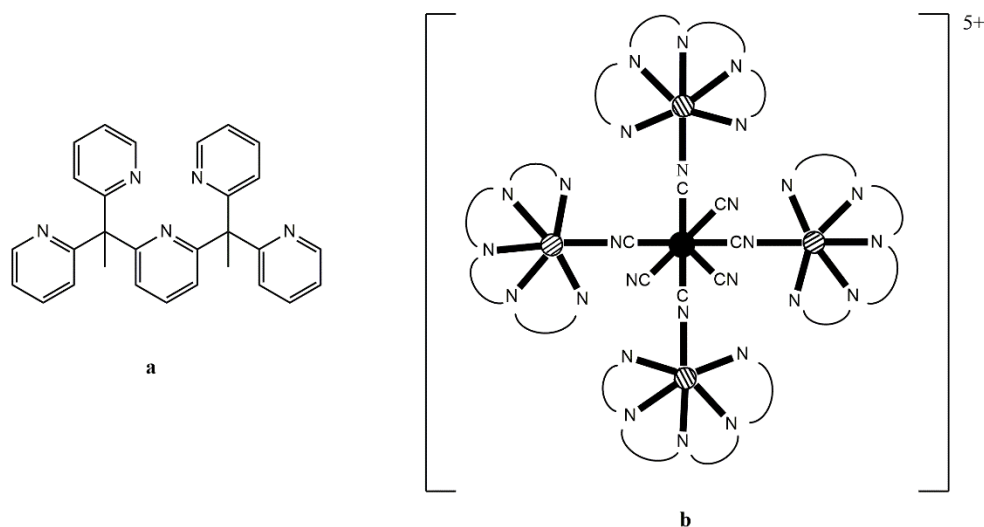

Figure 9. (**a**) The structural formula of the "open" pentadentate ligand PY5Me$_2$. (**b**) Schematic drawing of the molecular structure of the pentanuclear {Mn$^{II}_4$Re^{IV}} cation that is present in **13**; the solid circle represents the Re^{IV} atom, the semi-dashed circles represent the Mn^{II} atoms and N^N^N^N^N represents the pentadentate chelating ligand PY5Me$_2$, while the coordination bonds are drawn with bold lines.

Today the cyanido ligand is one of the most popular ligands in SMM chemistry [21,85], because of the variety of metalloligands that are available. For example, octacyanidometallates are unique building blocks that are useful in the construction of various types of magnetic clusters with topologies ranging from square, trigonal bipyramidal, octahedral, to pentadecanuclear six-capped-body-centered cubes and even larger molecules, some of which are SMMs [85].
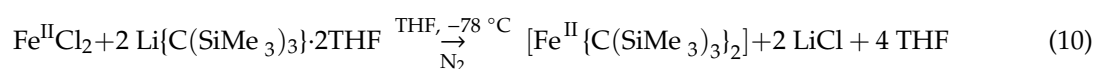
6. Tris(trimethylsilyl)methanide, an Old Organometallic "Friend" Joins the Chemistry of 3d-Metal SIMs

Several groups around the world re-investigate the magnetic anisotropies of complexes based on transition-metal ions in a general effort to find magnetic alternatives to the f-block metal ions. As it has already been mentioned in Section 1, mononuclear transition metal–ion complexes are not good candidates for large U_{eff} values because of their smaller magnetic moments and, for the 3d-metal ions, lower spin-orbit coupling constants. Also, the larger ligand-field splitting energies of the d orbitals lower the orbital contributions to the magnetic properties required to develop significant magnetic anisotropy. There are two manifestations of this effect: (i) The first-order orbital angular momentum can be quenched as the result of a Jahn–Teller distortion; and (ii) the second-order contribution to the magnetic anisotropy, i.e., the zero-field splitting, is becoming very small due to the large energy separation between ground and excited electronic states, which reduces the degree of mixing. These ligand-field effects can become much less important by synthesizing transition metal–ion complexes with very low coordination numbers [27]. In this way, the ligand-field splitting energies of the d orbitals fall within a narrow range, similar to the energies of the 4f orbitals in Ln(III) complexes. A linear two-coordinate geometry at the metal center is ideal for suppressing ligand-field effects in 3d-metal complexes and generating a large anisotropy barrier. For a strictly linear coordination geometry, with a local D$_{\infty h}$ symmetry at the metal ion, the energies of the

d orbitals are split as $(d_{xy}, d_{x^2-y^2}) < (d_{xz}, d_{yz}) < d_{z^2}$ (these relative energies do not consider the possibility of s-d_{z^2} mixing, which is known to lower the energy of d_{z^2} below that of the d_{xy}, d_{yz} pair), with the d_{z^2} and (d_{xz}, d_{yz}) orbital energies being destabilized by σ- and π-metal–ligand interactions, respectively; on the contrary, the $(d_{xy}, d_{x^2-y^2})$ orbitals have δ symmetry and are thus not participating in bonding with the ligands' orbitals. A high-spin $3d^6$ electron configuration is expected to give a large first-order contribution to orbital angular momentum that will not be quenched through a Jahn–Teller distortion; this maximizes the magnetic moment and the two donor atoms define an axis for its easy alignment [89].

One of the ligands that has played an important role in the chemistry of two-coordinate 3d-metal SIMs is the tris(trimethylsilyl)methanide, $^-C(SiMe_3)_3$. The neutral compound $HC(SiMe_3)_3$ and its conjugate base have their own history in organic [90,91] and organometallic [92,93] chemistry, respectively. The tris(trimethylsilyl)methanide ('trisyl') anion has been used as a very bulky ligand in main group and Ln(III) chemistry. The advantages of this group are numerous: (a) Due to its bulkiness, it can lead to very low coordination numbers and stabilize coordinatively unsaturated transition-metal complexes which often exhibit unusual structural features or exciting reactivity; (b) its steric bulk-which is estimated to be similar to that of Cp* anion or P(^{t}Bu)$_3$-confers kinetic stability to complexes; and (c) it lacks α-and β-hydrogens prohibiting undesired reactivity. In a sense, it may be viewed as combining the electronic features of a methyl anion and the steric requirements of the Cp* anion [93].

Complex $[Fe^{II}\{C(SiMe_3)_3\}_2]$ (**14**) was synthesized [93,94] by the reaction illustrated in Equation (10). $Li\{C(SiMe_3)_3\}·2THF$ can be prepared by the metallation of tris(trimethylsilyl)methane with MeLi in THF/Et$_2$O under reflux [92]. The two-coordinate Fe^{II} center sits on a crystallographic inversion center, resulting in a strictly linear geometry (C–Fe^{II}–C = 180.0°). Variable-temperature dc magnetic susceptibility data indicate a high-spin $3d^6$ Fe^{II} center ($t_{2g}^4 e_g^2$). Low-temperature magnetization data show a saturation value of 3.24 B.M.; this value is lower than 4 B.M. that would be expected for a spin-only $S = 2$ center. The results from the dc susceptibility and magnetization data indicate that **14** has a highly anisotropic magnetic moment. Both data sets could not be fit, suggesting that the magnetic anisotropy of the molecule is not due to spin-only phenomena [94]. Ac susceptibility data reveal slow magnetic relaxation under an external dc field. Arrhenius plots for the linear complex were fit by employing a sum of tunneling, direct, Raman and Orbach relaxations, resulting in a U_{eff} value of ~146 cm^{-1}. Theoretical calculations (CASSCF/NEVPT2 on the crystal structure) were performed to explore the influence of deviation from rigorous D$_{\infty h}$ geometry on the splittings of the 3d orbitals and the electronic state energies. The calculations suggest that the ligand field asymmetry quenches the orbital angular momentum of **14**, but finally spin-orbit coupling is strong enough to compensate and regenerate the orbital moment. The non-observation of a single Arrhenius behavior has been attributed to a combination of the asymmetry of the ligand field and the influence of vibronic coupling.

$$Fe^{II}Cl_2 + 2\,Li\{C(SiMe_3)_3\}·2THF \xrightarrow[\text{N}_2]{\text{THF, }-78\,°C} [Fe^{II}\{C(SiMe_3)_3\}_2] + 2\,LiCl + 4\,THF \qquad (10)$$

The observation of slow magnetic relaxation in **14**, and related mononuclear two-coordinate Fe(II) complexes, requires the application of an applied dc field which suppress fast magnetization reversal through QTM; the latter is very efficient for such systems because of the small non-Kramers $S = 2$ ground state prohibiting slow relaxation in zero magnetic field [27]. An alternative way to minimize tunneling of the magnetic moment, caused by mixing of the ground-state ± M_S levels, is employment of half-integer spin systems, according to the Kramers' theorem [95]. Such systems should not require the application of a dc field to display slow magnetic relaxation. The group of Long reported the structurally interesting and magnetically impressive two-coordinate SIM $[K(crypt-222)][Fe^I\{C(SiMe_3)_3\}_2]$ (**15**), which possesses a $S = 3/2$ ground state [96]; crypt is the ligand 4,7,13,16,21,24-hexaoxa-1,10-diazabicyclo[8,8,8]-hexacosane,

which chelates the K^+ ion though its six ether oxygen atoms. The synthesis of **15** was achieved by the one-electron reduction of **14** using KC_8 as reductant, Equation (11). The possibility of the one-electron reduction of the Fe(II) complex had been recognized by cyclic voltammetry studies in difluorobenzene, which show a reversible process corresponding to the $[Fe\{C(SiMe_3)_3\}_2]^{0/-1}$ couple. The product is obtained in yields of ~50% and has a bright yellow-green color. Single-crystal X-ray crystallography reveals a linear geometry around Fe^I (Figure 10a), the $C–Fe^I–C$ bond angle being 179.2°. The $SiMe_3$ groups are eclipsed, contrary to the structure of **14**, in which they are staggered. Complex **15** not only shows, as expected, one of the highest U_{eff} values [226(4) cm^{-1}] yet reported for SMMs and SIMs that contain transition-metal ions, magnetic hysteresis below 29 K and a T_B value of 4.5 K, but also has improved permanency in zero field [96,97]; the U_{eff} value starts to approach values that we meet in Ln(III)-based systems. Quantum-chemical and spectroscopic studies suggest an electronic structure (Figure 10b), which would not be expected by most coordination chemists. The theoreticians in the research team provided strong evidence that strong $4s$-$3d_z{}^2$ mixing stabilizes the $3d_z{}^2$ orbital. The result is supported by advanced spectroscopic characterization, and the calculated orbital degeneracies explain well the unquenched orbital moment. The U_{eff} value is close to the calculated energy gap between the ground $M_J = 7/2$ pair and the first excited $M_J = 5/2$ doublet, suggesting that the relaxation occurs via this latter state. Excellent ^{57}Fe-Mössbauer studies of **14** and **15** under zero applied dc field between 295 and 5 K yield their magnetization dynamics on a significantly faster time scale (the lifetime of the measurement is 10^{-8} to 10^{-9} s) than it is possible with ac magnetometry. From the modeling of the Mössbauer profiles, Arrhenius plots between 295 and 5 K were obtained for the two complexes [98]. The high-temperature regimes suggest Orbach relaxation with U_{eff} values of 178(9) (**14**) and 246(3) (**15**) cm^{-1}, in good agreement with the values obtained from magnetism. In **15**, two distinct high-temperature regimes of magnetic relaxation are observed with mechanisms corresponding to two distinct single-excitation Orbach processes within the ground-state spin–orbit coupled manifold of the Fe^I atom.

$$[Fe^{II}\{C(SiMe_3)_3\}_2] + KC_8 + crypt\text{-}222 \xrightarrow[N_2]{THF} [K(crypt\text{-}222)][Fe^I\{C(SiMe_3)_3\}_2] + 8\,C \tag{11}$$

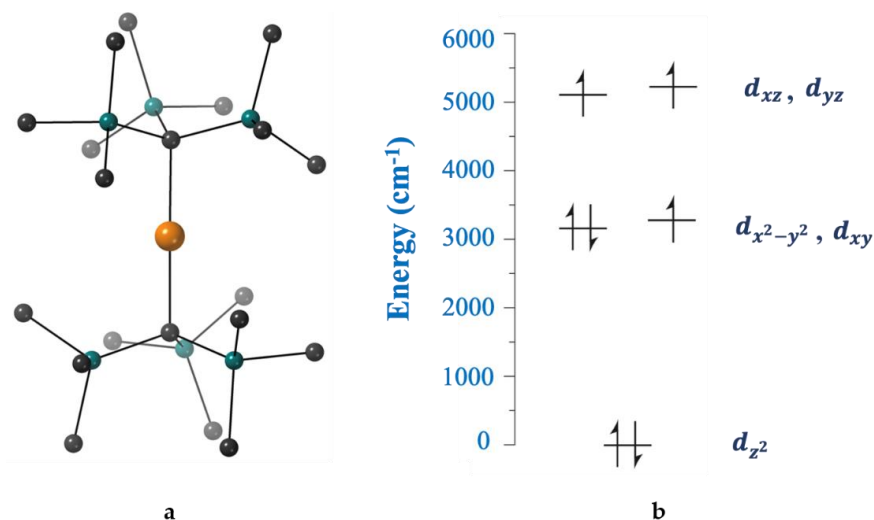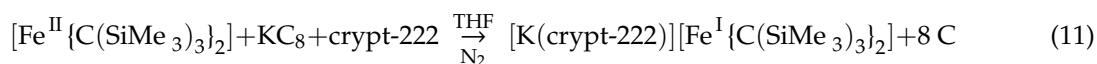**Figure 10.** (**a**) The molecular structure of the anion that is present in **15**. (**b**) Energy splitting of the 3d orbitals of $[Fe^I\{C(SiMe_3)_3\}_2]^-$ derived from an ab initio computational analysis; this orbital scheme is the origin of a strong magnetic moment along the z axis. Color code: Fe dark orange, Si turquoise, C black. H atoms have been omitted for clarity. Modified from reference [96].

　　It has become clear from the preceding information that orbital angular momentum L gives rise to magnetic anisotropy, an essential property for efficient SIMs. Unquenched L arises from an odd number of electrons in degenerate orbitals; this is observed only for free ions and in f-element complexes. In transition-metal complexes, however, the ligand field removes any orbital degeneracy, leading to practically zero L. Any magnetic anisotropy in such complexes is a weak effect arising from mixing of the electronic ground state and excited states induced by spin–orbit coupling. The maximum value L for a transition metal is 3 and, at first glance, it seems impossible. An $L = 3$ ground state in a linear complex requires two sets of degenerate orbitals, $(d_{x^2-y^2}, d_{xy})$ with $m_l = \pm 2$ and (d_{xz}, d_{yz}) with $m_l = \pm 1$, and an odd number of electrons in each. Such a system would imply a non-Aufbau configuration, wherein the electrons do not fill the d orbitals in the usual manner from lowest to highest energy, and likely exhibit a large magnetic anisotropy. Having as scientific arsenal: (A) The previous characterization of **15** with unquenched orbital angular momentum, large mangetic anisotropy and non-influence by Jahn–Teller distortions that would otherwise remove orbital degeneracy. (B) Experiments which have shown that Co atoms, deposited on a MgO surface under vacuum (referred to as adatoms) and adopting a coordination number of 1, have a $J = 9/2$ ($S = 3/2$, $L = 3$) ground state giving rise to near-maximal magnetic anisotropy [99]; and (C) Calculations on the hypothetical complex $[Co^{II}\{C(SiMe_3)_3\}_2]$ which have shown an $L = 3$ ground state arising from a non-Aufbau $(d_{x^2-y^2}, d_{xy})^3, (d_{xz}, d_{yz})^3 (d_{z^2})^1$ filling of the 3d orbitals and further predicting a gap of ~455 cm^{-1} between ground and first excited M_J states [100], a mutli-national research team led by Long, Neese and van Slageren set out efforts to synthesize and characterize $[Co^{II}\{C(SiMe_3)_3\}_2]$, i.e., the 3d^7 analogue of **14**.

　　The strongly reducing nature of the carbanion ligand $^-C(SiMe_3)_3$ hinders isolation of the desired compound [101]. Metathesis reactions of $\{C(SiMe)_3\}^-$ salts and CoX_2 (X = Cl, Br, I) gave only amorphous solids that could not be characterized. However, lowering the basicity of the central carbanion through the introduction of electron-withdrawing aryloxide groups provided access to the dialkyl complex $[Co^{II}\{C(SiMe_2ONaph)_3\}_2]$ (**16**), where Naph is the naphthyl group. The synthetic process is illustrated in Figure 11. The Zn(II) congener, $[Zn\{C(SiMe_2ONaph)_3\}_2]$ (**16a**) was obtained in an analogous manner. Using the same reaction conditions with a mixture of $ZnBr_2$ and $CoBr_2 \cdot THF$ (molar ratio ~900:1) enabled the preparation of the magnetically dilute sample $Co_{0.02}Zn_{0.98}\{C(SiMe_2ONaph)_3\}_2$ [101].
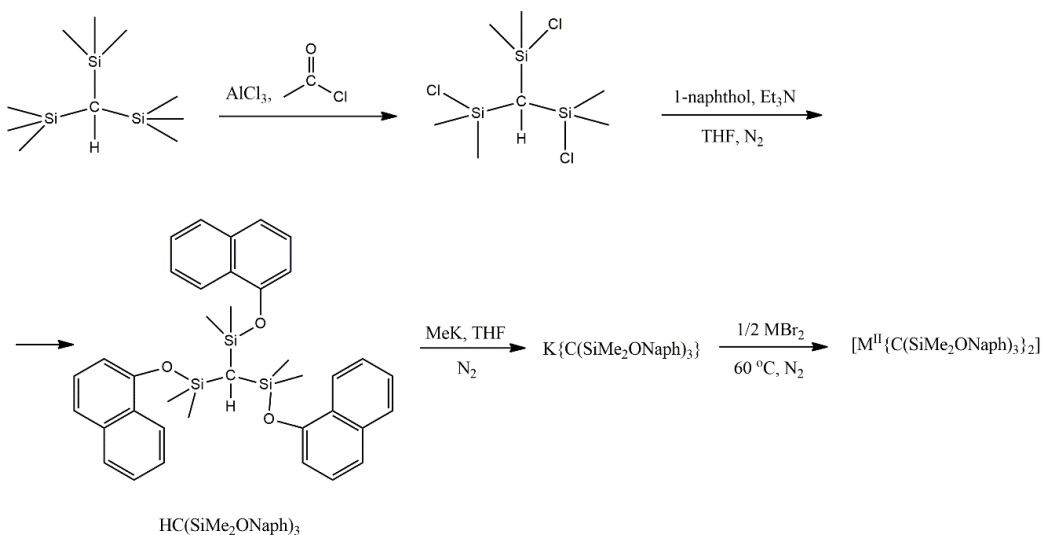

Figure 11. Synthetic scheme for the ligand HC(SiMe$_2$ONaph)$_3$ and preparation of the linear Co(II) and Zn(II) dialkyl compounds **16** and **16a**, M = Co, Zn.

Complexes **16** and **16a** are isomorphous and feature a linear C–M^{II}–C axis imposed by the S$_6$ site symmetry. The staggered orientation of the ligands facilitates close sp^3–CH···π and sp^2–CH···π contacts (2.69 and 2.82 Å, respectively). This indicates that interligand interactions contribute into the stabilization of the structures [101]. Ab initio calculations on **16** predict a ground state with $S = 3/2$, $L = 3$ and $J = 9/2$ which arises from the non-Aufbau electron configuration (d$_x{}^2{}_{-y}{}^2$, d$_{xy}$)^3(d$_{xz}$, d$_{yz}$)^3(d$_z{}^2$)^1, Figure 12; this deviates from the expected Aufbau filling of (d$_x{}^2{}_{-y}{}^2$, d$_{xy}$)^4(d$_{xz}$, d$_{yz}$)^2(d$_z{}^2$)^1. This deviation can be explained in terms of the competing effects of ligand-field stabilization and interelectron repulsion. As for Ln(III) complexes, the ligand field is weak so that interelectron repulsion and spin–orbit coupling determine the electronic ground state. Dc magnetic susceptibility results reveal a well-isolated $M_J = \pm 9/2$ ground state. Variable-field far-infrared spectra suggest a magnetically active excited state at ~450 cm^{-1} that, together with variable-temperature ac susceptometry and theoretical calculations, has assigned to the $M_J = \pm 7/2$ state. A d-orbital filling scheme with equally occupied of (d$_x{}^2{}_{-y}{}^2$, d$_{xy}$) and (d$_{xz}$, d$_{yz}$) orbital sets is also indicated by modeling of experimental charge density maps. The U_{eff} barrier of ~450 cm^{-1} determined for **16** is the largest reported to date for a transition-metal SMM or SIM. As a consequence of its large orbital angular momentum, the magnetically dilute sample Co$_{0.02}$Zn$_{0.98}${C(SiMe$_2$ONaph)$_3$}$_2$ exhibits a coercive field of 600 Oe at 1.8 K. Although its magnetic properties mainly pertain at very low temperature, the synthesis, structure and properties of **16** provide scientists with a valuable, general design principle [101].
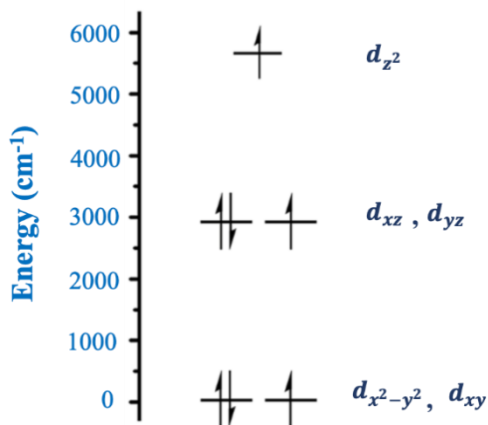

Figure 12. Energy diagram and occupations of the 3d orbitals by electrons in the linear complex **16**. Modified from reference [101].

7. Softer Ligands for More Efficient SIMs

The main advantage of transition-metal SIM chemistry is that the ground-state spin of the mononuclear molecule is fixed and D is the only parameter that affects U_{eff}. As we have seen, the orbital angular momentum is the main factor that dictates the magnitude of D; the former depends on the oxidation state and the coordination number/geometry of the 3d-metal ion (for first-row transition metals). Thus, scientists can fine-tune the electronic structure of the complex by playing with the oxidation state and the geometry of the metal ion. The classical approach involves the lowering of the coordination number which provides the system with a large orbital angular momentum resulting in high U_{eff} values [94,96,101,102]. In addition to this approach, several efforts have been performed to alter the spin Hamiltonian parameters of various metal ions by other methods [103]. Slow magnetization relaxation is normally not observed in integer-spin systems, even under application of external dc magnetic fields, because of underbarrier tunneling mechanisms. As a consequence of this, the interest has focused on non-integer spin systems for

a better design of SIMs. Cobalt is a good candidate for efficient SIMs due to strong first-order spin-orbit coupling displayed by the metal in its high-spin +II oxidation state [26,27]; this is particularly so in pseudotetrahedral symmetry. Several parameters can potentially be employed to stabilize easy-axis (or Ising-type) magnetic anisotropy including the softness (HSAB) of the donor atoms (and hence the Co^{II}–ligand covalency), the influence of the other commonly used coligands (e.g., halides) and the variation of the counter cation in anionic complexes. Representative examples are briefly described below.

The first transition-metal SIM without requiring the application of an external dc field to suppress quantum relaxation processes was the tetrahedral complex $(Ph_4P)_2[Co(SPh)_4]$ (**17**) [104], prepared as illustrated in Equation (12). The complex has an $S = 3/2$ spin ground state, with a large, negative, axial zero-field splitting ($D = -70$ cm^{-1}) and a low rhombicity ($E/D < 0.9$). The large magnetic anisotropy of the anion can be explained by examining Figure 13, derived from angular overlap model calculations. The near degeneracy of the filled $3d_{x^2-y^2}$ orbital and the singly occupied $3d_{xy}$ orbital leads to a low-lying electronic excited state that can couple to the ground electronic state through spin-orbit coupling, thus affording a large D value and resulting in a U_{eff} value of 21(1) cm^{-1}. Dilution of $[Co(SPh)_4]^{2-}$ within the isostructural $[Zn(SPh)_4]^{2-}$ matrix eliminates quantum tunneling pathways, indicating that they occur via intermolecular dipolar interactions [104].

$$CoCl_2 + 4\,K(SPh) + 2\,(Ph_4P)Br \xrightarrow[N_2]{MeCN} (Ph_4P)_2[Co(SPh)_4] + 2\,KCl + 2\,KBr \qquad (12)$$
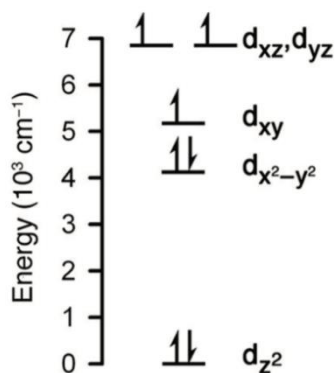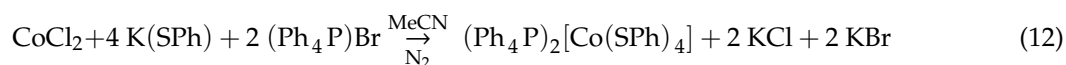

Figure 13. Electronic configuration and splitting of the 3d-orbital energy levels for the complex anion in **17**, derived using the angular overlap model. The diagram was reproduced from reference [104] with the permission of the American Chemical Society.

Continuing the above mentioned work, the group of Long prepared the salts of $[Co(EPh)_4]^{2-}$ (E = O, Se) $(Ph_4P)[Co(OPh)_4]$ (**18**), $K(Ph_4P)[Co(OPh)_4]$ (**18a**), $(Ph_4P)_2[Co(SePh)_4]$ (**19**), from reactions of $CoCl_2$ or CoI_2 with excess amounts of K(EPh) and $(Ph_4P)Br$ in MeCN [105]. All anions possess pseudotetrahedral coordination environments with tetragonal distortions to give exactly or approximately D_{2d} symmetry. One of the goals was to correlate D and U_{eff}. The values of the former are ~−11, −24 and −83 cm^{-1} for **18**, **18a** and **19**, respectively. Arrhenius plots of the ac data indicate U_{eff} values of 21(1) and 19(1) cm^{-1} for **18** and **19**, respectively, whereas the plot for **18a** shows substantial curvature indicating strong intermolecular interactions. Dilution experiments with $[Zn(OPh)_4]^{2-}$ allowed the observation of thermally-activated magnetic relaxation for **18a** with a U_{eff} value of 34.0(5) cm^{-1}. The trend in U_{eff} for **17**, **18**, **18a** and **19** does not follow the trend in D values; this possibly indicates that magnetization relaxation in **17**, **18a** and **19** is not fully thermally activated (the relation between D and U for an $S = 3/2$ system is $U = 2D$). An analysis of the four complexes within the framework of ligand field theory shows that the increase in $|D|$ takes place

in concert with a decrease in the Racah parameter *B*, i.e., increased covalency. This suggest the importance of soft donor ligands in the efforts to obtain systems with a large magnetic anisotropy.

The story does not end here. Inspired from the above described studies, the groups of Neese and Atanasov reported a systematic theoretical study developing magnetostructural correlations in the anions $[Co^{II}(EPh)_4]^{2-}$ (E = O, S, Se, Te; the Te derivative is hypothetical) based on multireference quantum chemical methods and ab initio-based ligand field theory; they also discussed the correlation of *D* with softness of the ligands, relativistic nephelauxetic effects and covalency [106]. The |*D*| value increases when the ligand field decreases across the series from O to Te. It has been shown that due to the π-anisotropy of the S and Se donor atoms, magnetostructural correlations in $[Co(OPh)_4]^{2-}$ and $[Co(EPh)_4]^{2-}$ (E = S, Se) differ. In the case of the isotropic PhO$^-$ ligand, only variations within the first coordination sphere of Co^{II} affect magnetic properties; in the case of the PhE$^-$ (E = S, Se) ligands, variations in the first and second coordination sphere affect equally the magnetic properties. The influence of the counter cations on the spin Hamitonian parameters was also studied in the two salts $(Ph_4P)_2[Co(SPh)_4]$ (**17**; D_{2d} symmetry) and $(Et_4N)_2[Co(SPh)_4]$ (**17a**; S_4 symmetry). The characterization techniques employed were high-field/high-frequency EPR, multifield SQUID magnetometry, frequency domain Fourier-transform THz-EPR and variable-field variable-temperature magnetic circular dichroism [107]. The $[Co(SPh)_4]^{2-}$ anion in **17** shows strong axial magnetic anisotropy as already was known [104,105], whereas the anion in **17a** shows rhombic anisotropy with *D* = +11 cm^{-1} and *E/D* = ~0.20 [107]. It has been verified, also with the help of multireference ab initio calculations, that the differences observed in the two complexes are associated with slight changes of the S–Co–S bond angles and C–S–Co–S torsion angles around the $\{Co^{II}S_4\}$ unit.

Another excellent experimental study on mononuclear Co(II) complexes is in agreement with the fact that ligands with heavier and softer main group donor atoms increase the magnetic anisotropy of the complexes, as evidenced by the increased |*D*| values [108]. The reactions of CoI_2 and the monodentate ligands quinoline (qun) and Ph_3P in anhydrous EtOH, and Ph_3As in $MeNO_2$, all under refluxing conditions, give complexes $[CoI_2(qun)_2]$ (**20**), $[CoI_2(Ph_3P)_2]$ (**21**) and $[CoI_2(Ph_3As)_2]$ (**22**) in good yields. The crystal structures of the complexes reveal a pseudo-tetrahedral local coordination environment around the central Co^{II} atom. The *D* value was found to vary from +9.2 cm^{-1} in **20** to −37 cm^{-1} in **21** and −75 cm^{-1} in **22**. However, the dynamic properties reveal only a minor effect on the U_{eff} value. Compound **20** does not show an out-of-phase ac magnetic susceptibility signal under a zero or applied dc field; complexes **21** and **22** exhibit slow magnetization relaxation below 4 K under an applied dc field of 1000 Oe with U_{eff} values of ~21 and ~23 cm^{-1}, respectively. It is obvious that the observed increase in the energy barrier for the As-based complex **22** (~−21 cm^{-1}→~−23 cm^{-1}) is much smaller than the corresponding increase in the D value (~−37 cm^{-1}→~−75 cm^{-1}).

Analogous studies have been performed by the groups of Rajaraman and Shanmugam [109]. They used the exocyclic mesoionic ligands 2,3-diphenyl-1,2,3,4-tetrazolium-5-olate (L$_1$) and 2,3-diphenyl-1,2,3,4-tetrazolium-5-thiolate (L$_2$), whose general structural formula is shown in Figure 14. Mesoionic ligands contain dipolar 5- or 6-membered rings whose canonical resonance structures cannot be represented without any additional charges in them. Their coordination chemistry is almost completely unexplored. Such ligands offer flexibility which allows researchers to selectively change the coordinating substituents and, thus, to investigate the influence of the donor atoms on the magnetic anisotropy. The 1:1 reactions of $CoX_2 \cdot 2H_2O$ (X = Cl, Br) with L$_1$ or L$_2$ in MeOH provide access to blue complexes $[CoX_2(L_1)(MeCN)]$ (X = Cl, **23a**; X = Br, **23b**) or green $[CoX_2(L_2)(MeCN)]$ (X = Cl, **24a**; X = Br, **24b**) when crystallized from MeCN; the preparation of **23a** and **23b** is illustrated in Equation (13). The complexes are pseudotetrahedral, the donor atoms of monodentate L$_1$ and L$_2$ being the exocyclic oxygen and sulfur atoms, respectively. The *D* values, deduced from magnetization data, are +15.6 cm^{-1} (**23a**), +11.2 cm^{-1} (**23b**), −11.3 cm^{-1} (**24a**) and −10.3 cm^{-1} (**24b**). Thus, simple substitution of L$_1$ (O-donor in **23a** and **23b**)

by L_2 (S-donor in **24a** and **24b**) switches the single-ion magnetic anisotropy parameter from positive to negative. All four complexes are field-induced SIMs with U_{eff} values of 10.3 cm^{-1} (**23a**), 8.2 cm^{-1} (**23b**), 20.2 cm^{-1} (**24a**) and 13.8 cm^{-1} (**24b**).

$$CoX_2 \cdot 6H_2O + L_1 + MeCN \xrightarrow[\Delta]{MeOH/MeCN} [CoX_2(L_1)(MeCN)] \tag{13}$$
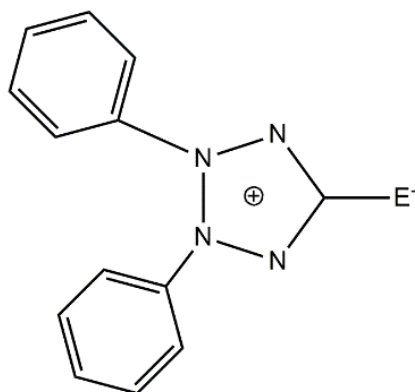

Figure 14. The general structural formula of the exocyclic mesoionic ligands L_1 (E = O) and L_2 (E = S).

8. Combined Metallacrown and Click Chemistry as a Tool for SMM Research

Metallacrowns (MCs) are analogues of crown ethers. They consist of a repeat unit of $-\{M'-N-O\}_n-$ in a cyclic arrangement where the ring metal ion and the nitrogen atom replace the methylene carbon atoms of a crown ether. MCs are named and abbreviated on the basis of the ring size and the number of oxygen atoms that act as donors. For example, in the abbreviation 12-MC-4, MC represents a metallacrown that is a 12-membered ring comprising 4 repeating $-\{M'-N-O\}-$ units with 4 donating oxygen atoms. The nomenclature/abbreviation also includes the bound central metal ion M, the ligand, and any bound or unbound ions. Thus, in the typical representation [MX{ring size-MC$_{M'Z(L)}$-ring oxygens}]Y, M is the bound central metal with its oxidation state, X is any bound anion, M′ is the ring metal with its oxidation state, Z is the third heteroatom of the ring (usually N), L is the organic ligand of the complex, and Y is any unbound anion. Sometimes there are unbound cations, which are placed before the bound central metal M. An example of the above naming scheme is [Gd^{III}(NO$_3$)$_2${15-MC$_{Cu}^{II}$$_{N(picha)}$-5}](NO$_3$), where H$_2$picha is picoline hydroxamic acid. The molecular structure of the hexanuclear cation is shown in Figure 15. The $-\{M'-N-O\}-$ repeat unit is now a quite general motif in inorganic chemistry and the connectivity has significantly grown to include a variety of bridges such as $-\{N-N\}-$, $-\{O-P\}-$, $-\{N-C-O\}-$, $-\{N-C-N\}-$, $-\{O-C-O\}-$ and $-\{X\}-$ (X is a nonmetal). After the initial great efforts to synthesize many MCs and to discover a great variety of structural types, the research activity in the past 15 years or so has shifted towards the use of these unique compounds for applications, e.g., for selective binding of cations or anions, as MRI contrast agents, in catalysis, as mimics of surface science, as building blocks for 1-, 2- and 3-dimensional solids, in liquid crystals and in various aspects of Molecular Magnetism [110]. Metallacrown chemistry has a brilliant potential for growth.

In addition to its use in inorganic chemistry (Section 4) as an anion, the azide functional group was widely used after the second world war in the synthesis of N-containing natural products and medicinal formulae. For example, the azide group is one of the most efficient amine precursors, and its ability to undergo 1,3-dipolar cycloadditions and diazo-transfer reactions is a valuable tool in organic synthesis. The [3 + 2] cycloadditions between azides and alkynes were first observed by Michael in 1893

and examined later by Huisgen [111]. The reaction has a high activation energy barrier and elevated temperatures or pressures are required to facilitate it. Almost 20 years ago, it was discovered that Cu(I) catalysis accelerates the rate of formal cycloaddition between azides and terminal alkynes, which proceeds at ambient temperatures and pressures affording 1,4-disubstitued 1,2,3-triazoles exclusively. This variant of the Huisgen cycloaddition has been termed CuAAC for <u>Cu</u>-catalyzed <u>a</u>zide <u>a</u>lkyne <u>c</u>ycloaddition. CuAAC is an exciting example of "click chemistry", a term used by Sharpless and coworkers to describe a category of chemical reactions that link two components in high yields and with minimal byproducts [112].
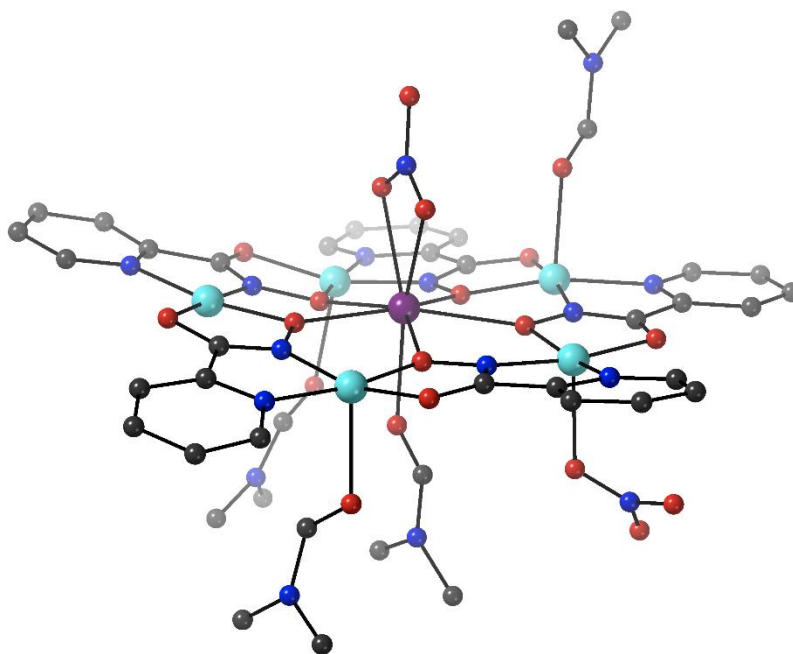

Figure 15. The molecular structure of the hexanuclear cation $[Gd^{III}Cu^{II}_5(NO_3)_2(picha)_5(DMF)_4]^+$ that is present in $[Gd^{III}(NO_3)_2\{15-MC_{Cu^{II}N(picha)}-5\}](NO_3)$. Color code: Gd^{III} dark mauve, Cu^{II} turquoise, O red, N dark blue, C, gray. Modified from reference [110].

The group of Rentschler has developed an approach which allows for the rational decoration of Cu(II) MCs with SIMs or SMMs using click chemistry [113]. The CuAAC is suitable for covalently linking magnetic building blocks which bear azide and terminal alkyne functional groups. Under mild conditions, the process leads selectively to a 1,4-disubstituted 1,2,3-triazole as a conjugated bridge which ensures communication between two or more magnetic building blocks. In order for the approach to be successful, several conditions must be satisfied: (i) To isolate thermodynamically stable complexes, polydentate chelating ligands are required. (ii) The number of introduced modified ligands must be limited to prevent an overloading of the complex. (iii) A short distance between the metal ions and the periphery of the ligands, as well as a conjugated π system are important to enable strong magnetic communication between the building blocks; and (iv) The latter should preserve their structural integrity in the reaction solvent. It is worth mentioning that this click concept can be further used in other challenging research areas of Molecular Magnetism, e.g., covalent anchoring of SMMs on surfaces, development of new cluster-based inorganic-organic hybrid materials, etc. We give an example of this strategy.

The two functionalized complexes are $(Me_4N)_2[Cu^{II}\{12-MC_{Cu(II)N(eshi)}-4\}]$ (**25**) [114] and $[Co^{II}(oda)(aterpy)]$ (**26**) [115]. Compound **25** was prepared by the high-yield reaction illustrated in Equation (14), where H_3eshi is 4-ethynylsalicylhydroxamic acid. In the centrosymmetric pentanuclear dianion

(Figure 16), each of the Cu^{II} atoms has an almost square planar coordination geometry. The peripheral four metal ions are bridged by N–O groups of the eshi^{3-} ligands forming a 12-membered metallacrown planar ring, which encapsulates the central Cu^{II} site through coordination of the μ_2 oxygen atoms of the N–O groups. The other two, terminally ligated oxygen atoms of each eshi^{3-} ligand complete coordination at neighboring Cu^{II} atoms. The four alkynyl groups protrude from the planar cluster dianion and each of them is orthogonal to its two neighbors. The complex exhibits an isolated $S = 1/2$ ground state with $J_1 = -158$ cm^{-1}, $J_2 = -65$ cm^{-1} and $g = 2.13$, adopting the Heisenberg Hamiltonian $\Sigma_{ij} (-2J_{ij} \cdot \hat{S}_i \cdot \hat{S}_j)$; J_1 and J_2 are the coupling constants corresponding to the radial magnetic interaction between the central Cu^{II} atom and the ring Cu^{II} atoms, and the tangential exchange interaction between two neighboring ring metal ions, respectively. The solution integrity of the pentanuclear dianion of **25** is proven by paramagnetic 1D and 2D ^{1}H NMR spectroscopy in d$_6$-DMSO and ESI-MS studies in a DMSO/MeOH solvent matrix. These results suggest that the 12-MC-4 Cu(II) complex is highly stable and thus suitable to perform CuAAC click reactions.

$$5 \, [Cu_2(O_2CMe)_4(H_2O)_2] + 8 \, H_3eshi + 4 \, (Me_4N)(O_2CMe) \xrightarrow{MeOH}$$
$$2 \, (MeN)_2[Cu_5(eshi)_4] + 24 \, MeCO_2H + 10 \, H_2O \tag{14}$$

Compound **26** was prepared [115] by the reaction illustrated in Equation (15) in ~30% yield; the neutral ligand aterpy is 4′-azido-2,2′:6′,2′′-terpyridine and oda is the oxodiacetate(−2) ligand. Complex [Zn(oda)(terpy)] (**26a**) was prepared in a similar manner (yield ~50%). The two complexes are isomorphous. The metal ion is in an octahedral coordination environment with rhombic (C_2) distortion because of the rigidity of the planar, tridentate chelating, tripodal aterpy and oda^{2-} ligands (Figure 16). The chelate effect of the two ligands provides the complexes with high thermodynamic stability in DMSO, as proven by ESI-MS and ^{1}H NMR (for the diamagnetic complex **26a**) studies. Thus, both complexes are suitable for CuAAC click reactions. Ac susceptibility data under a static dc field of 0.15 T reveal that the mononuclear Co(II) complex is a weak SIM.

$$[Co^{II}(oda)(H_2O)_2] + aterpy \xrightarrow[\Delta]{CHCl_3/H_2O} [Co^{II}(oda)(aterpy)] + 2 \, H_2O \tag{15}$$

The click reactions of **25** with **26** or **26a** in d$_6$-DMSO at 80 °C with copper(I) iodide as catalyst lead to complexes (Me$_4$N)$_2$[Cu^{II}\{12-MC$_{Cu(II)N([M(II)(oda)(ttshi)]}$-4\}] (**27**, M = Co; **27a**, M = Zn) [113,114], Equation (16) and Figure 15; H$_3$ttshi is 4-(2,2′:6′,2′′-terpyridyl-1H-[1–3]-triazol-4-yl)salicylhydroxamic acid. The nature and structural type of the complexes were verified by IR and UV/VIS spectroscopic techniques, ESI-MS studies, as well as by paramagnetic ^{1}H NMR methods for the {Cu$_5$Zn$_4$} cluster **27a**. Magnetic studies of **27a** indicate fairly strong antiferromagnetic Cu^{II}···Cu^{II} exchange interactions and an $S = 1/2$ ground state, similar to the behavior of the precursor complex **25**. Orbital contributions and spin-orbit coupling effects from the additional Co^{II} atoms make difficult the analysis of the magnetic properties of **27**. The important fact, however, is that ac susceptibility measurements of this complex reveal a weak out-of-phase signal at low temperatures and low-field oscillation frequencies. This is the first time (and a very promising approach) where the CuAAC click chemistry has been used to upgrade the magnetic properties of a simple copper(II) metallacrown with remarkable magnetic features from the attached Co(II) SIM units, opening new doors for the creation of interesting molecular magnetic materials and providing a contribution toward the future development of SMM-based quantum computers [113]; the latter require linking of SMMs/SIMs in a deliberate manner, like the click chemistry approach presented here. Whatever the future form of quantum technology will be, it is likely that the role of chemists will be the design and optimization of molecules that couple to an external stimulus in the adequate energy rate, while offering some elementar functionality [37]. SMMs/SIMs, being much more versatile than magnetic atoms, and yet microscopic are

among the quantum objects with the highest capacity to form non-trivial ordered states at the nanoscale and to be replicated in large numbers by means of chemical methods.

$$(Me_4N)_2[Cu_5(eshi)_4] + 4 [Co^{II}(oda)(aterpy)] \xrightarrow[\text{CuI}]{\text{DMSO, 80 °C}} (Me_4N)_2[Cu_5Co^{II}_4(oda)_4(ttshi)_4] \quad (16)$$
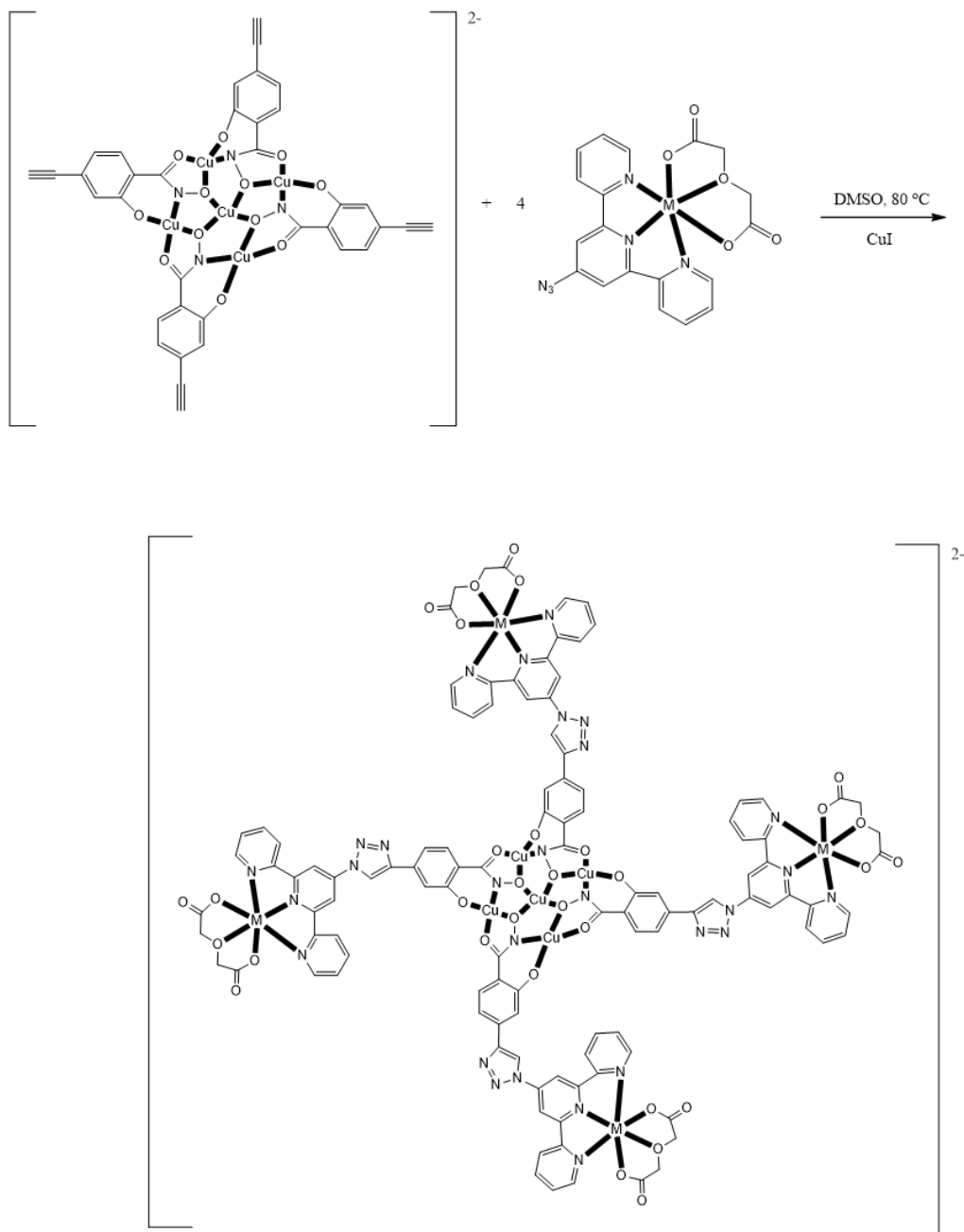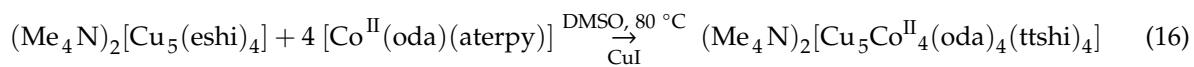

Figure 16. Representation of the CuAAC click reaction between **25** and **26/26a** that leads to the enneanuclear 3d/3d′ heterometallic clusters **27/27a**. The cations Me₄N⁺ are not shown. The coordination bonds are drawn with bold lines. M = Co, Zn.

9. Deprotonated 2-Pyridyl Alcohols: Central "Players" in the Chemistry of Transition-Metal SMMs

When developing routes and strategies for the synthesis of transition-metal SMMs, the design of bridging ligands is of paramount importance. In addition to bridging ability, the propagation of strong magnetic exchange interaction between the metal spin carriers and the simultaneous formation of chelating rings are highly desirable. The anions of 2-pyridyl alcohols (Figure 17) have proven to be versatile chelating and bridging groups that have yielded a number of 3d-metal, especially Mn, and 3d/4f-metal clusters with various structural motifs [116–133]. Moreover, the bridging deprotonated oxygen atom, i.e., the alkoxido group, often supports ferromagnetic coupling between the metal ions and has thus yielded polynuclear complexes with large S values and SMM properties. We give below examples from the use of such ligands in 3d-metal SMM chemistry.
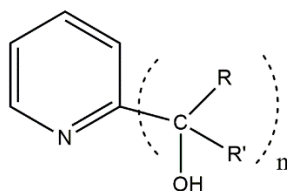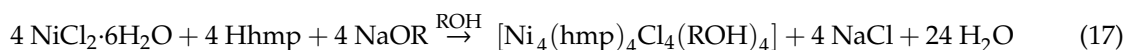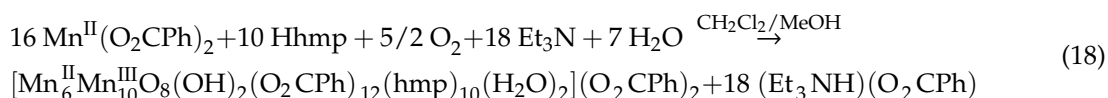

Figure 17. The general formula of the neutral 2-pyridyl alcohols; n can be 1 or 2, while R, R' are H and various non-donor organic groups (Me, Ph, …).

The 1:1:1 $NiCl_2 \cdot 6H_2O$/Hhmp/NaOR reaction mixtures in alcohols (MeOH, EtOH) give clusters $[Ni_4(hmp)_4Cl_4(ROH)_4]$ (**28**, R = Me; **28a**, R = Et), Equation (17); hmp is the anion of 2-(hydroxymethyl)pyridine (R = R' = H and $n = 1$ in Figure 17). The tetranuclear cluster molecules possess a distorted cubane $\{Ni_4(\mu_3\text{-OR''})_4\}^{4+}$ core, where R''– = (2-pyridyl)CH_2–, with the Ni^{II} atoms and the oxygen atoms from the 3.31 hmp$^-$ ligands (**B** with R = R' = H and $n = 1$ in Figure 4) occupying alternate vertices of the cube. A terminal chlorido ligand, an alcohol molecule and a 2-pyridyl nitrogen atom complete the octahedral coordination sphere of each metal ion [121]. Variable-temperature dc magnetic susceptibility studies indicate ferromagnetic $Ni^{II}\cdots Ni^{II}$ exchange interactions and a $S = 4$ ground state. Single-crystal high-frequency EPR spectra clearly suggest that each of the complexes has a total spin of 4 in the ground state with a negative D value. Magnetization vs. magnetic field measurements performed on single crystals with a micro-SQUID magnetometer show that these $\{Ni_4\}$ clusters are SMMs. An appreciable exchange bias is evident in the hysteresis loops. The first resonant tunneling step is shifted considerably from zero field by virtue of intermolecular antiferromagnetic exchange interactions between the tetranuclear molecules of **28** and **28a** in their crystals [121].

$$4\,NiCl_2 \cdot 6H_2O + 4\,Hhmp + 4\,NaOR \xrightarrow{ROH} [Ni_4(hmp)_4Cl_4(ROH)_4] + 4\,NaCl + 24\,H_2O \qquad (17)$$

Deprotonated 2-pyridyl alcohols have contributed a lot into the development of Mn SMMs. For example, the reaction of Hhmp with $Mn(O_2CPh)_2$ in the presence of Et_3N in CH_2Cl_2/MeOH leads to the isolation of $[Mn^{II}_6Mn^{III}_{10}O_8(OH)_2(O_2CPh)_{12}(hmp)_{10}(H_2O)_2](O_2CPh)_2$ (**29**) in 30% yield, Equation (18). The core structure consists of a linked pair of complete cubanes $\{Mn^{II}_2Mn^{III}_2(\mu_4\text{-O})_2(\mu_3\text{-OR''})_2\}^{4+}$, on either side of which is attached a tetrahedral $\{Mn^{II}Mn^{III}_3(\mu_4\text{-O})\}^{9+}$ unit. Among the ten hmp$^-$ groups, four are bridging within the central cubanes in a 3.31 mode (**B** with R = R' = H and $n = 1$ in Figure 4) and the other six are bridging within the outer tetrahedral units in a 2.21 mod (**C** with R = R' = H and $n = 1$ in Figure 4). The Mn ions are all six-coordinate with distorted octahedral geometry, except for the Mn^{II} atoms of the tetrahedral units which are 7-coordinate. Solid-state dc and ac magnetic susceptibility measurements on **29** establish that it possesses a $S = 8$ ground state. The complex displays frequency-dependent out-of-phase

(χ''_M) ac susceptibility signals below 3 K suggestive of SMM behavior. The D and U_{eff} value are -0.11 cm^{-1} and 7 cm^{-1}, respectively. Magnetization vs. applied dc field sweeps on single crystals of the complex down to 0.04 K exhibit hysteresis, confirming **29** to be a SMM, albeit weak [131]. Comparison of the structure of **29** ({Mn$_{16}$}) with {Mn$_{12}$} and {Mn$_6$} clusters obtained under the same reaction conditions but with two Me (R = R' = Me and n = 1 in Figure 17) or two Ph (R = R' = Ph and n = 1 in Figure 17) groups, respectively, added next to the alkoxido O atom of hmp$^-$ indicate their influence on the nuclearity and structure of the products [130,131] as being due to the overall bulk of the ligand plus the decreased ability of the deprotonated oxygen atom to bridge.

$$16\,\text{Mn}^{\text{II}}(\text{O}_2\text{CPh})_2 + 10\,\text{Hhmp} + 5/2\,\text{O}_2 + 18\,\text{Et}_3\text{N} + 7\,\text{H}_2\text{O} \xrightarrow{\text{CH}_2\text{Cl}_2/\text{MeOH}}$$
$$[\text{Mn}_6^{\text{II}}\text{Mn}_{10}^{\text{III}}\text{O}_8(\text{OH})_2(\text{O}_2\text{CPh})_{12}(\text{hmp})_{10}(\text{H}_2\text{O})_2](\text{O}_2\text{CPh})_2 + 18\,(\text{Et}_3\text{NH})(\text{O}_2\text{CPh}) \qquad (18)$$

The ligand Hhep (R = R' = H and n = 2 in Figure 17) also gives structurally and magnetically interesting clusters. The reaction of a 2:1 mixture of [Mn$^{\text{III}}_3$O(O$_2$CMe)$_6$(py)$_3$](ClO$_4$) and [Mn$^{\text{II,III,III}}_3$O(O$_2$CMe)$_6$(py)$_3$] with 4.5 equivs. of Hhep in MeCN affords cluster [Mn$^{\text{II}}_2$Mn$^{\text{III}}_{16}$O$_{14}$(O$_2$CMe)$_{18}$(hep)$_4$(Hhep)$_2$(H$_2$O)$_2$](ClO$_4$)$_2$ (**30**) in 20% yield. The core appears to be {Mn$_{18}$(μ_4-O)$_4$(μ_3-O)$_{10}$(μ_3-O$_{\text{acetato}}$)$_2$(μ_2-acetato)$_2$(μ_2-O$_{\text{hep}^-/\text{Hhep}}$)$_6$}$^{14+}$ [119,125]. It can be described as a central {Mn$_4$O$_6$} unit (containing a linear Mn$_4$ chain) linked by its μ_3-O^{2-} ions to two {Mn$_7$O$_9$} units, one on each side. Each of the heptanuclear units comprises a face-sharing set of one {Mn$_4$O$_4$} cubane and two {Mn$_3$O$_4$} partial cubanes. All the metal ions are six-coordinate. The hep$^-$ and Hhep groups behave as 2.21 (**C** with R = R' = H and n = 2 for hep$^-$ and **D** for Hhep in Figure 4) ligands. Fitting of magnetization data establish that **30** possesses a total spin of 13 in the ground state and a D value of -13 cm^{-1}. The complex is SMM (U_{eff} = 15 cm^{-1}), and this is confirmed by the appearance of hysteresis loops in magnetization vs. dc field sweeps on a single crystal. Below 0.2 K, the relaxation becomes temperature-independent, consistent with relaxation only by QTM through the anisotropy barrier via the lowest-energy M_S = ±13 levels of the S = 13 spin manifold. Although the high nuclearity of the complex is mostly due to the presence of 4.4- and 3.3-O^{2-} groups, as well as 4.31, 2.21 and 2.11 MeCO$_2^-$ ligands, the 2.21 hep$^-$ and Hhep moieties certainly contribute into its interesting magnetic properties.

2-pyridyl alcohols can be chiral leading to 3d-metal clusters with unprecedented structural motifs and interesting magnetic properties. The ligand α-methyl-2-pyridine-methanol (Hmpm; R = H, R' = Me and n = 1 in Figure 17) presents similar coordination features to Hhmp, but offers slightly different steric and electronic effects. The Hmpm ligand can be prepared via the reduction of 2-acetylpyridine by NaBH$_4$ [133]. The 2:1:2 reaction between Mn(O$_2$CPh)$_2$·2H$_2$O, rac-Hmpm and Et$_3$N in MeOH gives a deep red solution, which upon slow solvent evaporation at room temperature affords cluster [Mn$^{\text{II}}_2$Mn$^{\text{III}}_{28}$Mn$^{\text{IV}}$(OH)$_2$(OMe)$_{24}$O$_{24}$(O$_2$CPh)$_{16}$(rac-mpm)$_2$] (**31**) in ~30% yield, Equation (19). The core (Figure 18, left) can be described as a consecutive array of edge-sharing {Mn$_4$(μ_4-O)} tetrahedra and {Mn$_3$(μ_3-O)} triangles that are linked to each other via bridging MeO$^-$ and O^{2-} groups [133]. An alternative description of the core is as consisting of seven parallel layers (Figure 18, right) of four types (A, B, C, D) with an ABCDCBA arrangement. Layers A and B are simple Mn$^{\text{III}}$ monomeric and {Mn$^{\text{III}}_4$} butterfly subunits, respectively, attached to each other through a 4.4 oxido group. Layer C is a {Mn$^{\text{II}}$Mn$^{\text{III}}_3$} cluster moiety containing three edge-sharing {Mn$_3$} triangles. Layer D comprises a {Mn$^{\text{III}}_8$Mn$^{\text{IV}}$} rod-like cluster unit that can be further seen as a central, planar disk-like {Mn$^{\text{III}}_6$Mn$^{\text{IV}}$} moiety with two additional Mn$^{\text{III}}$ atoms above and below the disk. The layers are held together by a combination of bridging methoxido and oxido groups. The rac-mpm$^-$ groups behave as 2.21 ligands (**C** with R = H, R' = Me and n = 1 in Figure 4). The molecule is spherical with a diameter of ~2.5 nm. The cluster is: (i) One of the largest 3d-metal clusters, (ii) the second highest-nuclearity Mn complex containing an odd number of metal centers and the second

cluster with a nuclearity of 31, and (iii) the largest SMM (S = 23/2, U_{eff} = ~40 cm^{-1}) that possesses entirely resolved out-of-phase ac peaks and magnetization hysteresis loops below 5 K.

$$31\ Mn^{II}(O_2CPh)_2 \cdot 2H_2O + 2\ rac\text{-}Hmpm + 46\ Et_3N + 15/2O_2 + 24\ MeOH \xrightarrow{MeOH}$$

$$[Mn_2^{II}Mn_{28}^{III}Mn^{IV}(OH)_2(OMe)_{24}O_{24}(O_2CPh)_{16}(rac\text{-}mmp)_2] + 46\ (Et_3NH)(O_2CPh) + 51\ H_2O \tag{19}$$

Figure 18. The metal–oxygen core (left) and the four types of constituent layers (right) along the crystallographic c axis. H atoms have been omitted for clarity. Color code: Mn^{II} yellow, Mn^{III} blue, Mn^{IV} olive green, O red. Modified from reference [133].

10. Deprotonated Aliphatic Diols: Simple and Efficient Ligands in the Chemistry of 3d-Metal SMMs

Molecules with two hydroxyl groups on different aliphatic carbon atoms have some interesting chemical characteristics [134,135] which are more prominent for vicinal diols (*vic*-diols). In the last 15 years or so, there has been an intense interest in the use of diols in the chemistry of transition-metal clusters and SMMs [136]. The simplistic rationale here is that each deprotonated alkoxido oxygen atom can bridge two or three metal ions and the latter can be linked together into polymetallic arrays with hopefully large ground-state spins, anisotropies and SMM properties. The structures of the products depend on (i) the level of deprotonation of the ligand (singly or doubly deprotonated), (ii) the existence of other donor groups on the diol (e.g., a pyridyl group, –NH$_2$, –COOH, . . .), and (iii) the presence of other bridging co-ligands in the reaction system. A family of simple aliphatic diols, with no other donor groups, consist of 1,3-propanediol and its derivatives (Figure 19). We give below one notable example from the use of a member of this family in Mn SMM chemistry. The cited complexes belong to the class of giant homometallic 3d clusters (nuclearities higher than 30) with the metals in moderate oxidation states. Such giant clusters are of great interest not only for their impressive structures with nano dimensions, but also because they often display interesting magnetic properties (including SMM behavior). In addition, they possess the properties of both classical and quantum world, thus giving the opportunity for the discovery of new physical phenomena and the deeper understanding of the existing ones [137].

Figure 19. 1,3-propanediol (H$_2$pd; R = R′ = H) and its derivatives.

The 1:4:1 reaction of [Mn$^{II,III,III}_3$O(O$_2$CMe)$_6$(py)$_3$] with H$_2$pd and NaN$_3$ in MeCN leads to cluster [{Mn$^{II}_2$Mn$^{III}_8$NaO$_2$(O$_2$CMe)$_{13}$(pd)$_6$(py)$_2$}$_4$] (**32**) in 35% yield [138,139], Equation (20). Since the giant cluster contains Na$^+$ but not N$_3^-$, it has been assumed that NaN$_3$ is important as the source of Na$^+$ and perhaps to provide additional weak base (N$_3^-$) for ligand deprotonation and further oxide ion formation; however, the main sources for ligand deprotonation are the MeCO$_2^-$ ions, as shown in Eq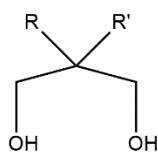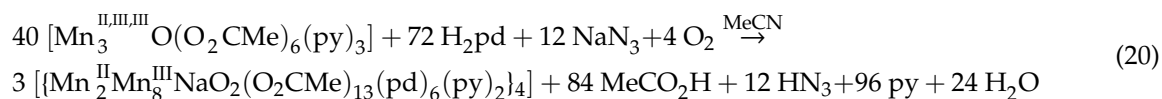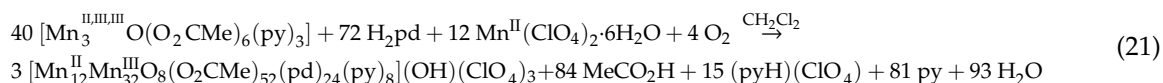uation (20), and/or the pyridine molecules. This is supported by the same reactions, but using NaCN, NaOCN, NaSCN or Na{N(CN)$_2$} instead of NaN$_3$, which all give **32** in slightly lower yields (18–26%). The molecule of **32** consists of four {Mn$^{II}_2$Mn$^{III}_8$} loops linked through four Na$^+$ ions to give a supramolecular aggregate with a saddle-like topology; one loop with one Na$^+$ ion is shown in Figure 20. The Mn ions are all in a distorted octahedral coordination environment; the eight high-spin 3d^4 Mn^{III} centers display the Jahn–Teller axial elongation, but the Jahn–Teller axes are not co-parallel. Each loop consists of two triangular {Mn$^{III}_3$(μ_3-O)}$^{7+}$ and two dinuclear {Mn^{II}Mn^{III}} subunits linked by the oxygen atoms of the six 3.22 pd^{2-} groups (**E** with R = R′ = H in Figure 4), as well as by 2.11 and 4.22 MeCO$_2^-$ ligands. The triangular subunits are connected by two pd^{2-} oxygen atoms, whereas the dinuclear subunits are connected by two pd^{2-} oxygen atoms and a 2.11 MeCO$_2^-$ ligand. The Mn^{II} and Mn^{III} atoms within each dinuclear subunit are bridged by a 2.11 acetato group, a pd^{2-} oxygen atom and an oxygen atom from a 4.22 MeCO$_2^-$ ligand. The Mn^{III} atoms of each triangular subunit are bridged by a 3.3 O^{2-} group, two oxygen atoms from two different pd^{2-} groups, one oxygen atom from a 4.22 MeCO$_2^-$ ligand and two 3.21 MeCO$_2^-$ ligands. The latter and an additional acetato group link each triangular subunit to a Na$^+$ ion; the two alkali metal ions attached to the decanuclear {Mn$^{II}_2$Mn$^{III}_8$} loop connect it in an equivalent manner to a neighboring loop giving a giant loop-of-loops aggregate. Four of the pd^{2-} groups bridge one Mn^{II} and two Mn^{III} centers, and the remaining two bridge three Mn^{III} ions. The crystal structure shows that the {Mn$^{II}_8$Mn$^{III}_{32}$Na$_4$} aggregates pack as tail-to-tail {Mn$^{II}_8$Mn$^{III}_{32}$Na$_4$}$_2$ dimers, thus leading to egg-shaped stacks. A detailed magnetic study of **32** reveals that each decanuclear loop has a $S = 4$ ground-state spin, and displays frequency-dependent in-phase and out-of-phase ac magnetic susceptibility signals. The aggregate also exhibits hysteresis loops. The hysteresis loops are not typical of SMM behavior because of the presence of interloop exchange interactions through the diamagnetic Na$^+$ ions, and also intermolecular interactions between different {Mn$^{II}_8$Mn$^{III}_{32}$Na$_4$} aggregates [137,139].

$$40\,[\text{Mn}_3^{II,III,III}\text{O}(\text{O}_2\text{CMe})_6(\text{py})_3] + 72\,\text{H}_2\text{pd} + 12\,\text{NaN}_3 + 4\,\text{O}_2 \xrightarrow{\text{MeCN}}$$
$$3\,[\{\text{Mn}_2^{II}\text{Mn}_8^{III}\text{NaO}_2(\text{O}_2\text{CMe})_{13}(\text{pd})_6(\text{py})_2\}_4] + 84\,\text{MeCO}_2\text{H} + 12\,\text{HN}_3 + 96\,\text{py} + 24\,\text{H}_2\text{O}$$

$$(20)$$

Once the heterometallic (Na/Mn) character of **32** and its influence on the magnetic properties had been studied, the synthesis of the magnetically discrete, homometallic {Mn$_{44}$} analogue of **32** was sought, as a means of strengthening the interloop exchange interactions and appearance of better SMM properties. The desired product [Mn$^{II}_{12}$Mn$^{III}_{32}$O$_8$(O$_2$CMe)$_{52}$(pd)$_{24}$(py)$_8$]$^{4+}$ was isolated [139] from the 1:5:1 [Mn$^{II,III,III}_3$O(py)$_3$]/H$_2$pd/Mn^{II}(ClO$_4$)$_2$·6H$_2$O reaction mixture in CH$_2$Cl$_2$, Equation (21), i.e., with the use of Mn^{II}(ClO$_4$)$_2$·6H$_2$O instead of NaN$_3$. The product is, as expected, cationic with the formula [Mn$^{II}_{12}$Mn$^{III}_{32}$O$_8$(O$_2$CMe)$_{52}$(pd)$_{24}$(py)$_8$](OH)(ClO$_4$)$_3$ (**33**) and its yield is ~25%. The molecular structure of the cation of **33** is very similar to that of the molecule of **32**, the main difference being the fact that the

$\{Mn^{II}_2Mn^{III}_8\}$ loops in the former are linked through Mn^{II} ions, whereas those of the latter by Na^+ ions; as a result the $\{Mn_{44}\}$ cluster is positively charged, whereas the $\{Mn_{40}Na_4\}$ aggregate is neutral. The packing of **33** is similar to that in **32**, and thus supramolecular $\{Mn_{44}\}_2$ dimers are formed in the crystal. In accord with the strongest magnetic exchange interactions between the four $\{Mn^{II}_2Mn^{III}_8\}$ loops mediated through the connecting Mn^{II} centers, magnetic susceptibility studies reveal that **33** has a $S = 6$ ground-state spin and displays frequency-dependent in-phase and out-of-phase signals. Magnetization vs. dc magnetic field sweeps on single crystals of **33** display hysteresis loops below 0.7 K whose coercivities increase with decreasing temperature and with increasing sweep rate, confirming that this giant cluster is one of the largest Mn SMMs.

$$40\,[Mn_3^{II,III,III}O(O_2CMe)_6(py)_3] + 72\,H_2pd + 12\,Mn^{II}(ClO_4)_2{\cdot}6H_2O + 4\,O_2 \xrightarrow{CH_2Cl_2}$$
$$3\,[Mn^{II}_{12}Mn^{III}_{32}O_8(O_2CMe)_{52}(pd)_{24}(py)_8](OH)(ClO_4)_3 + 84\,MeCO_2H + 15\,(pyH)(ClO_4) + 81\,py + 93\,H_2O \tag{21}$$

The ligand 2-methyl-1,3-propanediol (H_2mpd; R = H and R′ = Me in Figure 19) gives the heterometallic aggregate $[\{Mn^{II}_2Mn^{III}_8NaO_2(O_2CMe)_{13}(mpd)_6(py)_2\}_4]$ (**34**) [139], which is structurally and magnetically similar to **32**. The ligand pd^{2-} has been also used by Tasiopoulos' group to construct giant Mn/Co^{II} and Mn/Ni^{II} clusters with exciting structures and large ground-state spins, but with no SMM properties [140,141]. For example, cluster $[Mn^{II}_8Mn^{III}_{28}Ni^{II}_4O_{12}Cl_{10}(O_2CMe)_{26}(pd)_{24}(py)_4(H_2O)_2]$ (**35**) possesses an unprecedented "loop-of loops-and-supertetrahedra" structural topology and displays a high ground-state spin state value of 26 ± 1 [141].

Figure 20. The structure of one $\{Mn^{II}_2Mn^{III}_8NaO_2(O_2CMe)_{13}(pd)_6(py)_2\}$ loop that is present in **32**. Color code: Mn^{II} cyan, Mn^{III} dark blue, Na^+ dark yellow, O red, N green. Modified from reference [138].

11. Molecular and Supramolecular Approaches in the Chemistry of Manganese SMMs Using Simple and Elaborate 2-Pyridyl Oximes

The deprotonated oxime (oximate, R_2CNO^-) group has played an important role in the chemistry of 3d-metal clusters and SMMs. This diatomic group can bridge up to three metal ions and often propagates ferromagnetic exchange interactions; the latter property may lead to SMM properties. In most cases,

the oxime group is part of an organic ligand that possesses one or more other donor groups, often in a position that enables the formation of a stable chelating ring with the participation of the oximate nitrogen atom. The two most studied families of oxime groups in Molecular Magnetism are the salicyl aldo(keto)ximes and the 2-pyridyl aldo(keto)ximes, Figure 21. The former [142–155] have led to a variety of clusters with exciting molecular structures and magnetic properties; they have been used, among others, in the development of a synthetic process widely known as "ground-state spin switching and enhancing SMM properties via targeted structural distortion" strategy [56,142–145,147–149]. The latter [156–174], in addition to their involvement in the synthesis of 3d-metal SIMs [158], have provided access to interesting 3d-metal clusters and SMMs. They have also been used in the realization of a synthetic scheme best known as "'switching on' SMM properties upon conversion of low-spin complexes into high-spin ones without changing the core" strategy [168,169] and, when derivatized by design, in the development of an innovative approach which allows the covalent linking of SMMs by applying principles of supramolecular chemistry [172–174]. Below we describe briefly the molecular and supramolecular approaches in the chemistry of Mn SMMs by using 2-pyridyl ketoximes and its derivatives as key synthetic tools.
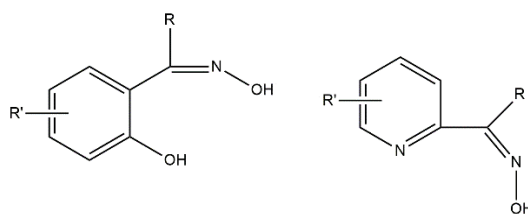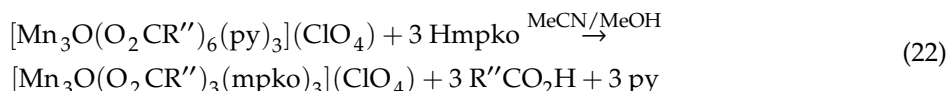

Figure 21. Salicyl aldo(keto)ximes (left) and 2-pyridyl aldo(keto)ximes (right), two families of ligands that have widely been used in the chemistry of transition-metal SMMs; R and R′ are various non-donor groups. When R = H the ligands are aldoximes and when R ≠ H the products are ketoximes.

An in-depth studied family of Mn(III) carboxylate clusters consists of the triply oxido-bridged, triangular complexes [Mn$_3$O(O$_2$CR″)$_6$L$_3$]X (R″ = Me, Et, Ph, . . . ; X = monoanionic counterions; L = neutral monodentate ligands) [175]. These complexes possess the {Mn^{III}$_3$(μ_3-O)}$^{7+}$ core with peripheral ligation provided by 2.11 carboxylato groups and terminal L ligands. The triangular cations are characterized by antiferromagnetic Mn^{III}···Mn^{III} exchange interactions and have low S values in the ground state; they are not thus SMMs. It was a general belief that this common triangular topology could never give complexes with SMM properties. Using 2-pyridyl ketoximes, however, these complexes can be converted into triangular clusters with the same {Mn$_3$(μ_3-O)}$^{7+}$ core, but with ferromagnetic Mn^{III}···Mn^{III} interactions. The strategy is illustrated in Figure 22. The 1:3 reaction between [Mn$_3$O(O$_2$CR″)$_6$(py)$_3$](ClO$_4$) (R″ = Me, **36a**; R″ = Et, **36b**; R″ = Ph, **36c**, see Figure 22, left) and methyl 2-pyridyl ketoxime (Hmpko; R = Me and R′ = H in Figure 21) in MeCN/MeOH give dark brown solutions; evaporation of the reaction solutions to dryness and crystallization of the residues from CH$_2$Cl$_2$/n-hexane give dark red crystals of [Mn$_3$O(O$_2$CR″)$_3$(mpko)$_3$](ClO$_4$) (R″ = Me, **37a**; R″ = Et, **37b**; R″ = Ph, **37c**) in high yields (>80%), Equation (22) [168]. The 1:3 molar ratio of the reactants was chosen to allow for the incorporation of one mpko$^-$ ligand onto each edge of the {Mn$_3$(μ_3-O)}$^{7+}$ core. The reaction can thus be described as a simple ligand substitution with the replacement of three R″CO$_2$$^-$ groups and three py ligands by three mpko$^-$ ones, without change of the Mn oxidation level. This reaction scheme is quite general and can be extended to other carboxylate groups and 2-pyridyl ketoximes (Figure 21), where R is a non-donor group.

$$[Mn_3O(O_2CR'')_6(py)_3](ClO_4) + 3\,Hmpko \overset{MeCN/MeOH}{\rightarrow}$$
$$[Mn_3O(O_2CR'')_3(mpko)_3](ClO_4) + 3\,R''CO_2H + 3\,py \tag{22}$$

Figure 22. Schematic drawing of the conversion of the low-spin cations of **36a**, **36b**, **36c** to the high-spin ($S = 6$) SMM cations **37a**, **37b**, **37c**. The large solid (●) and the single small open (o) circles represent the Mn^{III} centers and oxido (O^{2-}) groups, respectively. The curved solid lines represent triatomic carboxylate groups. The mixed dashed/solid lines represent the N,N (small dashed circles), O (small open circle) donor sets of the 2.111 mpko⁻ ligands. The coordination bonds are drawn with bold lines.

As in **36a**, **36b**, **36c**, the cations of **37a**, **37b**, **37c** (Figure 22, right) possess a $\{Mn^{III}_3(\mu_3\text{-}O)\}^{7+}$ triangular core, but each Mn_2 edge is now bridged by a 2.11 $R''CO_2^-$ and a 2.111 mpko⁻ (**G** with R = Me and R′ = H in Figure 4) group. The three $R''CO_2^-$ groups lie on one side of the plane defined by the Mn^{III} atoms and the three oximato groups on the other. The tridentate ligation mode of mpko⁻ causes a buckling of the formerly planar $\{Mn^{III}_3(\mu_3\text{-}O)\}^{7+}$ unit, giving rise to a relative twisting of the octahedra of the metal ions, a slight non-planarity of the Mn^{III}–N–O–Mn^{III} units and a displacement of the central oxido group which is ~0.3 Å above the $\{Mn^{III}_3\}$ plane on the same side as the carboxylate groups. These structural distortions lead to ferromagnetic $Mn^{III}\cdots Mn^{III}$ interactions resulting in a $S = 6$ ground state. Fits of dc magnetization data collected in the 10–70 KG and 1.8–10.0 K ranges confirm the ground-state spin and give a D value of ~−0.35 cm⁻¹. Complexes **37** exhibit frequency-dependent out-of-phase (χ''_M) ac magnetic susceptibility signals suggesting a possible SMM behavior. Relaxation rate vs. T data down to 1.8 K obtained from the χ''_M vs. T studies were supplemented with rate vs. T data measured to 0.04 K via magnetization vs. time decay studies, and these were used to construct Arrhenius plots from which U_{eff} values of ~8 cm⁻¹ were derived. Magnetization vs. dc field sweeps on single crystals of **37a**·3CH₂Cl₂ show hysteresis loops which exhibit steps due to QTM. The loops are temperature-independent below 0.3 K and this indicates only ground-state QTM between the $M_S = \pm 6$ levels. Complexes **37** were the first confirmed triangular SMMs of any transition metal. High-frequency EPR spectra of single crystals of **37a**·3CH₂Cl₂ give $D = -0.3$ cm⁻¹ and provide evidence of a rather significant transverse anisotropy ($|E| \geq 0.015$ cm⁻¹). DFT calculations provide strong evidence [169] that the unusual ferromagnetic exchange interactions in complexes **37** originate from a combination of several factors including the non-planarity (with respect to the $\{Mn^{III}_3\}$ plane) of the bridging oximato groups, the non-parallel alignment of the Jahn–Teller axes and the shift of the triply-bridging oxido group out of the plane defined by the three Mn^{III} ions. The above results demonstrate that structural distortions of a magnetic core imposed by peripheral ligands (deprotonated 2-pyridyl oximes in this case) can "switch on" SMM properties [168].

Ligands containing two 2-pyridyl ketoxime moieties are of special interest in the realm of the linking of SMMs [172–174]. Since SMMs have been proposed as qubits for quantum information processes and as components in molecular spintronics, a great challenge is their quantum mechanical coupling to

each other or to other components of a device, while maintaining the intrinsic properties of each SMM; this maintenance requires very weak coupling between the SMM precursors. Excluding utilization of hydrogen bonds, with which it is difficult to control oligomerization and to achieve retention of the supramolecular structure in solution, the best solution is the designed linking of SMMs via coordination bonds. The groups of Papaefstathiou, Escuer, Brechin and Christou [150–153,170–174], among others, have used building-block strategies to link SMMs together employing carefully chosen linkers that provide inter-SMM interactions and ensure the formation of discrete oligomeric (and not polymeric) species.

The SMM cations of **37a**, **37b** and **37c** (Figure 22, right) are excellent candidates to be used as building blocks for such a strategy. They have their $R''CO_2^-$ and $mpko^-$ ligands on opposite sites of the $\{Mn^{III}_3\}$ plane. The tripodal arrangement of the carboxylato and oximato groups suggests that their replacement with dicarboxylato [170] or bis(2-pyridyl) dioximato groups [172–174], respectively, could lead to discrete aggregates (oligomers) rather than polymeric complexes. We give an example in which a bis(2-pyridyl) dioxime provides the inter-SMM linkage.

The ligand of choice was H_2dpd (Figure 23) and its selection was based on principles of the supramolecular chemistry field [174]. The molecule can be seen as a fusion of two Hmpko units (Figure 21, right, with R = Me and R′ = H) at the Me group. The single sp^3 central carbon atom reduces the conformational flexibility, and according to the directional bonding approach of supramolecular chemistry, the combination of a tritopic $\{Mn^{III}_3\}$ unit with a ~109° ditopic dioximate should give a $\{Mn^{III}_3\}_2$ "dimer" with three linkers and parallel $\{Mn^{III}_3\}$ planes. It was also expected that the coordination by tridentate 2-pyridyloximate groups of three dpd^{2-} ligands would give a rigidity in the resulting dimeric product, a favorable fact for the retention of the structure in solution. All these design principles turned out to be successful, Equation (23). The I_3^- counterions, which are present in the product $[Mn_6O_2(O_2CMe)_6(dpd)_3](I_3)_2$ (**38**), come from I_2 in the reaction mixture, probably from reductive agents, e.g., EtOH, through the $2e^- + 3\,I_2 \rightarrow 2\,I_3^-$ process.

$$2\,[Mn_3^{III}O(O_2CMe)_6(py)_3](ClO_4) + 3\,H_2dpd + 2\,H^+ + 2\,I_3^- \xrightarrow{CH_2Cl_2/EtOH}$$
$$[Mn_6^{III}O_2(O_2CMe)_6(dpd)_3](I_3)_2 + 2\,(pyH)(ClO_4) + 4\,(pyH)(O_2CMe) + 2\,MeCO_2H \tag{23}$$

H_2dpd

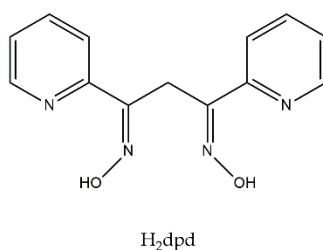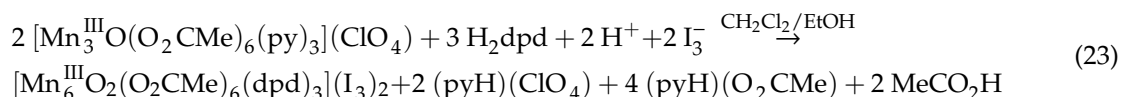**Figure 23.** The free ligand 1,3-di(pyridin-2-yl)propane-1,3-dione dioxime which has been used for the synthesis of a covalently linked dimer of $\{Mn^{III}_3\}$ SMMs.

At targeted by the selection of H_2dpd, the structure of the hexanuclear dication consists of two $\{Mn^{III}_3(\mu_3\text{-O})\}^{7+}$ subunits connected by three 4.111111 dpd^{2-} ligands (**H** in Figure 5) to give a $\{Mn^{III}_3\}$ "dimer" of D_3 symmetry; the two $\{Mn^{III}_3\}$ planes are thus parallel. Each triangular subunit is structurally very similar to that of the "monomer" **37a**. Solid-state dc and ac magnetic susceptibility studies show that each $\{Mn^{III}_3\}$ subunit of the "dimer" is a separate SMM with an $S = 6$ ground state and that the two subunits are very weakly ferromagnetically exchange-coupled. Single-crystal high-frequency EPR spectra on **38** display signal splittings suggesting quantum superposition/entanglement of the two SMM subunits. Remarkably, the same spectral behavior is observed in MeCN/toluene (1:1 *v/v*) frozen solutions,

indicating that the structure of the "dimer" is retained in solution and the weak inter-SMM interaction persists. This work proves that the synthesis of covalently linked oligomers of exchange-coupled SMMs is feasible, with a careful ligand design, and the products can retain their oligomeric nature and inter-SMM quantum mechanical coupling in solution. These results provide scientists with a good background as efforts of using solution methods for deposition of SMMs on surfaces and other substrates continue.

12. Concluding Comments and Brief Prognosis for the Future

We hope that this review has provided the readers with a taste of the synthetic chemistry and reactivity studies of 3d-, 4d- and 5d-metal SIMs and SMMs, with emphasis on some ligands or families of ligands that have been used successfully in this area. Other authors could have selected other ligands from a plethora available. We do believe that some of the ligands discussed, e.g., the azido and cyanido groups, ligands containing soft donor atoms, aliphatic diols and oxime-based ligands, are promising for further developments.

Although the current interest in this field is shifted to f-elements, it is our opinion that the chemistry of transition-metal SMMs and SIMs has brilliant perspectives. In the SMM area, the major advantage of using d-block metal ions is their ability to create strongly coupled systems; this is in contrast to the situation with the lanthanoid ions (with the exception of radical-bridged 4f-metal SMMs [176]) where the core-like character of the 4f orbitals prohibits this. The d-block SIM chemistry appears to grow exponentially and it is striking that few of the compounds reported to date are SIMs in zero field. One approach to increase the number of zero-field d-metal SIMs is to design ligand-field environments, which can preserve strict axial symmetry around the metal ion. In both areas, and from a synthetic inorganic chemistry point of view, the synthesis of 4d- and 5d-metal SIM and SMM systems is expected to gain more and more attention. The spin-orbit coupling constants of these metal ions are larger than their first-row counterparts, and this can lead to improved SIM properties. Moreover, the increased radial extension of the 4d and 5d orbitals gives the possibility for stronger magnetic exchange interactions, a crucial consideration in the design of efficient SMMs.

Regardless of how the chemistry of SIMs and SMMs develops over the next few years, one thing is certain: the design and synthesis of new ligands, and the proper use of existing ones will remain to the fore.

Concluding, we hope that synthetic inorganic chemists active in the transition-metal SIM and SMM areas or scientists who just enter into this field will find this review useful. We shall be happy if the readers enjoy the review as much we enjoyed writing it.

References

1. Kahn, O. *Molecular Magnetism*; Wiley-VCH: New York, NY, USA, 1993.
2. Housecroft, C.E.; Sharpe, A.G. *Inorganic Chemistry*, 5th ed.; Pearson: Harlow, UK, 2018; pp. 661–795.
3. Miessler, G.L.; Fischer, P.J.; Tarr, D.A. *Inorganic Chemistry*, 5th ed.; Pearson: Boston, MA, USA, 2014; pp. 313–470.

4. Murrie, M.; Price, D.J. Molecular Magnetism. *Annu. Rep. Prog. Chem. Sect.* **2007**, *103*, 20–38. [CrossRef]

5. Kahn, O. Dinuclear complexes with predictable magnetic properties. *Angew. Chem. Int. Ed. Engl.* **1985**, *24*, 834–850.

6. Coronado, E.; Drillon, M.; Nugteren, P.R.; de Jongh, L.J.; Beltran, D.; Georges, R. Low-Temperature investigation of the ferrimagnetic chains MnM′(EDTA)·6H$_2$O (M′ = Co, Ni, and Cu(II)): Thermal and magnetic properties. *J. Am. Chem. Soc.* **1989**, *111*, 3874–3880.

7. Caneschi, A.; Gatteschi, D.; Sessoli, R.; Rey, P. Toward molecular magnets: The metal-radical approach. *Acc. Chem. Res.* **1989**, *22*, 392–398. [CrossRef]

8. Stumpf, H.O.; Quahab, L.; Pei, Y.; Grandjean, D.; Kahn, O. A molecular-based magnet with a fully interlocked 3-dimensional structure. *Science* **1993**, *261*, 447–449. [CrossRef]

9. Ferlay, S.; Mallah, T.; Quahes, R.; Veillet, P.; Verdaguer, M. A room-temperature organometallic magnet based on Prussian blue. *Nature* **1995**, *378*, 701–703. [CrossRef]

10. Holmes, S.M.; Girolami, G.S. Sol-Gel Synthesis of KV^{II}[Cr^{III}(CN)$_6$]·2H$_2$O: A Crystalline molecule-based magnet with a magnetic ordering temperature above 100 °C. *J. Am. Chem. Soc.* **1999**, *121*, 5593–5594. [CrossRef]

11. Manriquez, J.M.; Yee, G.T.; McLean, R.S.; Epstein, A.J.; Miller, J.S. A Room-Temperature molecular/organic-based magnet. *Science* **1991**, *252*, 1415–1417. [CrossRef] [PubMed]

12. Gütlich, P.; Garcia, Y.; Goodwin, H.A. Spin crossover phenomena in Fe(II) complexes. *Chem. Soc. Rev.* **2000**, *29*, 419–427. [CrossRef]

13. Brooker, S. Spin crossover with thermal hysteresis: Practicalities and lessons learnt. *Chem. Soc. Rev.* **2015**, *44*, 2880–2892. [PubMed]

14. Lada, Z.G.; Andrikopoulos, K.S.; Chrissanthopoulos, A.; Perlepes, S.P.; Voyiatzis, G.A. A known Iron(II) Complex in Different Nanosized Particles: Variable-Temperature Raman Study of Its Spin-Crossover Behavior. *Inorg. Chem.* **2019**, *58*, 5183–5195. [CrossRef] [PubMed]

15. Aguilà, D.; Prado, Y.; Koumousi, E.S.; Mathonière, C.; Clérac, R. Switchable Fe/Co Prussian blue networks and molecular analogues. *Chem. Soc. Rev.* **2016**, *45*, 203–224. [CrossRef] [PubMed]

16. Linares, J.; Codjovi, E.; Garcia, Y. Pressure and temperature spin crossover sensors with optical detection. *Sensors* **2012**, *12*, 4479–4492. [CrossRef] [PubMed]

17. Molnár, G.; Rat, S.; Salmon, L.; Nicolazzi, W.; Bousseksou, A. Spin crossover nanomaterials: From fundamental concepts to devices. *Adv. Mater.* **2018**, *30*, 1703862. [CrossRef]

18. Kahn, O.; Jay Martínez, C. Spin-transition polymers: From molecular materials toward memory devices. *Science* **1998**, *279*, 44–48. [CrossRef]

19. Coronado, E. Molecular magnetism: From chemical design to spin control in molecules, materials and devices. *Nat. Rev. Mater.* **2020**, *5*, 87–104. [CrossRef]

20. Gatteschi, D.; Bogani, L.; Cornia, A.; Mannini, M.; Sorace, L.; Sessoli, R. Molecular magnetism, status and perspectives. *Solid State Sci.* **2008**, *10*, 1701–1709. [CrossRef]

21. Launay, J.-P.; Verdaguer, M. *Electrons in Molecules*, revised ed.; Oxford University Press: Oxford, UK, 2018; pp. 187–190, 207–223.

22. Gatteschi, D.; Sessoli, R.; Villain, J. *Molecular Nanomagnets*; Oxford University Press: Oxford, UK, 2006.

23. Bagai, R.; Christou, G. The Drosophila of single-molecule magnetism: [Mn$_{12}$O$_{12}$(O$_2$CR)$_{16}$(H$_2$O)$_4$]. *Chem. Soc. Rev.* **2009**, *38*, 1011–1026. [CrossRef]

24. Thomas, L.; Lionti, F.; Ballou, R.; Gatteschi, D.; Sessoli, R.; Barbara, B. Macroscopic quantum tunneling of magnetization in a single crystal of nanomagnets. *Nature* **1996**, *383*, 145–147. [CrossRef]

25. Friedman, J.R.; Sarachik, M.P.; Tejada, J.; Ziolo, R. Macroscopic measurement of resonant magnetization tunneling in high-spin molecules. *Phys. Rev. Lett.* **1996**, *76*, 3830–3833. [CrossRef]

26. Craig, G.A.; Murrie, M. 3d-single ion magnets. *Chem. Soc. Rev.* **2015**, *44*, 2135–2147. [CrossRef] [PubMed]

27. Frost, J.M.; Harriman, K.L.M.; Murugesu, M. The rise of 3d single-ion magnets in molecular magnetism: Towards materials from molecules? *Chem. Sci.* **2016**, *7*, 2470–2491. [CrossRef] [PubMed]

28. Martínez-Lillo, J.; Mastropierto, T.F.; Lhotel, E.; Paulsen, C.; Cano, J.; De Munno, G.; Faus, J.; Lloret, F.; Julve, M.; Nellutla, S.; et al. Highly anisotropic Rhenium(IV) complexes: New examples of mononuclear single-molecule magnets. *J. Am. Chem. Soc.* **2013**, *135*, 13737–13748. [CrossRef] [PubMed]

29. Feng, M.; Tong, M.-L. Single ion magnets from 3d to 5f: Developments and strategies. *Chem. Eur. J.* **2018**, *24*, 7574–7594. [CrossRef]

30. Harriman, K.L.M.; Errulat, D.; Murugesu, M. Magnetic axiality: Design principles from molecules to materials. *Trends Chem.* **2019**, *1*, 425–439. [CrossRef]

31. Woodruff, D.N.; Winpenny, R.E.P.; Layfield, R.A. Lanthanide single-molecule magnets. *Chem. Rev.* **2013**, *113*, 5110–5148. [CrossRef]

32. Pointillart, F.; Cador, O.; Le Guennic, B.; Quahab, L. Uncommon lanthanide ions in purely 4f Single Molecule Magnets. *Coord. Chem. Rev.* **2017**, *346*, 150–175. [CrossRef]

33. Gupta, S.K.; Murugavel, R. Enriching lanthanide single-ion magnetism through symmetry and axiality. *Chem. Commun.* **2018**, *54*, 3685–3696. [CrossRef]

34. Meihaus, K.R.; Long, J.R. Actinide-based single-molecule magnets. *Dalton Trans.* **2015**, *44*, 2517–2528. [CrossRef]

35. Ishikawa, N.; Sugita, M.; Ishikawa, T.; Koshihara, S.-U.; Kaizu, Y. Lanthanide double-decker complexes functioning as magnets at the single-molecule level. *J. Am. Chem. Soc.* **2003**, *125*, 8694–8695. [CrossRef]

36. Guo, F.-S.; Day, B.M.; Chen, Y.-C.; Tong, M.-L.; Mansikkamäki, A.; Layfield, R.A. Magnetic hysteresis up to 80 Kelvin in a Dysprosium metallocene single-molecule magnet. *Science* **2018**, *362*, 1400–1403. [CrossRef] [PubMed]

37. Gaita-Ariño, A.; Luis, F.; Hill, S.; Coronado, E. Molecular spins for quantum computation. *Nat. Chem.* **2019**, *11*, 301–309. [CrossRef] [PubMed]

38. Miyasaka, H.; Julve, M.; Yamashita, M.; Clérac, R. Slow Dynamics of the Magnetization in One-dimensional coordination polymers: Single-chain magnets. *Inorg. Chem.* **2009**, *48*, 3420–3437. [CrossRef] [PubMed]

39. Rams, M.; Jochim, A.; Böhme, M.; Lohmiller, T.; Ceglarska, M.; Rams, M.M.; Schnegg, A.; Plass, W.; Näther, C. Single-Chain magnet based on Cobalt(II) thiocyanate as XXZ spin chain. *Eur. J. Inorg. Chem.* **2020**, 2837–2851. [CrossRef]

40. Caneschi, A.; Gatteschi, D.; Lalioti, N.; Sangregorio, C.; Sessoli, R.; Venturi, G.; Vindigni, A.; Rettori, A.; Pini, M.G.; Novak, M.A. Cobalt(II)-Nitronyl nitroxide chains as molecular magnetic nanowires. *Angew. Chem. Int. Ed.* **2001**, *40*, 1760–1763. [CrossRef]

41. Maspoch, D.; Ruiz-Molina, D.; Wurst, K.; Domingo, N.; Cavallini, M.; Biscarini, F.; Tejada, J.; Rovira, C.; Veciana, J. A nanoporous molecular magnet with reversible solvent-induced mechanical and magnetic properties. *Nat. Mater.* **2003**, *2*, 190–195. [CrossRef]

42. Coronado, E.; Gómez-Garcia, C.J.; Nuez, A.; Romero, F.M.; Waerenborgh, J.C. Synthesis, chirality and magnetic properties of bimetallic Cyanide-bridged Two-dimensional ferromagnets. *Chem. Mater.* **2006**, *18*, 2670–2681.

43. Train, C.; Gheorge, R.; Krstic, V.; Chamoreau, L.-M.; Ovanesyan, N.S.; Rikken, G.L.J.A.; Gruselle, M.; Verdaguer, M. Strong magneto-chiral dichroism in enantiopure chiral ferromagnets. *Nat. Mater.* **2008**, *7*, 729–734.

44. Coronado, E.; Galán-Mascarós, J.R.; Gómez-Garcia, C.J.; Laukhin, V. Coexistence of ferromagnetism and metallic conductivity in a molecule-based layered compound. *Nature* **2000**, *408*, 447–449.

45. Errulat, D.; Marin, R.; Gálico, D.A.; Harriman, K.L.M.; Pialat, A.; Gabidullin, B.; Iikawa, F.; Couto, J.O.D.D.; Moilanen, J.O.; Hemmer, E.; et al. A Luminescent thermometer exhibiting slow relaxation of the magnetization: Toward Self-Monitored building blocks for Next-Generation optomagnetic devices. *ACS Cent. Sci.* **2019**, *5*, 1187–1198. [CrossRef]

46. Anastasiadis, N.C.; Granadeiro, C.M.; Mayans, J.; Raptopoulou, C.P.; Bekiari, V.; Cunha-Silva, L.; Psycharis, V.; Escuer, A.; Balula, S.S.; Konidaris, K.F.; et al. Multifunctionality in two families of dinuclear Lanthanide(III) complexes with a tridentate schiff-base ligand. *Inorg. Chem.* **2019**, *58*, 9581–9585. [CrossRef] [PubMed]

47. Aromi, G.; Aguilà, D.; Gamez, P.; Luis, F.; Roubeau, O. Design of magnetic coordination complexes for quantum computing. *Chem. Soc. Rev.* **2012**, *41*, 537–546. [CrossRef] [PubMed]

48. Katoh, K.; Isshiki, H.; Komeda, T.; Yamashita, M. Molecular spintronics based on single-molecule magnets composed of mutliple-decker phthalocyaninato Terbium(III) complex. *Chem. Asian J.* **2012**, *7*, 1154–1169. [CrossRef] [PubMed]

49. Fernandez, A.; Ferrando-Soria, J.; Moreno Pineda, E.; Tuna, F.; Vitorica-Yrezabal, I.J.; Knappke, C.; Ujma, J.; Muryn, C.A.; Timco, G.A.; Barran, P.E.; et al. Making hybrid [n]-rotaxanes as supramolecular arrays of molecular electron spin qubits. *Nat. Commun.* **2016**, *7*, 10240.

50. Pedersen, K.S.; Perlepe, P.S.; Aubey, M.L.; Woodruff, D.N.; Reyes-Lillo, S.E.; Reinholdt, A.; Voigt, L.; Li, Z.; Borup, K.; Rouzières, M.; et al. Formation of the layered conductive magnet $CrCl_2(pyrazine)_2$ through redox-active coordination chemistry. *Nat. Chem.* **2018**, *10*, 1056–1061.

51. Minguez Espallargas, G.; Coronado, E. Magnetic functionalities in MOFs: From the framework to the pore. *Chem. Soc. Rev.* **2018**, *47*, 533–557.

52. Ribas Gispert, J. *Coordination Chemistry*; Wiley-VCH: Weinheim, Germany, 2008; pp. XXXIX, XL, 31–57.

53. Cotton, F.A.; Wilkinson, G.; Murillo, C.A.; Bochmann, M. *Advanced Inorganic Chemistry*, 6th ed.; Wiley: New York, NY, USA, 1999.

54. Busch, D.H. The Compleat coordination chemistry-one practioner's perspective. *Chem. Rev.* **1993**, *93*, 847–860. [CrossRef]

55. Lada, Z.G.; Katsoulakou, E.; Perlepes, S.P. Synthesis and Chemistry of Single-molecule Magnets. In *Single-Molecule Magnets: Molecular Architectures and Building Blocks for Spintronics*; Holynska, M., Ed.; Wiley-VCH: Weinheim, Germany, 2019; pp. 245–313.

56. Maniaki, D.; Pilichos, E.; Perlepes, S.P. Coordination clusters of 3d-metals that behave as Single-Molecule Magnets (SMMs): Synthetic routes and strategies. *Front. Chem.* **2018**, *6*, 461. [CrossRef]

57. Bar, A.K.; Pichon, C.; Sutter, J.-P. Magnetic anisotropy in two- to eight-coordinated transition-metal complexes: Recent developments in molecular magnetism. *Coord. Chem. Rev.* **2016**, *308*, 346–380. [CrossRef]

58. Beltran, L.M.; Long, J.R. Directed assembly of metal cyanide cluster magnets. *Acc. Chem. Res.* **2005**, *38*, 325–334. [CrossRef]

59. Aromi, G.; Brechin, E.K. Synthesis of 3d metallic single-molecule magnets. *Struct. Bond.* **2006**, *122*, 1–67.

60. Milios, C.J.; Winpenny, R.E.P. Cluster-based single-molecule magnets. *Struct. Bond.* **2015**, *164*, 1–109.

61. Coxall, R.A.; Harris, S.G.; Henderson, D.K.; Parsons, S.; Tasker, P.A.; Winpenny, R.E.P. Inter-ligand reactions: In situ formation of new polydentate ligands. *J. Chem. Soc. Dalton Trans.* **2000**, 2349–2356. [CrossRef]

62. Escuer, A.; Aromi, G. Azide as a bridging ligand and magnetic coupler in transition metal clusters. *Eur. J. Inorg. Chem.* **2006**, *2006*, 4721–4736. [CrossRef]

63. Escuer, A.; Esteban, J.; Perlepes, S.P.; Stamatatos, T.C. The bridging azido ligand as a central "player" in high-nuclearity 3d-metal cluster chemistry. *Coord. Chem. Rev.* **2014**, *275*, 87–129. [CrossRef]

64. Stamatatos, T.C.; Christou, G. Azide groups in higher oxidation state manganese cluster chemistry. *Inorg. Chem.* **2009**, *48*, 3308–3322. [CrossRef]

65. Schweinfurth, D.; Sommer, M.G.; Atanasov, M.; Demeshko, S.; Hohlock, S.; Meyer, F.; Neese, F.; Sarkar, B. The ligand field of the azido ligand: Insights into bonding parameters and magnetic anisotropy in a Co(II)-Azido complex. *J. Am. Chem. Soc.* **2015**, *137*, 1993–2005. [CrossRef]

66. Papaefstathiou, G.S.; Perlepes, S.P.; Escuer, A.; Vicente, R.; Font-Bardia, M.; Solans, X. Unique single-atom binding of pseudohalogeno ligands to four metal ions induced by their trapping into high-nuclearity cages. *Angew. Chem. Int. Ed.* **2001**, *40*, 884–886. [CrossRef]

67. Papaefstathiou, G.S.; Escuer, A.; Vicente, R.; Font-Bardia, M.; Solans, X.; Perlepes, S.P. Reactivity in polynuclear transition metal chemistry as a means to obtain high-spin molecules: Substitution of μ_4-OH$^-$ by η^1,μ_4-N$_3^-$ increases nine times the ground state S value of a nonanuclear Nickel(II) cage. *Chem. Commun.* **2001**, 2414–2415. [CrossRef]

68. Boudalis, A.K.; Donnadieu, B.; Nastopoulos, V.; Clemente-Juan, J.M.; Mari, A.; Sanakis, Y.; Tuchagues, J.-P.; Perlepes, S.P. A Nonanuclear Iron(II) single-molecule magnet. *Angew. Chem. Int. Ed.* **2004**, *43*, 2266–2270. [CrossRef]

69. Boudalis, A.K.; Sanakis, Y.; Clemente-Juan, J.M.; Donnadieu, B.; Nastopoulos, V.; Mari, A.; Coppel, Y.; Tuchagues, S.P.; Perlepes, S.P. A family of enneanuclear Iron(II) single-molecule magnets. *Chem. Eur. J.* **2008**, *14*, 2514–2526.

70. Stamatatos, T.C.; Rentschler, E. Organic chelate-free and azido-rich metal clusters and coordination polymers from the use of Me$_3$SiN$_3$: A new synthetic route to complexes with beautiful structures and diverse magnetic properties. *Chem. Commun.* **2019**, *55*, 11–26. [CrossRef]

71. Alexandropoulos, D.I.; Vignesh, K.R.; Stamatatos, T.C.; Dunbar, K.R. Rare "Janus"-faced {Fe^{II}$_7$} single-molecule magnet exhibiting intramolecular ferromagnetic interactions. *Chem. Sci.* **2019**, *10*, 1626–1633. [CrossRef]

72. Alexandropoulos, D.I.; Cunha-Silva, L.; Escuer, A.; Stamatatos, T.C. New classes of ferromagnetic materials with exclusively end-on Azido Bridges: From single-molecule magnets to 2D molecule-based magnets. *Chem. Eur. J.* **2014**, *20*, 13860–13864. [CrossRef]

73. Alexandropoulos, D.I.; Fournet, A.; Cunha-Silva, L.; Christou, G.; Stamatatos, T.C. "Molecular Nanoclusters": A 2-nm-Sized {Mn$_{29}$} cluster with a spherical structure. *Inorg. Chem.* **2016**, *55*, 12118–12121.

74. Coronado, E.; Dunbar, K.R. Preface for the forum of molecular magnetism: The role of inorganic chemistry. *Inorg. Chem.* **2009**, *48*, 3293–3295. [CrossRef] [PubMed]

75. Ludi, A. Prussian blue, an inorganic evergreen. *J. Chem. Educ.* **1981**, *58*, 1013.

76. Waldmann, O. A criterion for the anisotropy barrier in single-molecule magnets. *Inorg. Chem.* **2007**, *46*, 10035–10037. [CrossRef] [PubMed]

77. Sokol, J.J.; Hee, A.G.; Long, J.R. A cyano-bridged single-molecule magnet: Slow magnetic relaxation in a trigonal prismatic MnMo$_6$(CN)$_{18}$ cluster. *J. Am. Chem. Soc.* **2002**, *124*, 7656–7657. [PubMed]

78. Schelter, E.J.; Prosvirin, A.V.; Dunbar, K.R. Molecular cube of Re^{II} and Mn^{II} that exhibits single-molecule magnetism. *J. Am. Chem. Soc.* **2004**, *126*, 15004–15005. [CrossRef] [PubMed]

79. Schelter, E.J.; Karadas, F.; Avendano, C.; Prosvirin, A.V.; Wernsdorfer, W.; Dunbar, K.R. A family of mixed-metal cyanide cubes with alternating octahedral and tetrahedral corners exhibiting a variety of magnetic behaviors including single molecule magnetism. *J. Am. Chem. Soc.* **2007**, *129*, 8139–8149. [PubMed]

80. Freedman, D.E.; Jenkins, D.M.; Lavarone, A.T.; Long, J.R. A redox-switchable single-molecule magnet incorporating [Re(CN)$_7$]$^{3-}$. *J. Am. Chem. Soc.* **2008**, *130*, 2884–2885. [PubMed]

81. Zadrozny, J.M.; Freedman, D.E.; Jenkins, D.M.; Harris, T.D.; Lavarone, A.T.; Mathionière, C.; Clérac, R.; Long, J.R. Slow Magnetic relaxation and charge-transfer in cyano-bridged coordination clusters incorporating [Re(CN)$_7$]$^{3-/4-}$. *Inorg. Chem.* **2010**, *49*, 8886–8896. [CrossRef] [PubMed]

82. Feng, X.; Liu, J.; Harris, T.D.; Hill, S.; Long, J.R. Slow magnetic relaxation induced by a large transverse zero-field splitting in a Mn^{II}Re^{IV}(CN)$_2$ single-chain magnet. *J. Am. Chem. Soc.* **2012**, *134*, 7521–7529. [CrossRef]

83. Pinkowicz, D.; Southerland, H.I.; Avendaño, C.; Prosvirin, A.; Sanders, C.; Wernsdorfer, W.; Pedersen, K.S.; Dreiser, J.; Clérac, R.; Nehrkorn, J.; et al. Cyanide single-molecule magnets exhibiting solvent dependent reversible "on" and "off" exchange bias behavior. *J. Am. Chem. Soc.* **2015**, *137*, 14406–14422.

84. Wang, X.-Y.; Avendaño, C.; Dunbar, K.R. Molecular magnetic materials based on 4d and 5d transition metals. *Chem. Soc. Rev.* **2011**, *40*, 3213–3238.

85. Pinkowicz, D.; Rodgajny, R.; Nowicka, B.; Chorazy, S.; Reczyński, M.; Sieklucka, B. Magnetic clusters based on octacyanidometallates. *Inorg. Chem. Front.* **2015**, *2*, 10–27. [CrossRef]

86. Rebilly, J.-N.; Mallah, T. Synthesis of Single-Molecule Magnets Using Metallocyanates. In *Single-Molecule Magnets and Related Phenomena*; Winpenny, R.E.P., Ed.; Springer: Berlin, Germany, 2006; pp. 103–131.

87. Schelter, E.J.; Bera, J.K.; Basca, J.; Galán-Mascarós, J.R.; Dunbar, K.R. New paramagnetic Re(II) compounds with nitrile and cyanide ligands prepared by homolytic scission of dirhenium complexes. *Inorg. Chem.* **2003**, *42*, 4256–4258.

88. Bennett, M.V.; Long, J.R. New cyanometalate building units: Synthesis and characterization of [Re(CN)$_7$]$^{3-}$ and [Re(CN)$_8$]$^{3-}$. *J. Am. Chem. Soc.* **2003**, *125*, 2394–2395. [CrossRef]

89. Atanasov, M.; Zadrozny, J.M.; Long, J.R.; Neese, F. A theoretical analysis of chemical bonding, vibronic coupling and magnetic anisotropy in linear Iron(II) complexes with single-molecule magnet behavior. *Chem. Sci.* **2013**, *4*, 139–156. [CrossRef]

90. Beagley, B.; Pritchard, R.G.; Eaborn, C.; Washburne, S.S. A gas-phase electron diffraction study of tris(trimethylsilyl)methane. A C–H bond of high p-character. *J. Chem. Soc. Chem. Commun.* **1981**, 710–711. [CrossRef]

91. Longshaw, A.I.; Carland, M.W.; Krenske, E.H.; Coote, M.L.; Sherburn, M.S. Tris(trimethylsilyl)methane is not an effective mediator of radical reactions. *Tetrahedron Lett.* **2007**, *48*, 5585–5588. [CrossRef]

92. Cook, M.A.; Eaborn, C.; Jukes, A.E.; Walton, D.R.M. [Tris(trimethylsilyl)methyl]lithim: An alkyllithium compound of unusual stability. *J. Organomet. Chem.* **1970**, *24*, 529–535. [CrossRef]

93. LaPointe, A.M. Fe[C(SiMe₃)₃]₂: Synthesis and reactivity of a monomeric homoleptic Iron(II) alkyl complex. *Inorg. Chim. Acta* **2003**, *345*, 359–362. [CrossRef]

94. Zadrozny, J.M.; Atanasov, M.; Bryan, A.M.; Lin, C.-Y.; Rekken, B.D.; Power, P.P.; Neese, F.; Long, J.R. Slow magnetization dynamics in a series of two-coordinate Iron(II) complexes. *Chem. Sci.* **2013**, *4*, 125–138.

95. Kramers, H.A. A general theory of paramagnetic rotation in crystals. *Proc. R. Acad. Sci. Amst.* **1930**, *33*, 959–972.

96. Zadrozny, J.M.; Xiao, D.J.; Atanasov, M.; Long, G.J.; Grandjean, F.; Neese, F.; Long, J.R. Magnetic blocking in a linear Iron(I) complex. *Nat. Chem.* **2013**, *5*, 577–581. [CrossRef]

97. Bill, E. Iron lines up. *Nat. Chem.* **2013**, *5*, 556–557. [CrossRef]

98. Zadrozny, J.M.; Xiao, D.X.; Long, J.R.; Atanasov, M.; Neese, F.; Grandjean, F.; Long, G.J. Mössbauer spectroscopy as a probe of magnetization dynamics in the linear Iron(I) and Iron(II) complexes [Fe(C(SiMe₃)₃)₂]$^{1-/0}$. *Inorg. Chem.* **2013**, *52*, 13123–13131. [CrossRef]

99. Rau, I.G.; Baumann, S.; Rusponi, S.; Donati, F.; Stepanow, S.; Gragnaniello, L.; Dreiser, J.; Piamonteze, C.; Nolting, F.; Gangopadhyay, S.; et al. Reaching the magnetic anisotropy limit of a 3d metal atom. *Science* **2014**, *344*, 988–992. [CrossRef]

100. Atanasov, M.; Aravena, D.; Suturina, E.; Bill, E.; Maganas, D.; Neese, F. First principles approach to the electronic structure, magnetic anisotropy and spin relaxation in mononuclear 3d-transition metal single molecule magnets. *Coord. Chem. Rev.* **2015**, *289–290*, 177–214. [CrossRef]

101. Bunting, P.C.; Atanasov, M.; Damgaard-Møller, E.; Perfetti, M.; Crassee, I.; Orlita, M.; Overgaard, J.; van Slageren, J.; Long, J.R. A linear Cobalt(II) complex with maximal orbital angular momentum from a non-Aufbau ground state. *Science* **2018**, *362*, 7319. [CrossRef] [PubMed]

102. Yao, X.-N.; Du, J.-Z.; Zhang, Y.-Q.; Leng, X.-B.; Yang, W.-W.; Jiang, S.-D.; Wang, Z.-X.; Quyang, Z.-W.; Deng, L.; Wang, B.-W.; et al. Two-Coordinate Co(II) Imido complexes as outstanding single-molecule magnets. *J. Am. Chem. Soc.* **2017**, *139*, 373–380. [CrossRef] [PubMed]

103. Vaida, S.; Shulka, P.; Tripathi, S.; Rivière, E.; Mallah, T.; Rajaraman, G.; Shanmugam, M. Substituted versus naked thiourea ligand containing pseudotetrahedral Cobalt(II) complexes: A comparative study on its magnetization relaxation dynamics phenomenon. *Inorg. Chem.* **2018**, *57*, 3371–3386. [CrossRef] [PubMed]

104. Zadrozny, J.M.; Long, J.R. Slow magnetic relaxation at zero field in the tetrahedral complex [Co(SPh)₄]$^{2-}$. *J. Am. Chem. Soc.* **2011**, *133*, 20732–20734. [CrossRef] [PubMed]

105. Zadrozny, J.M.; Telser, J.; Long, J.R. Slow magnetic relaxation in the tetrahedral Cobalt(II) complexes [Co(EPh)₄]$^{2-}$ (E = O, S, Se). *Polyhedron* **2013**, *64*, 209–217. [CrossRef]

106. Suturina, E.A.; Maganas, D.; Bill, E.; Atanasov, M.; Neese, F. Magneto-Structural correlations in a series of pseudotetrahedral [Co^{II}(XR)₄]$^{2-}$ single molecule magnets: An ab initio ligand field study. *Inorg. Chem.* **2015**, *54*, 9948–9961. [CrossRef]

107. Suturina, E.; Nehrkorn, J.; Zadrozny, J.M.; Liu, J.; Atanasov, M.; Weyhermüller, T.; Maganas, D.; Hill, S.; Schnegg, A.; Bill, E.; et al. Magneto-Structural correlations in pseudotetrahedral forms of the [Co(SPh)₄]$^{2-}$ complex probed by magnetometry, MCD spectroscopy, advanced EPR techniques, and ab initio electronic structure calculations. *Inorg. Chem.* **2017**, *56*, 3102–3118. [CrossRef]

108. Saber, M.R.; Dunbar, K.R. Ligand effects on the magnetic anisotropy of tetrahedral Cobalt complexes. *Chem. Commun.* **2014**, *50*, 12266–12269. [CrossRef]

109. Vaidya, S.; Upadhyay, A.; Singh, S.K.; Gupta, T.; Tewary, S.; Langley, S.K.; Walsh, J.P.S.; Murray, K.S.; Rajaraman, G.; Shanmugan, M. A synthetic strategy for switching the single ion anisotropy in tetrahedral Co(II) complexes. *Chem. Commun.* **2015**, *51*, 3739–3742. [CrossRef]

110. Mezei, G.; Zaleski, C.M.; Pecoraro, V.L. Structural and functional evolution of metallacrowns. *Chem. Rev.* **2007**, *107*, 4933–5003. [CrossRef] [PubMed]

111. Baskin, J.M.; Bertozzi, C.R. Copper-Free click chemistry: Bioorthogonal reagents for tagging azides. *Aldrichim. Acta* **2010**, *43*, 15–23.

112. Kolb, H.C.; Finn, M.G.; Sharpless, K.B. Click chemistry: Diverse chemical function from a few good reactions. *Angew. Chem. Int. Ed.* **2001**, *40*, 2004–2021. [CrossRef]

113. Happ, P.; Plenk, C.; Rentschler, E. 12-MC-4 metallacrowns as versatile tools for SMM research. *Coord. Chem. Rev.* **2015**, *289–290*, 238–260. [CrossRef]

114. Plenk, C.; Krause, J.; Beck, M.; Rentschler, E. Rational linkage of magnetic molecules using click chemistry. *Chem. Commun.* **2015**, *51*, 6524–6527. [CrossRef]

115. Plenk, C.; Krause, J.; Rentschler, E. A Click-Funtionalized single-molecule magnet based on Cobalt(II) and its analogous Manganese(II) and Zinc(II) compounds. *Eur. J. Inorg. Chem.* **2015**, *2015*, 370–374. [CrossRef]

116. Bolcar, M.A.; Aubin, S.M.J.; Folting, K.; Hendrickson, D.N.; Christou, G. A new Manganese cluster topology capable of yielding high-spin species: Mixed-valence $[Mn_7(OH)_3Cl_3(hmp)_9]^{2+}$ with S ≥ 10. *Chem. Commun.* **1997**, 1485–1486. [CrossRef]

117. Boscovic, C.; Brechin, E.K.; Streib, W.E.; Folting, K.; Hendrickson, D.N.; Christou, G. A new class of single-molecule magnets: Mixed-valent $[Mn_{12}O_8Cl_4(O_2CPh)_8(hmp)_6]$. *Chem. Commun.* **2001**, 467–468. [CrossRef]

118. You, J.; Yamaguchi, A.; Nakano, M.; Krzystek, J.; Streib, W.E.; Brunel, L.-C.; Ishimoto, H.; Christou, G.; Hendrickson, D.N. Mixed-Valence tetranuclear single-molecule magnets. *Inorg. Chem.* **2001**, *40*, 4604–4616. [CrossRef]

119. Brechin, E.K.; Boskovic, C.; Wernsdorfer, W.; You, J.; Yamaguchi, A.; Sañudo, E.C.; Concolino, T.R.; Rheingold, A.L.; Ishimoto, H.; Hendrickson, D.N.; et al. Quantum tunneling of magnetization in a new $[Mn_{18}]^{2+}$ single-molecule magnet with S = 13. *J. Am. Chem. Soc.* **2002**, *124*, 9710–9711. [CrossRef]

120. Sañudo, E.C.; Brechin, E.K.; Boskovic, C.; Wernsdorfer, W.; Yoo, J.; Yamaguchi, A.; Concolino, T.R.; Abboud, K.A.; Rheingold, A.L.; Ishimoto, H.; et al. $[Mn_{18}]^{2+}$ and $[Mn_{21}]^{4+}$ single-molecule magnets. *Polyhedron* **2003**, *22*, 2267–2271. [CrossRef]

121. Yang, E.-C.; Wernsdorfer, W.; Hill, S.; Edwards, R.S.; Nakano, M.; Maccagnano, S.; Zakharov, L.N.; Rheingold, A.L.; Christou, G.; Hendrickson, D.N. Exchange bias in Ni₄ single-molecule magnets. *Polyhedron* **2003**, *22*, 1727–1733. [CrossRef]

122. Boskovic, C.; Brechin, E.K.; Streib, W.E.; Folting, K.; Bollinger, J.C.; Hendrickson, D.N.; Christou, G. Single-Molecule magnets: A new family of Mn₁₂ clusters of formula $[Mn_{12}O_8X_4(O_2CPh)_8L_6]$. *J. Am. Chem. Soc.* **2002**, *124*, 3725–3736. [PubMed]

123. Harden, N.C.; Bolcar, M.A.; Wernsdorfer, W.; Abboud, K.A.; Streib, W.E.; Christou, G. Heptanuclear and decanuclear Manganese complexes with the anion of 2-hydroxymethylpyridine. *Inorg. Chem.* **2003**, *42*, 7067–7076. [CrossRef] [PubMed]

124. Sañudo, E.C.; Wernsdorfer, W.; Abboud, K.A.; Christou, G. Synthesis, structure, and magnetic properties of a Mn₂₁ single-molecule magnet. *Inorg. Chem.* **2004**, *43*, 4137–4144.

125. Brechin, E.K.; Sañudo, E.C.; Wernsdorfer, W.; Boskovic, C.; Yoo, J.; Hendrickson, D.N.; Yamaguchi, A.; Ishimoto, I.; Concolino, T.E.; Rheingold, A.L.; et al. Single-Molecule magnets: Structure and properties of $[Mn_{18}O_{14}(O_2CMe)_{18}(hep)_4(hepH)_2(H_2O)_2](ClO_4)_2$ with S = 13. *Inorg. Chem.* **2005**, *44*, 502–511.

126. Stamatatos, T.C.; Abboud, K.A.; Wernsdorfer, W.; Christou, G. High-Nuclearity, high-symmetry, high-spin molecules: A Mixed-Valence Mn₁₀ cage possessing rare T symmetry and an S = 22 ground state. *Angew. Chem. Int. Ed.* **2006**, *45*, 4134–4137.

127. Stamatatos, T.C.; Boudalis, A.K.; Pringouri, K.V.; Raptopoulou, C.P.; Terzis, A.; Wolowska, J.; McInnes, E.J.L.; Perlepes, S.P. Mixed-Valence Cobalt(II/III) carboxylate clusters: $Co^{II}_4Co^{III}_2$ and $Co^{II}Co^{III}_2$ complexes from the use of 2-(Hydroxymethyl)pyridine. *Eur. J. Inorg. Chem.* **2007**, 5098–5104. [CrossRef]

128. Stamatatos, T.C.; Poole, K.M.; Abboud, K.A.; Wernsdorfer, W.; O'Brien, T.A.; Christou, G. High-Spin Mn₄ and Mn₁₀ molecules: Large spin changes with structure in mixed-valence $Mn^{II}_4Mn^{III}_6$ clusters with azide and alkoxide-based ligands. *Inorg. Chem.* **2008**, *47*, 5006–5021.

129. Efthymiou, C.G.; Papatriantafyllopoulou, C.; Alexopoulou, N.I.; Raptopoulou, C.P.; Boča, R.; Mrozinski, J.; Bakalbassis, E.G.; Perlepes, S.P. A mononuclear complex and a cubane cluster from the initial use of 2-(hydroxymethyl)pyridine in Nickel(II) carboxylate chemistry. *Polyhedron* **2009**, *28*, 3373–3381. [CrossRef]

130. Taguchi, T.; Daniels, M.R.; Abboud, K.A.; Christou, G. Mn_4, Mn_6 and Mn_{11} clusters from the use of bulky diphenyl(pyridine-2-yl)methanol. *Inorg. Chem.* **2009**, *48*, 9235–9245.

131. Taguchi, T.; Wernsdorfer, W.; Abboud, K.A.; Christou, G. Mn_8 and Mn_{16} clusters from the use of 2-(Hydroxymethyl)pyridine, and comparison with the products from bulkier chelates: A new high nuclearity single-molecule magnet. *Inorg. Chem.* **2010**, *49*, 10579–10589. [CrossRef] [PubMed]

132. Papatriantafyllopoulou, C.; Abboud, K.A.; Christou, G. Carboxylate-Free $Mn^{III}_2Ln^{III}_2$ (Ln = Lanthanide) and $Mn^{III}_2Y^{III}_2$ complexes from the use of (2-hydroxymethyl)pyridine: Analysis of spin frustration effects. *Inorg. Chem.* **2011**, *50*, 8959–8966. [CrossRef] [PubMed]

133. Abbasi, P.; Quinn, K.; Alexandropoulos, D.I.; Damjanovich, M.; Wernsdorfer, W.; Escuer, A.; Mayans, J.; Pilkington, M.; Stamatatos, T.C. Transition metal single-molecule magnets: A {Mn_{31}} Nano-sized Cluster with a large energy barrier of ~60 K and magnetic hysteresis at ~5 K. *J. Am. Chem. Soc.* **2017**, *139*, 15644–15647. [CrossRef] [PubMed]

134. March, J. *Advanced Organic Chemistry*, 4th ed.; Wiley: New York, NY, USA, 1992; pp. 882–883.

135. Wilkinson, S.G. Alcohols. In *Comprehensive Organic Chemistry*; Barton, D., Ollis, D., Eds.; Pergamon Press: Oxford, UK, 1979; Volume 1, Chapter 4.1; pp. 579–706.

136. Tasiopoulos, A.J.; Perlepes, S.P. Diol-type ligands as central 'players' in the chemistry of high-spin molecules and single-molecule magnets. *Dalton Trans.* **2008**, 5537–5555. [CrossRef]

137. Papatriantafyllopoulou, C.; Moushi, E.E.; Christou, G.; Tasiopoulos, A.J. Filling the gap between the quantum and classical worlds of nanoscale magnetism: Giant molecular aggregates based on paramagnetic 3d metal ions. *Chem. Soc. Rev.* **2016**, *45*, 1597–1628. [CrossRef]

138. Moushi, E.E.; Lampropoulos, C.; Wernsdorfer, W.; Nastopoulos, V.; Christou, G.; Tasiopoulos, A.J. A large [$Mn_{10}Na$]$_4$ loop of four linked Mn_{10} loops. *Inorg. Chem.* **2007**, *46*, 3795–3797.

139. Moushi, E.E.; Lampropoulos, C.; Wernsdorfer, W.; Nastopoulos, V.; Christou, G.; Tasiopoulos, A.J. Inducing single-molecule magnetism in a family of loop-of-loops aggregates: Heterometallic $Mn_{10}Na_4$ Clusters and the homometallic Mn_{44} analogue. *J. Am. Chem. Soc.* **2010**, *132*, 16146–16155.

140. Charalambous, M.; Moushi, E.E.; Nguyen, T.N.; Papatriantafyllopoulou, C.; Nastopoulos, V.; Christou, G.; Tasiopoulos, A.J. Giant heterometallic [$Mn_{36}Ni_4$]$^{0/2-}$ and [$Mn_{32}Co_8$] "loop-of-loops-and-supertetrahedra" molecular aggregates. *Front. Chem.* **2019**, *7*, 96. [CrossRef]

141. Charalambous, M.; Moushi, E.E.; Papatriantafyllopoulou, C.; Wernsdorfer, W.; Nastopoulos, V.; Christou, G.; Tasiopoulos, A.J. A $Mn_{36}Ni_4$ 'loop-of-loops-and-sypertetrahedra' aggregate possessing a high $S_T = 26 \pm 1$ spin ground state. *Chem. Commun.* **2012**, *48*, 5140–5142. [CrossRef]

142. Milios, C.J.; Piligkos, S.; Brechin, E.K. Ground state spin-switching via targeted structural distortion: Twisted single-molecule magnets from derivatised salicylaldoximes. *Dalton Trans.* **2008**, 1809–1817. [CrossRef] [PubMed]

143. Jones, L.F.; Inglis, R.; Cochrane, M.E.; Mason, K.; Collins, A.; Parsons, S.; Perlepes, S.P.; Brechin, E.K. New structural types and different oxidation levels in the family of Mn_6-oxime single-molecule magnets. *Dalton Trans.* **2008**, 6205–6210. [CrossRef] [PubMed]

144. Milios, C.J.; Inglis, R.; Vinslava, A.; Prescimone, A.; Parsons, S.; Perlepes, S.P.; Christou, G.; Brechin, E.K. Turning up the spin, turning on single-molecule magnetism: From S = 1 to S = 7 in a [Mn_8] cluster via ligand induced structural distortion. *Chem. Commun.* **2007**, 2738–2740. [CrossRef] [PubMed]

145. Inglis, R.; Jones, L.F.; Milios, C.J.; Datta, S.; Collins, A.; Parsons, S.; Wernsdorfer, W.; Hill, S.; Perlepes, S.P.; Piligkos, S.; et al. Attempting to understand (and control) the relationship between structure and magnetism in an extended family of Mn_6 single-molecule magnets. *Dalton Trans.* **2009**, 3403–3412. [CrossRef] [PubMed]

146. Milios, C.J.; Vinslava, A.; Whittaker, A.G.; Parsons, S.; Wernsdorfer, W.; Christou, G.; Perlepes, S.P.; Brechin, E.K. Microwave-Assisted synthesis of a hexanuclear Mn^{III} single-molecule magnet. *Inorg. Chem.* **2006**, *45*, 5272–5274. [CrossRef]

147. Milios, C.J.; Inglis, R.; Bagai, R.; Wernsdorfer, W.; Collins, A.; Moggach, S.; Parsons, S.; Perlepes, S.P.; Christou, G.; Brechin, E.K. Enhancing SMM properties in a family of [Mn$_6$] clusters. *Chem. Commun.* **2007**, 3476–3478. [CrossRef]

148. Milios, C.J.; Raptopoulou, C.P.; Terzis, A.; Lloret, F.; Vicente, R.; Perlepes, S.P.; Escuer, A. hexanuclear Manganese(III) single-molecule magnets. *Angew. Chem. Int. Ed.* **2004**, *43*, 210–212. [CrossRef]

149. Milios, C.J.; Inglis, E.; Vinslava, A.; Bagai, E.; Wernsdorfer, W.; Parsons, S.P.; Perlepes, S.P.; Christou, G.; Brechin, E.K. Toward a magnetostructural correlation for a family of Mn$_6$ SMMs. *J. Am. Chem. Soc.* **2007**, *129*, 12505–12511. [CrossRef]

150. Cordero, B.; Roubeau, O.; Teat, S.J.; Escuer, A. Building of a novel single molecule magnet by assembly of anisotropic {Mn$_3$(μ_3-O)(salox)$_3$}$^+$ triangles. *Dalton Trans.* **2011**, *40*, 7127–7129. [CrossRef]

151. Inglis, R.; Katsenis, A.D.; Collins, A.; White, F.; Milios, C.J.; Papaefstathiou, G.S.; Brechin, E.K. Assembling molecular triangles into discrete and infinite architectures. *Cryst. Eng. Commun.* **2010**, *12*, 2064–2072. [CrossRef]

152. Stoumpos, C.C.; Inglis, R.; Karotsis, G.; Jones, L.F.; Collins, A.; Parsons, S.; Milios, C.J.; Papaefstathiou, G.S.; Brechin, E.K. Supramolecular entanglement from interlocked molecular nanomagnets. *Cryst. Growth Des.* **2009**, *9*, 24–27. [CrossRef]

153. Inglis, R.; Papaefstathiou, G.S.; Wernsdorfer, W.; Brechin, E.K. Ferromagnetic [Mn$_3$] single-molecule magnets and their supramolecular networks. *Aust. J. Chem.* **2009**, *62*, 1108–1118. [CrossRef]

154. Manoli, M.; Inglis, R.; Piligkos, S.; Yanha, L.; Wernsdorfer, W.; Brechin, E.K.; Tasiopoulos, A.J. A hexameric [Mn$^{III}_{18}$Na$_6$] wheel based on [Mn$^{III}_3$O]$^{7+}$ sub-units. *Chem. Commun.* **2016**, *52*, 12829–12832. [CrossRef] [PubMed]

155. Manoli, M.; Inglis, R.; Manos, M.J.; Nastopoulos, V.; Wernsdorfer, W.; Brechin, E.K.; Tasiopoulos, A.J. A [Mn$_{32}$] double-decker wheel. *Angew. Chem. Int. Ed.* **2011**, *50*, 4441–4444. [CrossRef]

156. Milios, C.J.; Stamatatos, T.C.; Perlepes, S.P. The coordination chemistry of pyridyl oximes. *Polyhedron* **2006**, *25*, 134–194. [CrossRef]

157. Abele, E.; Abele, R.; Lukevics, E. Pyridine oximes: Synthesis, reactions, and biological activity. *Chem. Heterocycl. Compd.* **2003**, *39*, 825–865. [CrossRef]

158. Pavlov, A.A.; Savkina, S.A.; Belov, A.S.; Nelyubina, Y.V.; Efimov, N.N.; Voloshin, Y.Z.; Novikov, V.V. Trigonal prismatic tris-pyridineoximate transition metal complexes: A Cobalt(II) compound with high magnetic anisotropy. *Inorg. Chem.* **2017**, *56*, 6943–6951. [CrossRef]

159. Escuer, A.; Vlahopoulou, G.; Maunter, F.A. Use of 6-methylpyridine-2-carbaldehydeoxime in Nickel(II) carboxylate chemistry: Synthetic, structural and magnetic properties of penta and hexanuclear complexes. *Dalton Trans.* **2011**, *40*, 10109–10116. [CrossRef]

160. Esteban, J.; Ruiz, E.; Font-Bardia, M.; Calvet, T.; Escuer, A. Triangular nickel complexes derived from 2-Pyridylcyanoxime: An approach to the mangetic properties of the [Ni$_3$(μ_3-OH){pyC(R)NO}$_3$]$^{2+}$ core. *Chem. Eur. J.* **2012**, *18*, 3637–3648. [CrossRef]

161. Escuer, A.; Vlahopoulou, G.; Perlepes, S.P.; Mautner, F.A. Trinuclear, tetranuclear, and polymeric Cu^{II} complexes from the first use of 2-Pyridylcyanoxime in transition metal chemistry: Synthetic, structural, and magnetic studies. *Inorg. Chem.* **2011**, *50*, 2468–2478. [CrossRef]

162. Papatriantafyllopoulou, C.; Stamatatos, T.C.; Wernsdorfer, W.; Teat, S.J.; Tasiopoulos, A.J.; Escuer, A.; Perlepes, S.P. Combining Azide, carboxylate, and 2-Pyridyloximate ligands in transition-metal chemistry: Ferromagnetic Ni$^{II}_5$ clusters with a bowtie skeleton. *Inorg. Chem.* **2010**, *49*, 10486–10496. [CrossRef]

163. Alexandropoulos, D.I.; Papatriantafyllopoulou, C.; Aromi, G.; Roubeau, O.; Teat, S.J.; Perlepes, S.P.; Christou, G.; Stamatatos, T.C. The Highest-Nuclearity manganese/oximate complex: An unusual Mn$^{II/III}_{15}$ cluster with an S = 6 ground state. *Inorg. Chem.* **2010**, *49*, 3962–3964. [CrossRef]

164. Lampropoulos, C.; Stamatatos, T.C.; Manos, M.J.; Tasiopoulos, A.J.; Abboud, K.A.; Christou, G. New mixed-valence Mn$^{II/III}_6$ complexes bearing oximato and azido ligands: Synthesis, and structural and magnetic characterization. *Eur. J. Inorg. Chem.* **2010**, 2244–2253. [CrossRef]

165. Milios, C.J.; Piligkos, S.; Bell, A.R.; Laye, R.H.; Teat, S.J.; Vicente, R.; McInnes, E.; Escuer, A.; Perlepes, S.P.; Winpenny, R.E.P. A rare mixed-valence state manganese (II/IV) tetranuclear cage formed using phenyl 2-pyridyl ketone oxime and azide as ligands. *Inorg. Chem. Commun.* **2006**, *9*, 638–641. [CrossRef]

166. Milios, C.J.; Stamatatos, T.C.; Kyritsis, P.; Terzis, A.; Raptopoulou, C.P.; Vicente, R.; Escuer, A.; Perlepes, S.P. Phenyl 2-Pyridyl ketone and its oxime in manganese carboxylate chemistry: Synthesis, characterization, *X*-ray studies and magnetic properties of mononuclear, trinuclear and octanuclear complexes. *Eur. J. Inorg. Chem.* **2004**, 2885–2901. [CrossRef]

167. Adebayo, O.A.; Abboud, K.A.; Christou, G. Mn_3 single-molecule magnets and Mn_6/Mn_9 clusters from the use of Methyl 2-Pyridyl ketone oxime in manganese phosphinate and phosphonate chemistry. *Inorg. Chem.* **2017**, *56*, 11352–11364. [CrossRef] [PubMed]

168. Stamatatos, T.C.; Foguet-Albiol, D.; Lee, S.-C.; Stoumpos, C.C.; Raptopoulou, C.P.; Terzis, A.; Wernsdorfer, W.; Hill, S.O.; Perlepes, S.P.; Christou, G. "Switching On" the properties of single-molecule magnetism in triangular Manganese(III) complexes. *J. Am. Chem. Soc.* **2007**, *129*, 9484–9499. [CrossRef] [PubMed]

169. Cano, J.; Cauchy, T.; Ruiz, E.; Milios, C.J.; Stoumpos, C.C.; Stamatatos, T.C.; Perlepes, S.P.; Christou, G.; Brechin, E.K. On the origin of ferromagnetism in oximato-based $[Mn_3O]^{7+}$ triangles. *Dalton Trans.* **2008**, 234–240. [CrossRef]

170. Mowson, A.M.; Nguyen, T.N.; Abboud, K.A.; Christou, G. Dimeric and tetrameric supramolecular aggregates of single-molecule magnets via carboxylate substitution. *Inorg. Chem.* **2013**, *52*, 12320–12322. [CrossRef] [PubMed]

171. Nguyen, T.N.; Abboud, K.A.; Christou, G. MOF-like supramolecular network of Mn_3 single-molecule magnets formed by extensive π–π stacking. *Polyhedron* **2016**, *103*, 150–156. [CrossRef]

172. Nguyen, T.N.; Wernsdorfer, W.; Abboud, K.A.; Christou, G. A supramolecular aggregate of four exchange-biased single-molecule magnets. *J. Am. Chem. Soc.* **2011**, *133*, 20688–20691. [CrossRef] [PubMed]

173. Nguyen, T.N.; Wernsdorfer, W.; Shiddiq, M.; Abboud, K.A.; Hill, S.; Christou, G. Supramolecular aggregates of single-molecule magnets: Exchange-biased quantum tunneling of magnetization in a rectangular $[Mn_3]_4$ tetramer. *Chem. Sci.* **2016**, *7*, 1156–1173. [PubMed]

174. Nguyen, T.N.; Shiddiq, M.; Ghosh, T.; Abboud, K.A.; Hill, S.; Christou, G. Covalently linked dimer of Mn_3 Single-Molecule magnets and retention of its structure and quantum properties in solution. *J. Am. Chem. Soc.* **2015**, *137*, 7160–7168.

175. Vincent, J.B.; Chang, H.-R.; Folting, K.; Huffman, J.C.; Christou, G.; Hendrickson, D.N. Preparation and physical properties of trinuclear oxo-centered manganese complexes of the general formulation $[Mn_3O(O_2CR)_6L_3]^{0,+}$ (R = Me or Ph; L = a neutral donor group) and the crystal structures of $[Mn_3O(O_2CMe)_6(pyr)_3](pyr)$ and $[Mn_3O(O_2CPh)_6(pyr)_2(H_2O)]\cdot0.5MeCN$. *J. Am. Chem. Soc.* **1987**, *109*, 5703–5711.

176. Efthymiou, C.; Winterlich, M.; Papatriantafyllopoulou, C. Breakthrough in radical-bridged single-molecule magnets. In *Single-Molecule Magnets: Molecular Architectures and Building Blocks for Spintronics*; Holynska, M., Ed.; Wiley-VCH: Weinheim, Germany, 2019; pp. 315–351.